

ORIGIN AND NATURE OF THE REGIONAL
DETACHMENT FAULT IN THE AREA OF THE
DEEP GALICIA MARGIN

Dissertation
zur Erlangung des Doktorgrades
der Mathematisch-Naturwissenschaftlichen Fakultät
der Christian-Albrechts-Universität zu Kiel

vorgelegt von
Thomas Leythaeuser

Kiel 2004

Referent : Prof. Dr. Timothy Reston

Korreferent : Prof. Dr. Ernst R. Flüh

Tag der mündlichen Prüfung : 02.07.2004

Zum Druck genehmigt : Kiel, 14.07.2004

Der Dekan

TABLE OF CONTENTS

SUMMARY	1
ZUSAMMENFASSUNG	5
1.0 INTRODUCTION	9
1.1 Structure and Evolution of Iberia Margin	10
1.2 Study area and objectives	13
2.0 METHODS OF SEISMIC DATA PROCESSING	17
2.1 Poststack Time Migration	18
2.2 Prestack Depth Migration	25
2.3 Full Waveform Inversion	27
3.0 INTERPRETATION OF THE MCS DATA OF LINE ISE-2	35
3.1 Poststack Time Migration	35
3.2 Prestack Depth Migration	38
3.3 Full Waveform Inversion	46
4.0 INTERPRETATION OF THE MCS DATA OF LINE ISE-1	55
4.1 Poststack Time Migration	55
4.2 Prestack Depth Migration	55
5.0 DISCUSSION	63
5.1 Origin of the S-reflector	63
5.2 Nature of the S-reflector	84
6.0 DANKSAGUNG	93
7.0 LITERATURE	95

SUMMARY

The Iberia margin is a classical example of a non-volcanic rifted margin. Rifting of continental crust has produced there a number of typical structural configurations such as e.g. rows of landward tilted fault blocks of thin continental crust underlain by a widespread low-angle detachment which is imaged as a bright seismic reflection and known as the S-reflector. The present study area is located in the northern part of this margin which is known as the deep Galicia margin. This area belongs to the continent-ocean-transition zone which has been studied intensively for many years by several marine seismic experiments and ODP drilling activities. Consequently, the history of rifting, continental break-up and extension with respect to the evolution of this margin is well understood and documented in the literature.

In an area of the deep Galicia margin which is crossed by many MCS reflection lines two seismic lines (ISE-1 and ISE-2) have been processed and interpreted in the course of the present study. Its main objective was to attempt clarification of the precise nature and origin of the S-reflector. For this purpose a full waveform inversion was carried out for a selected CMP gather from line ISE-2 besides prestack depth migration and conventional poststack seismic data processing of both lines.

Interpretation of seismic cross sections of both ISE-lines lead to the following observations and conclusions:

- a) Most conclusions documented in the previous literature about the evolution of this margin and its structural configuration can be confirmed, e.g. S represents a low-angle detachment fault which has played a crucial role in continental break-up and extension. The S-reflector passes without offset beneath the rotated fault blocks of the thinned continental crust. In both ISE-lines there are places where stretching was so advanced that complete separation of the continental crustal blocks has occurred.
- b) Several hitherto little, or not recognised structural features were observed. In line ISE-2 the S-reflector can be traced directly up to the reflection of the eastern flank of the peridotite ridge. A possible explanation is that the latter reflection may have originated from an originally seaward extending S which was later

warped upwards with the rise of the peridotite ridge. Another noteworthy structural configuration imaged in line ISE-2 is a lenticular shaped body at the foot of a tilted fault block which is interpreted as a clastic wedge which had slid down the originally oversteepened fault scarp.

- c) Also, some evidence is obtained in line ISE-1 suggesting that multiple phases of faulting has occurred during extension of the continental crust.

Full waveform inversion of a selected CMP gather from line ISE-2 lead to the conclusion that the S-reflector is at this location represented by an approx. 50 m thick low-velocity zone superimposed on an increase in seismic velocities which forms the topmost interval of the mantle. For this zone a compressional wave velocity of 5.2 km/s was determined as compared to 5.45 km/s for the overlying continental crust and 7.0 km/s for the mantle interval below. These p-wave velocity contrasts in the uppermost mantle are interpreted to result from a particular serpentinization history. It may have occurred in two separate stages in analogy to processes which have been documented for several ODP sites along the Iberia margin on the basis of detailed mineralogical and petrophysical studies. During an early stage the upper 2-3 km of the mantle peridotite may have been serpentinised in a high temperature regime (200°-400°C) to a moderate degree due to slow pervasive infiltration of sea water. At a later and more advanced stretching stage deep normal faults penetrating the mantle allowed influx of sea water leading to the second stage of serpentinization. This resulted in a continuation of the serpentinization process in a low temperature regime (50°-150°C) in the fractured mantle volume around each normal fault. With progress of serpentinization reactions a series of interdependent processes is triggered, which leads ultimately to the formation of a detachment fault : i) heat-driven convection of aqueous fluids due to the exothermic nature of serpentinisation leading to ii) sealing of the fault near the crust/mantle interface by hydrothermal mineral precipitation, causing iii) overpressuring of trapped pore fluids below aided also by generation of methane gas due to serpentinization and heating of pore fluids due to the exothermic serpentinization reaction, and iv) squeezing of serpentine masses into the crust/mantle contact zone where a thin interval of material with reduced density is formed, which is seismically imaged as S-reflector.

The effects of these processes are illustrated in a qualitative model (Figs. 5.1.3, 5.1.4 and 5.2.2). The possible mechanism of overpressuring of pore fluids is examined on the basis of a volume balance of the serpentinization reaction, i.e. quantification of volume expansion of the solid phase versus water consumption and replenishment. On the basis of these results it is suggested that volume expansion and focussed local generation of pore fluid overpressures in the vicinity of fault zones due to serpentinization have played an important role with respect to the formation of the low-angle detachment, which is seismically imaged as the S-reflector.

ZUSAMMENFASSUNG

Der West-Iberische Kontinentalrand gilt als typisches Beispiel für einen nicht-vulkanischen Kontinentalrand. Die Extension der kontinentalen Kruste hat dort eine Reihe charakteristischer tektonischer Strukturen erzeugt wie z.B. eine Staffelung von landwärts gekippten Krustenblöcken, die durch westwärts einfallende Abschiebungen begrenzt werden. An ihrer Unterkante wird über weite Regionen ein Detachment beobachtet, das seismisch als deutlicher Reflektor ausgebildet ist. Er wird in diesem Gebiet als S-Reflektor bezeichnet. Das Untersuchungsgebiet der vorliegenden Arbeit liegt im nördlichen Teil dieses Kontinentalrands, der als der tiefe galizische Kontinentalrand bezeichnet wird. In diesem Gebiet befindet sich eine breite Übergangszone von ozeanischer zu kontinentaler Kruste (OCT), die anhand zahlreicher seismischer Profile sowie durch Bohrungen im Rahmen von Fahrten des internationalen Tiefseebohrprogramms (ODP) relativ gut untersucht ist. Deshalb ist die erdgeschichtliche Entwicklung dieses Kontinentalrands vom Riftstadium zum Stadium der Krustenextension und Kontinentseparierung in Einzelheiten gut rekonstruiert und in zahlreichen Arbeiten in der Literatur dokumentiert. Die vorliegende Arbeit basiert auf der Bearbeitung seismischer Daten mittels Standardmethoden und der iterativen Tiefenmigration vor dem Stapeln, sowie der geologischen Interpretation von zwei seismischen Linien (ISE-1 und ISE-2) in einem Teilgebiet des tiefen galizischen Kontinentalrands, in dem schon viele reflexionsseismische Linien vermessen und z.T. von Mitarbeitern der Kieler Arbeitsgruppe „Marine Geodynamik“ im GEOMAR-Zentrum interpretiert wurden. Die übergeordnete Zielsetzung der vorliegenden Arbeit galt der Klärung der Ausprägung und Entstehung dieses S-Reflektors. Zu diesem Zweck wurde für eine ausgewählte CMP Familie aus dem Profil ISE-2 mittels Softwarepaketen, die am „Southampton Oceanography Centre“ vorhanden sind, eine „full waveform inversion“ durchgeführt.

Die Interpretation der beiden bearbeiteten ISE-Linien erlaubt folgende Beobachtungen und Schlußfolgerungen :

a) Ein Großteil der Untersuchungsergebnisse, die in der Literatur zur Evolution und dem strukturellen Bau dieses Kontinentalrandes dokumentiert sind, können bestätigt

werden, z.B. die Beobachtung, daß der S-Reflektor eine sehr flach einfallende Detachment-Störung darstellt, die eine zentrale Rolle gespielt hat beim Aufbrechen und der Extension der kontinentalen Kruste, sowie die Beobachtung, daß die die Krustenblöcke begrenzenden Abschiebungen abrupt beim Kontakt mit dem S-Reflektor enden. In beiden ISE-Linien ist die Krustendehnung so weit fortgeschritten, daß es lokal zu einer völligen Trennung benachbarter Krustenblöcke kam.

b) Einige bemerkenswerte strukturgeologische Konfigurationen konnten charakterisiert werden, die in den bisher interpretierten seismischen Profilen dieses Gebiets nur undeutlich oder überhaupt nicht beobachtet worden waren. Im Profil ISE-2 kann der S-Reflektor durchverfolgt werden bis zum direkten Kontakt mit der Reflexion der Ostflanke des Peridotitrückens. Als mögliche Erklärung wird vorgeschlagen, daß die Reflexion der Ostflanke des Peridotitrückens die ursprüngliche ozeanwärts ausgebildete Fortsetzung des S-Reflektors darstellt, die mit dem Aufstieg des Peridotitrückens hochgebogen wurde. Eine weitere strukturgeologisch interessante Detailbeobachtung im Profil der Linie ISE-2 betrifft einen größeren linsenförmigen Körper am Fuß eines gekippten Krustenblocks, der als eine keilförmige, klastische Rutschmasse interpretiert wird, die möglicherweise infolge Übersteilung der durch die Abschiebung gebildeten Steilstufe abgerutscht ist.

c) Einige in der Linie ISE-1 schwach ausgebildete Reflexionen können als Anzeichen für eine während der Extension abgelaufene mehrphasige Bruchtektonik gedeutet werden.

Die Ergebnisse der „full waveform inversion“ der Daten des ausgewählten „CDP gathers“ der Linie ISE-2 lassen die Schlußfolgerung zu, daß der S-Reflektor an dieser Lokation eine ca. 50 m mächtige Niedriggeschwindigkeitszone darstellt, die zwischen einer sprunghaften Zunahme der P-Wellengeschwindigkeit eingeschoben ist. Für diese oberste Mantelzone wurde eine P-Wellengeschwindigkeit von 5.2 km/s ermittelt, während die überlagernde Kruste bzw. der unterlagernde Mantel P-Wellengeschwindigkeiten von 5.45 bzw. 7.0 km/s zeigen. Diese deutlichen Unterschiede in den P-Wellengeschwindigkeiten im Grenzbereich zwischen der Kruste und dem Mantel können als Ergebnis eines besonderen Ablaufs der Serpentinisierung dieser obersten Zone des Mantels erklärt werden. In einer gewissen Analogie zu dem gut

dokumentierten Ablauf der Serpentinisierungsprozesse, der in mehreren ODP-Bohrungen am West-Iberischen Kontinentalrand anhand mineralogischer und petrophysikalischer Untersuchungen rekonstruiert wurde, wird die Hypothese vorgeschlagen, daß die Serpentinisierung in zwei Phasen erfolgt sein könnte. In einer ersten Phase kann der Mantelperidotit infolge einer Infiltration von Meerwasser, das die Gesteinsmatrix der ausgedünnten Kruste langsam durchdringt, bis in Tiefen von 2-3 km unterhalb der Kruste/Mantel-Grenze partiell serpentiniert werden. Diese Alteration erfolgte in größerer Tiefe und unter erhöhten Temperaturen (200-400°C) nicht zu einem vollständigen Ausmaß, da das Angebot an Meerwasser limitiert war. In einem späteren Stadium der fortgeschrittenen Krustenextension konnten große Abschiebungen bis weit in den Mantel eindringen. Dies hatte einen lokal auf die Störungszonen fokussierten und volumenmäßig erheblichen Eintrag von Meerwasser in den Mantel in der Umgebung jeder Störungszone zur Folge. Dort kam es zur vollständigen Serpentinisierung des Mantelperidotites, die infolge des diesmal raschen Meeresswassereintrags in einem niedrigeren Temperaturbereich erfolgte (50-150°C). Im Verlauf dieser lokal begrenzten Serpentinisierungsprozesse kam es durch folgende Umstände zur Ausbildung der markanten Detachment-Störung, die seismisch als S-Reflektor erfaßbar ist :

- a) Ausbildung einer hydrothermalen Konvektionszelle in der geklüfteten Störungszone als Folge der exothermen Natur der Serpentinisierungsreaktionen, dies führte
- b) schließlich zur Versiegelung der Störungszone nahe der Kruste/Mantel-Grenze durch hydrothermale Mineralausfällungen, wodurch c) sich in den residualen Porenfluiden der Störungszone unterhalb dieser Permeabilitätsbarriere als kombinierter Effekt mehrerer Prozesse überhydrostatische Druckverhältnisse einstellten (Volumenexpansion der festen Mineralphase bei vollständiger Serpentinisierung ; Bildung von Methan als Folge der Serpentinisierung ; Erwärmung der Porenfluide durch die exothermen Serpentinisierungsreaktionen), in den so entstandenen lokal begrenzten Mantelvolumina stellten sich auf diese Weise duktile Bedingungen ein, die dazu führten, daß d) die duktil verformbaren Serpentinmassen als Folge tektonischer Beanspruchung bei einer erneut einsetzenden Extensionsphase entlang der Kruste/Mantel-Grenze mobilisiert wurden. Diese in einer dünnen Zone so mobilisierten Serpentinmassen haben infolge eines niedrigen Reibungskoeffizienten als Schmiermittel bei der Rotation und Extension der Krustenblöcke gewirkt.

Der hypothetische Ablauf dieser Prozesse der Serpentinisierung und ihrer Folgeerscheinungen wird in einem konzeptionellen, qualitativen Modell schematisch dargestellt (Abb. 5.1.3, 5.1.4, und 5.2.2). Mögliche Mechanismen der Porenfluid-Überdruckbildung werden diskutiert auf der Basis einer Bilanzierung der mit der Serpentinisierung von Mantelperidotit verbundenen Volumenexpansion diskutiert. Aufgrund dieser Ergebnisse erscheint es wahrscheinlich, daß eine lokale, auf tiefgehende Störungszonen im oberen Mantel fokussierte Ausbildung von Porenfluidüberdrücken eine wichtige Rolle gespielt hat bei der Entstehung der regionalen Detachment-Störung, die seismisch als S-Reflektor ausgeprägt ist.

1.0 INTRODUCTION

Continental extension and rifting can either lead to the initiation of seafloor spreading, or the process stops at an intermediate stage resulting in a failed rift zone. In the first case a combination of tectonic and magmatic processes leads to the formation of new oceanic crust and new ocean basins. In the second case proto-rift and rift basins are formed (e.g. Rockall Trough). The geological and geophysical processes which control the evolution of continental extension and rifting in either case is not completely understood.

With respect to the case of continental extension and rifting leading to the initiation of seafloor spreading two types of continental margins can be formed: Volcanic-rifted margins and non-volcanic rifted margins. Volcanic rifted margins are associated with considerable synrift magmatic activity leading to the formation of thick and regionally extensive basalt layers known in seismic sections as seaward-dipping reflectors (Hinz et al. 1981). The East Greenland margin and the South Atlantic margin offshore Argentina and Namibia are classical examples of this type of continental margins. At non-volcanic rifted margins there is little or no magmatic activity observed. Here the continental crust is often thinned to an extreme degree such that mantle unroofing has occurred. This type of continental margin is represented e.g. by the Iberia margin (Boillot and Winterer 1988, Whitmarsh et al. 1996) and the conjugate Newfoundland margin (Reid, 1994) as well as by the proto-Alpine margin (Froitzheim and Manatschal 1996). Common features of these margins concerns rifting of relatively thin and cool continental crust and certain similarities in terms of structural styles e.g. large-scale detachment faults and unroofed mantle peridotite as crucial structural elements. Among the best known and most intensively studied non-volcanic rifted continental margins worldwide is the Iberia margin. This is the result of three ODP legs (Nrs. 103, 149 and 173) including the relevant pre-site geophysical surveys as well as several reflection and refraction seismic studies (Reston et al. 1996, Chian et al. 1999, Dean et al. 2000).

1.1 STRUCTURE AND EVOLUTION OF THE IBERIA MARGIN

The evolution of the Iberia margin was initiated by several phases of continental rifting dated between the Triassic and early Cretaceous (Pinheiro et al. 1992). Separation from the conjugate Newfoundland margin occurred during early Cretaceous times due to seafloor spreading propagating from south to north. The plate tectonic situation of the study area at that time is shown in Fig. 1.1.1. Evidence of the first Triassic rifting event is observed in the Lusitanian Basin onshore Portugal (Wilson et al. 1990). In the north the Lusitanian basin extends offshore to the Galicia Interior basin, which represents an aborted rift bordered to the west by the Galicia Bank. The Galicia Interior basin is believed to have originated due to extension during Valanginian times (Murillas et al. 1990). As shown by the bathymetry in Fig. 1.1.2 the Iberian margin itself is divided into three segments : The Tagus Abyssal Plain, the Iberia Abyssal Plain and the Deep Galicia Margin. The magnetic anomaly J as the oldest one occurring offshore Iberia and offshore the conjugate Newfoundland margin allows an estimate of the age of the final break-up event. This anomaly is age-dated between seafloor spreading isochrons M0 and M2 of the Central Atlantic (Rabinowitz et al. 1978, Tucholke and Ludwig 1982). The initiation of actual seafloor spreading is believed to have started at anomaly M11 in the area of the Tagus Abyssal Plain (Pinheiro et al. 1992), during anomaly M3 in the area of the Iberia Abyssal Plain (Whitmarsh and Miles 1995) and during late Aptian in the area of the Deep Galicia Margin (Boillot and Winterer 1988).

In the region of the Iberia Abyssal Plain and the Deep Galicia Margin there is no well defined boundary between the thinned continental and the normal oceanic crust. Instead a so called continent-ocean transition zone (COT) was recognized, where the geophysical nature of the crust cannot be classified as continental or as oceanic. This margin is characterized by the exhumation of mantle peridotite during the final stages of breakup. Subsequently the shallow mantle rocks were then transformed to serpentinite by interaction with seawater (Whitmarsh et al. 1996, Chian et al. 1999, Whitmarsh et al. 2000). However lithospheric thinning was accompanied by little or no decompressional melting of the asthenospheric mantle. As shown in Fig. 1.1.2 the width

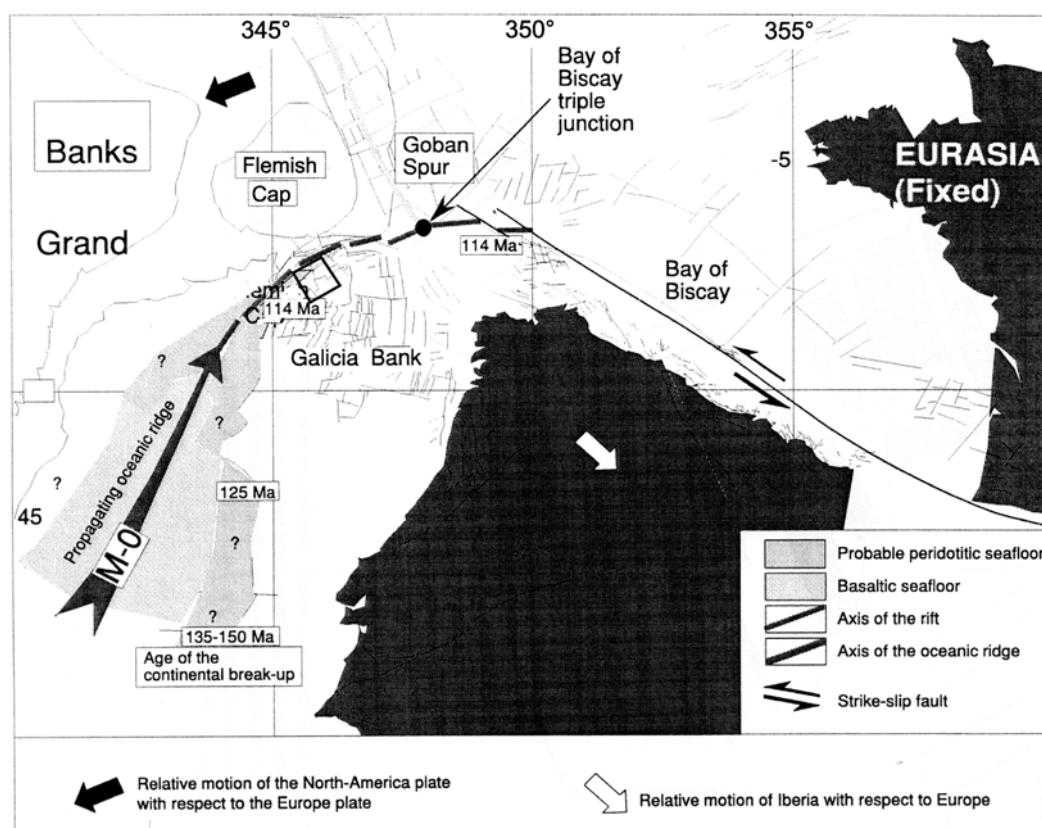


Fig. 1.1.1 : Plate tectonic situation of the Iberia Margin during M0 (reproduced from Malod and Mauffret 1990) when continental break-up and separation from the Newfoundland margin occurred along with northward propagation of oceanic ridge. Approximate location of study area (box) is adjacent of Flemish Cap.

of the continent-ocean transition zone exhibiting serpentinized mantle varies along strike the Iberian margin. While this transitional zone is about 100 km wide in the southern Iberia Abyssal Plain (Dean et al. 2000), it narrows considerably in the study area off Galicia Bank (Whitmarsh et al. 1996). In this zone, neither clearly defined fault blocks of stretched continental crust nor typically linear magnetic anomalies of oceanic crust are observed (Pickup et al. 1996, Krawzyck et al. 1996, Reston et al. 1996, Whitmarsh and Miles 1995). The most characteristic structural features of this COT zone concerns detachment faults located between very thin continental crust above and serpentinised mantle rocks below. Landward of these detachment faults the basement consists of continental rocks, while in a seaward direction exhumed and serpentinized mantle make up the basement. Like other similar plate tectonic settings these detachment faults appear to have played a crucial role in the thinning of the continental crust

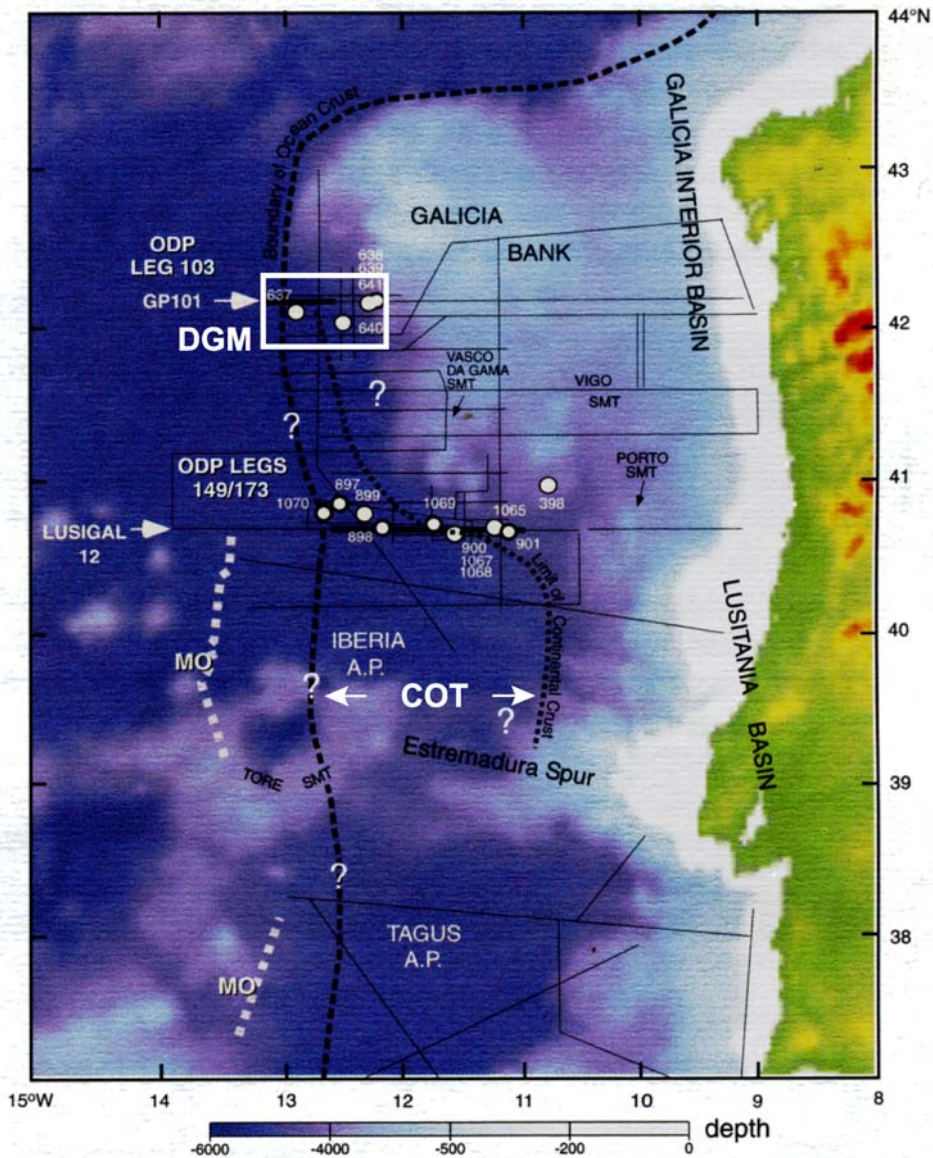


Fig. 1.1.2 : Location of study area (box) in relationship to the continent-ocean-transition zone (COT), the location of drill sites of ODP-legs 103, 149 and 173 as well as seismic lines measured in this region (reproduced from Larsen 2002, Fig. 3)

as well as in the crustal separation and exhumation of mantle peridotites (e.g. Reston et al. 1996). The origin, nature and structural style of this continent-ocean transition zone is poorly understood (Chian et al. 1999, Dean et al. 2000, Whitmarsh and Sawyer 1996). However, there is a general agreement that a better understanding of these aspects would be a key to resolve the problem how and under which conditions continental rifting evolves into a regime of oceanic spreading.

1.2 STUDY AREA AND OBJECTIVES

The present work is based on detailed processing of seismic lines ISE-1 and ISE-2 (Fig. 1.2.1). Line ISE-2 is 85 km long running across the Deep Galicia Margin, while line ISE-1, which is nearly identical with line GP-12, is only 55 km long (Fig. 1.2.2). Both seismic lines were acquired in the framework of the Iberia Seismic Experiment (ISE) in the Summer of 1997, which was a joint USA-German project including scientists from Rice University, Houston, University of Texas in Austin, and Geomar, Kiel. These lines were surveyed utilising the RV Maurice Ewing and its 4 km long, 160 channel streamer. A tuned source array of 20 air guns with 8385 cu inch total volume was fired every 50m (20 sec) resulting in 40-fold cmp data for lines ISE-1 and ISE-2.

A striking feature in most previously interpreted seismic lines of the study area concerns the so called S reflector. As an example Fig. 1.2.3 shows S as a continuous, seaward inclined reflector. Most previous authors agreed that this S reflector has played a crucial role within the extension of the crust leading to continental break-up (Mauffret and Montadert 1987). However, there is no agreement in the literature with respect to the interpretation of the origin and precise nature of the S reflector. Several authors have suggested that S has played an important role as a brittle-ductile transition during crustal stretching (e.g. de Charpal et al. 1978). A group of other authors have interpreted the S reflector as a major detachment fault whereby two alternatives have been proposed with respect to its position and dip, either intracrustal (Sibuet 1992) or at the crust-mantle boundary (Boillot et al. 1989). A completely different interpretation was proposed by Horsefield (1992), who suggested that a similar type reflector in other non-volcanic passive continental margin settings of the North Atlantic might represent the top of a zone of magmatic underplating above the Moho. Bright intracrustal reflections have also been interpreted as sill-type igneous intrusions (Litak and Hauser 1992, Goodwin et al. 1990, Barnes and Reston 1992, Pratt 1991) and in the case of the Siljan impact structure in Sweden have been documented by drilling to represent dolerite sills (Juhlin 1990).

Galicia Margin

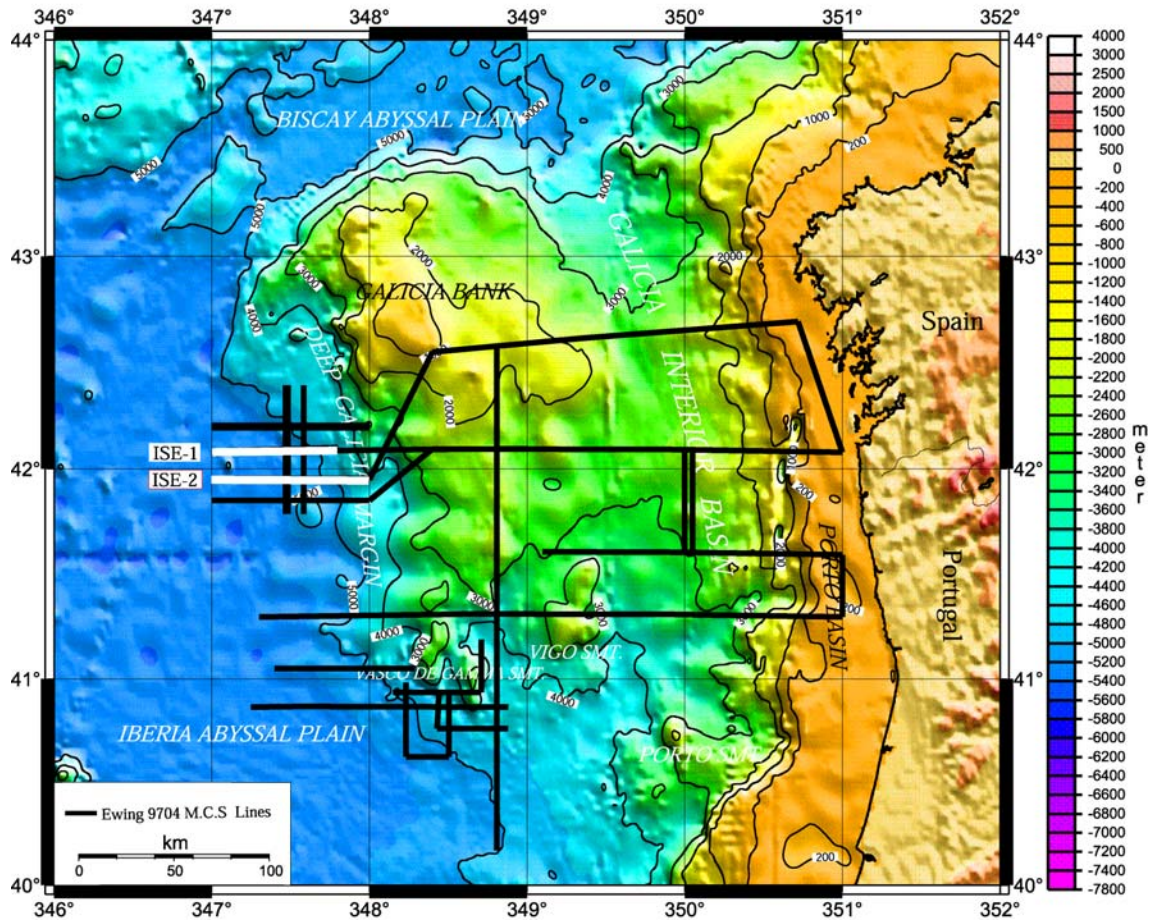


Fig. 1.2.1 : Location of all seismic lines acquired in the framework of the Iberia Seismic Experiment (ISE). Seismic lines ISE-1 and ISE-2 processed and interpreted in the present study are indicated.

The overall objective of the present study is to improve the understanding of the formation and evolution of non-volcanic rifted margins. For that part of the margin which is close to, or partly overlapping with the present study area the evolution of rifting and continental extension has been studied for many years by Reston and coworkers (for summary see e.g. Reston et al. 1996) on the basis of the time and depth migrated GP-seismic sections (Fig. 1.2.2). Pérez-Gussinyé et al. (2001) have in addition modeled the thermal, magmatic and rheological evolution of this margin during extension depending on initial lithospheric structure, rift duration and stretching factors. The main focus of the present work was directed towards clarification of the precise nature and role of the S reflector during the evolution of this rifted margin. In this con-

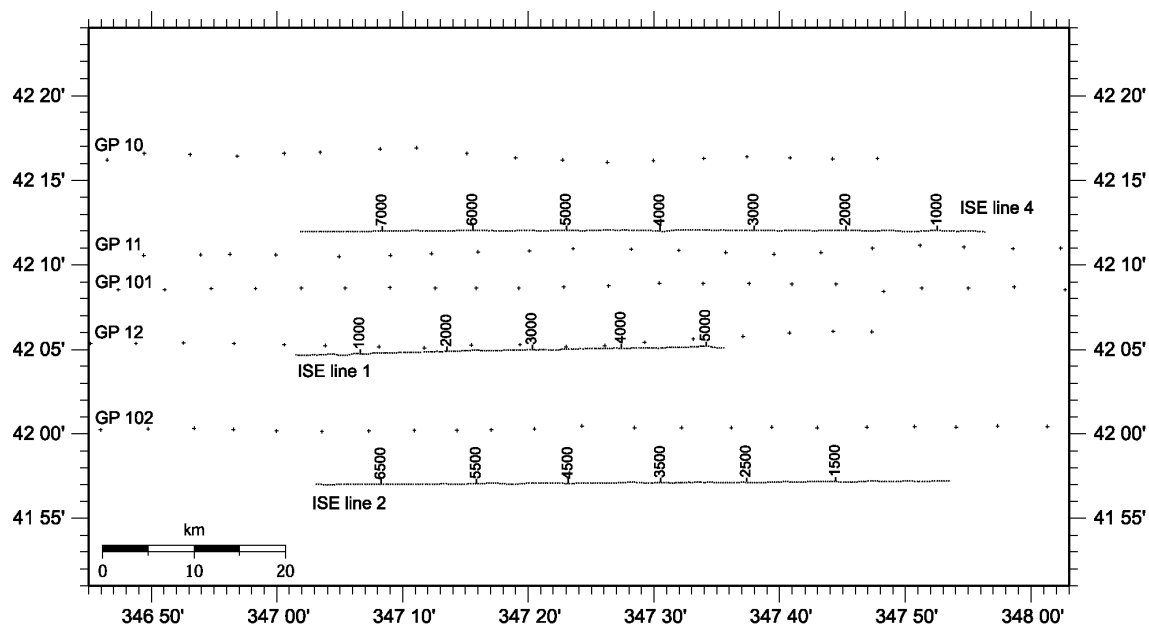


Fig. 1.2.2 : Location of seismic lines ISE-1 and ISE-2 processed in the present study in comparison with the GP-lines interpreted by Reston et al. (1996).

text the following questions are relevant:

What is the nature of S i.e. is it a reflection from a single interface or alternatively from a thin layer of a significantly different velocity ?

How did the S-reflector originate and evolve during stretching ?

What is the evidence that S represents a detachment structure ?

Can a break-away point be recognised based on the lateral shape of S ?

In order to obtain evidence which would answer these and other questions seismic lines ISE-2 and ISE-1 were processed with several processing software packages, each resulting in information of a somewhat different nature. Routine poststack time migration was performed to image basic structural features in two-way travelttime. However, no true structural dips and no depth related information is obtained. To get a true depth related image iterative prestack depth migration was performed. As a final step a full waveform inversion was carried out for a selected CMP of line ISE-2 to characterize the nature of S locally in high resolution. This was done during an eight months stay at the Southampton Oceanographic Centre (SOC) under the supervision of Dr. T. Minshall.

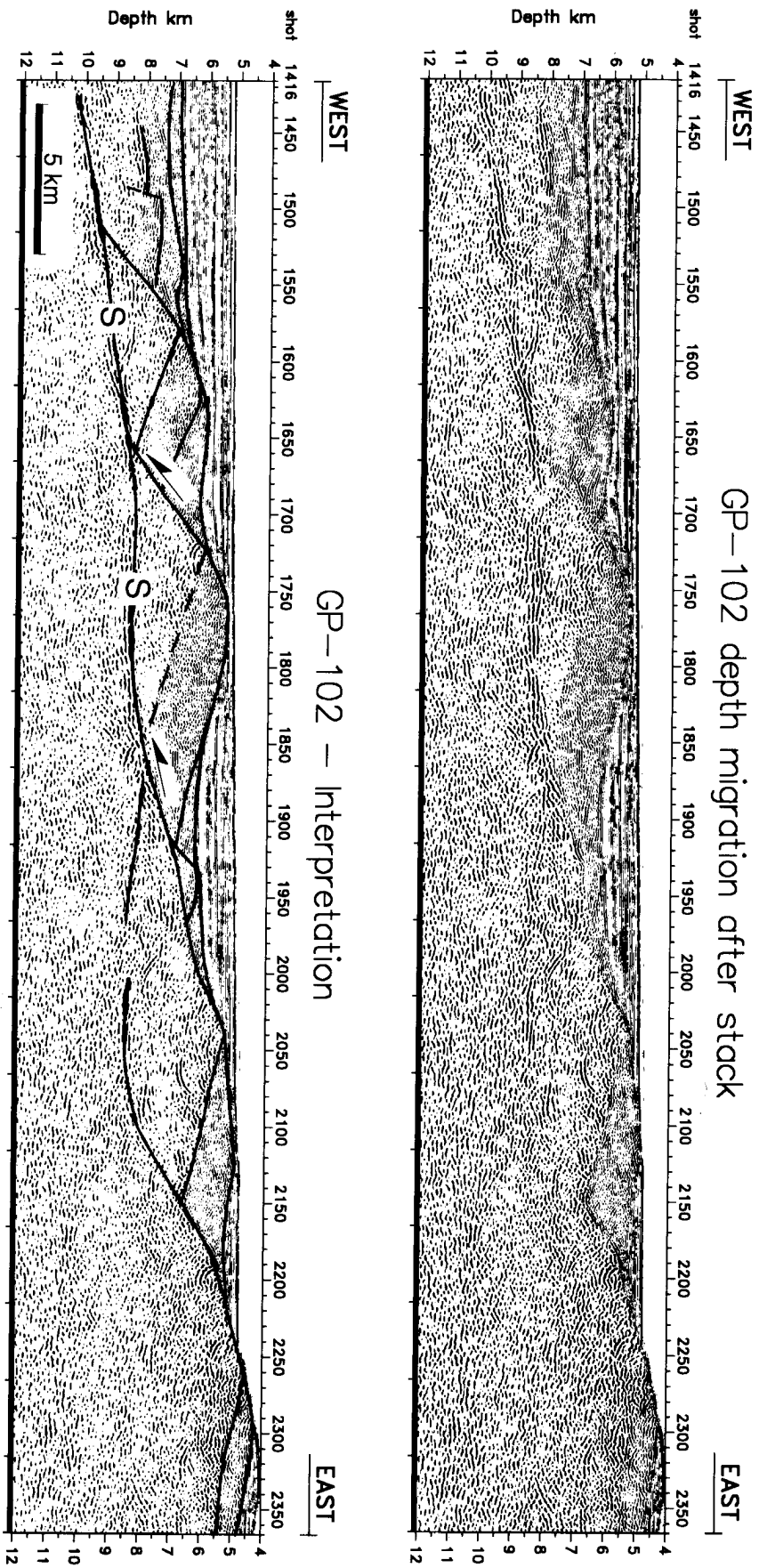


Fig. 1.2.3 : Depth-migrated seismic line GP-102 showing the S-reflector continuously dipping in a seaward direction without offsetting the block-bounding faults (reproduced from Reston et al. 1996).

2.0 METHODS OF SEISMIC DATA PROCESSING

The ultimate goal of seismic data recording is to recover an image of the geological structures in the subsurface which resembles a geological cross section and can be interpreted. To achieve this image the recorded seismic data have to be processed. Seismic data processing can generally be classified to consist of three main phases. A first phase of data processing includes all processes meant to enhance the signal-to-noise ratio of the recorded data. This first phase generally includes despiking, frequency filtering, multiple suppression and deconvolution. In a second phase subsurface velocities have to be estimated. Classically this is done by a velocity analysis deriving stacking velocities. Based on these stacking velocities, normal-move-out (NMO) corrections are applied and a first intermediate image of the subsurface is achieved by stacking the NMO corrected data. The third processing phase involves a process called migration by which a final image representing a geological cross section is achieved. In a more general sense migration is also termed imaging. Classically the stacked seismic section is time migrated to derive the final subsurface image representing a geological cross section.

The above outlined processing sequence is termed conventional processing as this is the classical scheme for multi-channel seismic (MCS) data processing. However, this processing sequence should not be thought of as a fixed scheme but a general sequence as the processing sequence applied should be specially adopted to the specific data set to achieve an optimal result. The processing steps applied to the multi-channel seismic data within the conventional processing sequence are described in section 2.1

As post-stack time migration does not account for effects like raypath bending and refraction the subsurface image derived can still show considerable distortions. This holds especially true in environments with laterally strongly varying velocity domains like the continental margin transects presented in this study. Here, sediment filled halfgrabens, representing domains of relatively low velocity, are juxtaposed against continental fault blocks, representing domains of relatively high velocity. These laterally strongly varying velocity distribution causes considerable raypath bending

leading to distortions in the stack and the subsequent post-stack time migration imaging process. To overcome the shortcomings in imaging by conventional post-stack time migration a prestack depth migration was performed. Pre-stack depth migration yields a geometrically more accurate subsurface image. As it accounts for raypath bending, it represents a superior imaging technique compared to conventional post-stack time migration. On the downside pre-stack depth migration is far more computationally demanding than post-stack time migration. The pre-stack depth migration is described in detail in section 2.2 .

To study the nature of the S-reflector in detail, a full waveform inversion was conducted for a selected CMP gather. Full waveform inversion aims at finding a subsurface model such that the observed data and synthetic data, calculated based on the subsurface model, match with respect to amplitude, phase and travel time. Section 2.3 deals with the method of the full waveform inversion in detail.

2.1 POSTSTACK TIME MIGRATION

The flowchart in Fig. 2.1.1 was prepared as an overview to facilitate the following discussion of the processing methods.

Trace Editing

Preceding the actual data processing a thorough visual inspection of the raw data to check for recording inconsistencies was performed. This so-called trace editing included the removal of obviously bad traces caused by malfunctioning channels in the recording system. Additionally a few traces in each shotgather turned out to be overmodulated. These were weighted such that they matched the average amplitude level of their neighbouring traces. Furthermore specific channels within each shotgather showed a consistent static shift in the order of 1 - 2 samples which were subsequently corrected. Of the 160 traces within each shot gather about 5 - 6 had to be removed due to mal-

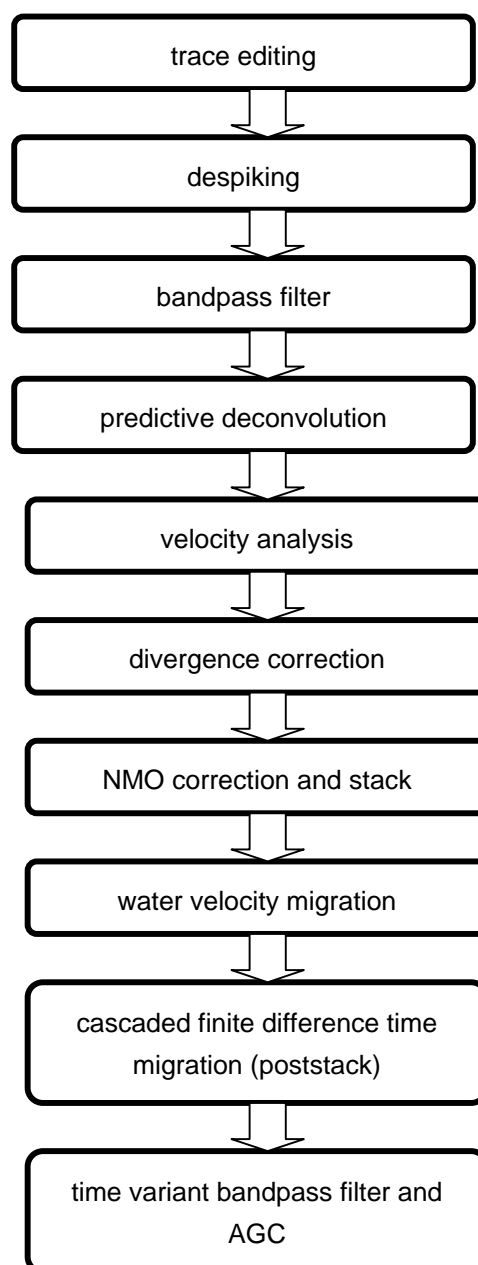


Figure 2.1.1 : Flowchart showing the processing sequence adopted for the ISE seismic data to achieve a poststack time migrated image of the subsurface.

functioning recording channels, about 2 - 3 traces had to be rescaled due to overmodulation and a static shift had to be applied to another 2 traces.

Despiking

Randomly distributed spikes introduced by the recording system are not only considered as noise, but furthermore in subsequent processing (frequency filtering, deconvolution) spikes can cause processing artefacts. These artefacts can considerably decrease the resolution of the processed data, thus spikes have to be removed before further processing. By calculating average amplitude values within characteristic time gates and subsequent correlation within each CMP gather, the randomly distributed spikes can be identified and erased.

Bandpass Filter

The data were frequency filtered with a minimum phase, time variant bandpass filter (ormsby filter). Within the sedimentary sequence the filter flanks were set to 4/6 - 50/60 Hz, within deeper crustal levels the bandpass is narrowed to 3/5 – 40/50 Hz. The narrowing of the bandpass for later travel times reflects that the earth itself acts as a lowpass filter with respect to seismic waves. For increasing travel times an increasing amount of the high frequencies of the seismic signal are attenuated. Thus this filter aims to suppress noise outside the main frequency content of the source signal.

Predictive Deconvolution

Deconvolution is a process which aims to recover the true subsurface reflectivity series. It is based on a model where the recorded seismogram $s(t)$ is approximated by the convolution of the earth's impulse response $e(t)$ with the seismic source wavelet $w(t)$, plus an unknown random noise component $n(t)$:

$$s(t) = [w(t) * e(t)] + n(t)$$

Seismogram = Source wavelet * earth impulse response + random noise

Deconvolution then tries to recover the reflectivity series, that is the earth's impulse response. Let S_k denote the seismogram, F_k the deconvolution filter to be determined and E_k the earth impulse response. Then the optimum wiener filter F_k is the one that

makes the difference between the desired output and the actual output a minimum in the least squares sense :

$$\sum_{k=0}^n (e_k - s_k * f_k)^2 = 0$$

developing this becomes :

$$\sum_{j=0}^n \Phi_{ww} (i - j) f = \Phi_{we}$$

where Φ_{ww} is the autocorrelation of the source wavelet and Φ_{we} the crosscorrelation of the source wavelet with the earth impulse response (Yilmaz,1987). Since the source wavelet is not known, its autocorrelation is approximated by that of the seismic trace. This is possible if the earth impulse response $e(t)$ and the noise $n(t)$ are random series and thus their autocorrelation is a constant value.

To compute the Wiener statistical deconvolution operator in practice one has to specify input values for the prediction lag, the filter length and the time gate for the computation of the filter. These processing parameters have to be acquired through running a number of tests and subsequent comparison of results. Finally the prediction lag was set to 16 ms and the filter length to 160 ms.

The convolutional model described above does not take into account the attenuation of higher frequencies as the source wavelet travels through the earth, thereby gradually but continuously changing the shape of the waveform. To take this effect into account the Wiener filter was calculated in two different time gates. The time gates were defined to contain a characteristic frequency content of the earth impulse response. Each time gate was 2 – 3 seconds long, the first time gate was centered at the sediments, whereas the second time gate contained the basement. Each deconvolution operator was applied 100% at the center of each time gate and then interpolated between the time gates. Through this gated Wiener deconvolution the change in waveform with increasing traveltimes is accounted for.

Velocity Analysis and NMO Correction

Reflections from a single point in the subsurface map along a hyperbolic travel time curve in a CMP gather. Before stacking a CMP gather a normal-move-out correction (NMO correction) has to be applied. The NMO correction transforms the travel time hyperbola into a horizontal line at the travel time of its apex. To achieve this the time difference Δt_{NMO} between the apex of the hyperbola and every point along the reflection hyperbola has to be calculated. Assuming a subsurface consisting of horizontal layers of constant velocity, Δt_{NMO} is described as a function of the root mean square velocity V_{rms} and the source-receiver offset x

$$\Delta t_{\text{NMO}} = \frac{x^2}{2 V_{\text{rms}}^2 t_0} \quad \text{where} \quad V_{\text{rms}}^2 = \frac{\sum_{i=1}^n V_i^2 \Delta t_i}{\sum_{i=1}^n \Delta t_i}$$

for n layers $i=1, \dots, n$. V_i is the velocity of each layer, Δt_i is the time the wave travels through layer i and t_0 is the time of the apex of the hyperbola.

However, as subbasement structures are generally not horizontally layered, reflections from these dipping structures do not align along a perfect hyperbola. The velocity which gives the best fit hyperbola to data which is not perfectly hyperbolic is the so called stacking velocity. These stacking velocities are determined in a velocity analysis. The velocity analysis consists of two sets of panels. In the first panel the NMO correction is applied on a single CMP gather for a range of velocities between 1500 – 7000 m/sec. In the second panel constant velocity stacks of 100 consecutive CMPs are calculated for the same CMP as in the first panel. For shallow reflections the velocities are best picked on the first panel showing individual NMO corrected CMPs as the normal moveout is most significant for shallow levels. Deeper reflections are picked on the constant velocity stacks where the horizontal continuity of events can be better controlled. Each reflection being picked is checked in the brute stack to avoid picking reflections originating from diffractions or multiples.

Stacking

The NMO correction is applied onto the CMP gathers; thus reflections align horizontally and the traces within each CMP gather are summed up or stacked. By stacking coherent reflections within a CMP gather interfere positively and thereby get amplified whereas incoherent reflections interfere negatively and thus are suppressed. Finally a stacked seismic section is achieved.

Divergence Correction

As the seismic signal propagates through the earth its amplitude is attenuated. First of all, due to radial spreading of the wavefront the energy of the expanding body wave per square unit decreases. Additionally, the increase of velocity with depth further attenuates the amplitude of the seismic wave. To correct for these effects a process has to be applied to correct for the attenuation of the amplitude of the seismic wave at late traveltimes. This process is called spherical divergence correction.

The seismic signal produced by an airgun can be considered as a point source which generates a spherical expanding body wave. Assuming the total energy density of the expanding wavefront remains constant (no energy loss e.g. through friction), it has to be inversely proportional to the square of the distance to the source r , to $1/r^2$. As the wave amplitude is proportional to the square root of the energy density, it turns out that as the wave front propagates, its amplitude decreases proportional to $1/r$.

The process outlined above holds true for a homogeneous medium. In case of a non-homogeneous medium (as the earth) the amplitude of the seismic wave is further attenuated. This attenuation caused by the increase of velocity with depth can be expressed as $1/V_{rms}^2 \cdot t$. Thus to compensate for this effect in a non-homogeneous medium, one has to scale the amplitudes proportional to $V_{rms}^2 \cdot t$. However, this is a first order approximation which does not take into account effects like focussing and defocussing, but nevertheless it presents a reasonable amplitude balancing approach of the zero-offset section prior to migration.

To achieve a geologically reasonable V_{rms} velocity model with depth, the stacking velocities are converted to interval velocities, laterally smoothed along the seismic line

and where necessary corrected to a geologically meaningful value.

Cascaded Time Migration

In the stacked seismic section events originating from a dipping reflector generally do not map onto their correct subsurface position. In general dipping events in a stacked seismic section show too shallow dips compared with their true subsurface dip. Therefore, a processing process is required which migrates dipping events of the stacked seismic section into their true subsurface position. This process is called migration. The ultimate goal of seismic migration is to make the stacked section appear similar to a geological cross section along a seismic line.

Here a finite-difference time migration in the x-t domain was used. A finite-difference migration is considered to be very robust and tolerates relatively large lateral and vertical velocity variations (Yilmaz 1987). In practice the time migration was carried out in a two step approach through a cascaded migration (Larner and Beasley 1987). A cascaded migration aims at improving the accuracy of mapping steeply dipping events. In the first step a water velocity migration is performed utilizing a finite difference algorithm in the frequency space domain (stolt migration). The velocity depth function is kept constant at 1500 m/s (water velocity) through the whole seismic section. This results in a sharp image of the seafloor, whereas the subseafloor structures are only partially migrated. However subseafloor dipping events are imaged a bit shallower and thus can be migrated into their true position with better accuracy in a following second migration step. Furthermore, side swipes resulting from out-of-plane reflections can now be identified and subsequently carefully weighted down. In the second step of the cascaded migration a residual migration of the already water velocity migrated section is carried out using the geological velocity model.

Time variant bandpass filter and AGC

Before plotting the obtained migrated sections a bandpass filter with a time variant frequency filter was applied as well as a automatic gain control (AGC). This so called post-processing is performed to enhance the quality of the final plots.

2.2 PRESTACK DEPTH MIGRATION

Pre-stack depth migration aims at obtaining a seismic section in depth (as opposed to travel time). As it corrects for the refraction and bending of rays at velocity interfaces and gradients it is a superior imaging technique as compared to conventional processing (post-stack time migration). Especially in complex geological settings, such as rifted margins, where tilted fault blocks of high-velocity crust juxtapose low-velocity sediments, these bending effects become particularly important and may degrade the image derived by conventional processing. A prestack depth migration can achieve a geometrically more correct and accurate image of the subsurface as a conventional time migration, even if followed by a time-to-depth conversion. As a byproduct to the depth migration a detailed velocity model is achieved. It is created iteratively down from the seafloor to deeper levels through depth-focussing analysis, which compares apparent and focussing depth of reflected and diffracted energy. Source and receivers are continued downwards to the depth of the reflector using a defined propagation velocity. If this defined propagation velocity is the correct velocity, the energy is perfectly focused when the operator reaches the reflector depth. If an incorrect propagation velocity was used, maximum focussing occurs either before or after the downward continuation operator reaches the reflector. Determining the difference between the depth focussing and the apparent depth of the reflector with the used velocity function allows the velocity error to be calculated and a new, correct velocity model may be defined. The velocity model is created iteratively from top to bottom of the section, determining the velocity in one layer at a time, because the velocity structure of the upper layers affects the accuracy of the velocity determination from deeper levels.

For the pre-stack depth migration the Kirpack module of the Sirius software was used. The pre-stack depth migration algorithm is based on a downward continuation of the wavefield in the source-receiver-frequency domain combined with an interactive focussing analysis to determine errors in the velocity model used for the migration. A detailed description of the pre-stack depth migration process can be found in Denelle et al. (1986) and Audebert and Diet (1990).

Downward movement of the source from $z=0$ to z_1 is performed by the phase shift operator, which reduces the travel time t to $t=z_1/V$ assuming a velocity V of the medium. This operator is applied in the frequency domain, in which a downward shift results in a phase shift. The focussing operator sums energy along diffraction trajectories resulting in partial focussing.

The effect of these operations on a reflection in the shot or receiver gather is shown in Fig. 2.2.1. Beginning at $z=0$, if the velocity V is correct, the more energy is focussed at zero offset the more z approaches z_R . Focussing is perfect at $z=z_R$. If the medium velocity is too high, the focussing operator focusses the energy at a shallower depth than the exact depth, whereas the phase shift operator moves reflections deeper than the actual depth. Thus the exact depth is between the focussing depth z_f and the migration depth z_m . Similarly, if the medium velocity V is too low, z_f is too deep and z_m is too shallow.

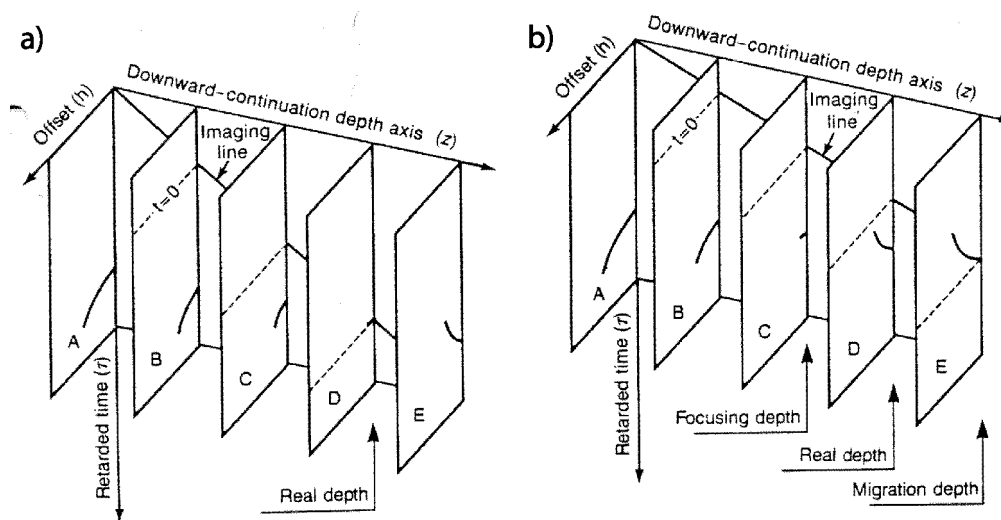


Fig. 2.2.1 : Schematic diagram illustrating the principle of depth focussing error analysis (reproduced from Denelle et al. 1986). **a)** maximum focussing occurs when downward continuation operator reaches actual depth of the reflector. **b)** In case an incorrect migration velocity is used, there is a discrepancy between the depth of maximum focussing and the depth of the reflector. By analysing this discrepancy and subsequent correction, the velocity model can be achieved.

2.3 FULL WAVEFORM INVERSION

One of the main objectives of the present study is to characterise the nature of the S reflector in detail. For this purpose a full waveform inversion was applied to a selected CMP gather to resolve its fine-scale velocity structure.

The waveform inversion aims at finding a seismic model of the subsurface such that the sample-by-sample misfit in the frequency-slowness domain between synthetic and observed seismograms is minimised. As the misfit function is highly nonlinear, which means that it contains numerous local optima and thus requires a Monte Carlo random search to confirm that a global minimum is found. Since this approach is quite time consuming, the inversion strategy consists of the following two steps:

- 1.) the construction of a reliable background velocity model to represent the long wavelength global minimum.
- 2.) A local search to estimate the short wavelength variations.

Fig. 2.3.1 gives an overview of the inversion process applied in this study. The local search implies a generalized least squares inversion method, based on the estimation of velocities by minimising the misfit in the frequency-slowness domain. The inversion method is a one-dimensional, isotropic, full waveform inversion. It is based around the conjugate gradient optimisation scheme (Kormendi and Dietrich 1991) to minimise the misfit, and the generalized reflection and transmission matrix method of Kennett and Kerry (1979) to calculate the reflectivity of the subsurface. Convolution with the source wavelet yields the synthetic seismograms. The generalized reflection and transmission matrix method accurately treats multiples and mode conversions in the medium, and thus includes all nonlinear effects.

The misfit function $S(\mathbf{m})$ is calculated in a least squares sense between synthetic data, \mathbf{d} , and the real data, \mathbf{d}_{obs} . The misfit function $S(\mathbf{m})$ is defined as :

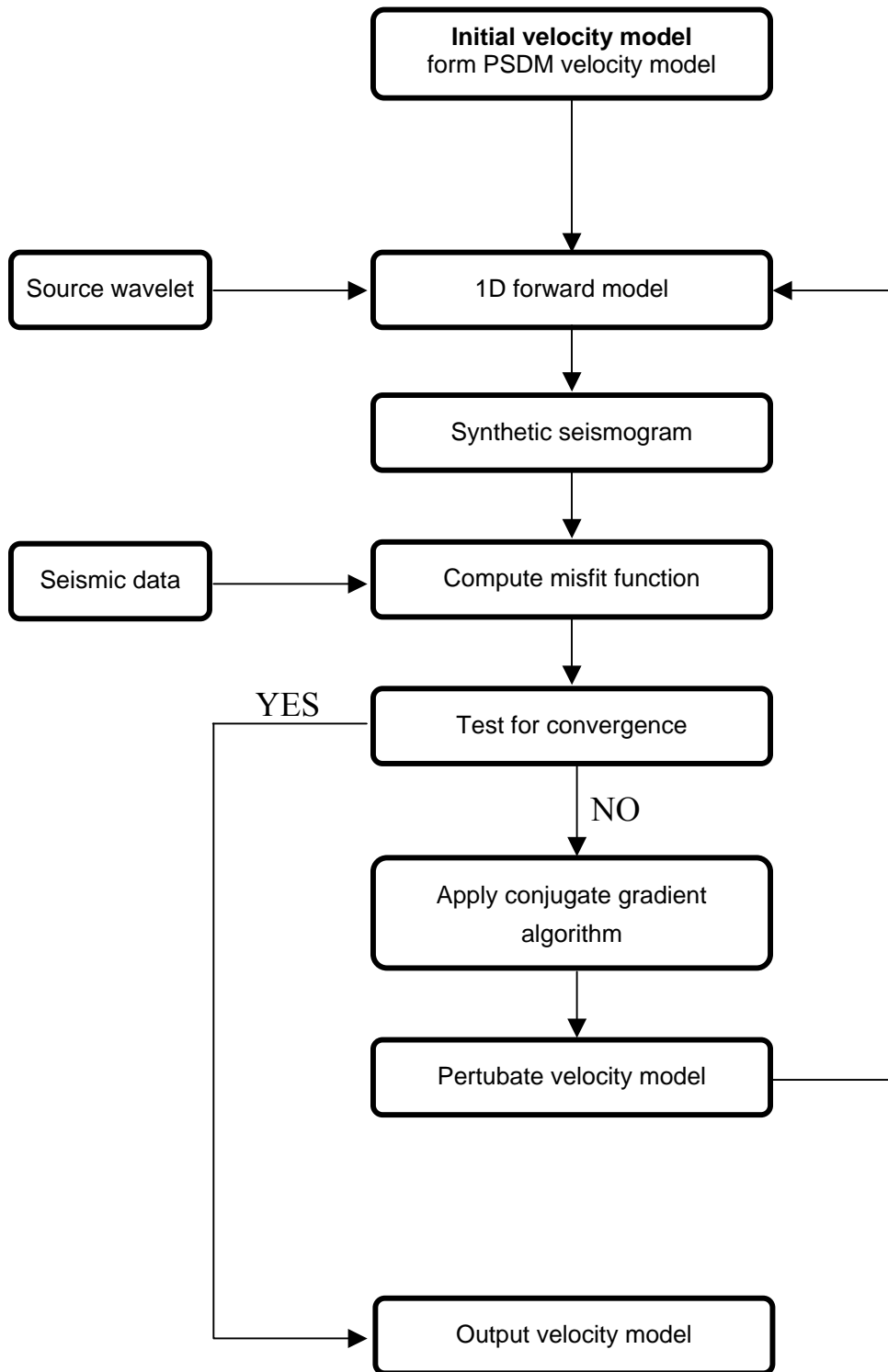


Fig. 2.3.1 : Schematic flowchart of the seismic full waveform inversion applied in this study.

$$S(\mathbf{m}) = \frac{1}{2} \left(\|\mathbf{d}_{\text{cal}}(p, \omega) - \mathbf{d}_{\text{obs}}(p, \omega)\|_D^2 + \|\mathbf{m} - \mathbf{m}_0\|_M^2 \right)$$

where $\mathbf{d}_{\text{cal}}(p, \omega) = \mathbf{f}(\mathbf{m})$ is the calculated wavefield, \mathbf{f} is the forward modeling operator, \mathbf{m}_0 is the initial starting model. The vector \mathbf{m} contains the properties of the discrete stratified medium, P- and S-wave velocity (Vp and Vs), density (ρ), and quality factors Qp and Qs for P- and S-waves respectively. The norms $\|\dots\|_D$ and $\|\dots\|_M$ are the weighted L_2 norms defined as

$$\|\mathbf{d}\|_D^2 = \mathbf{d}^{*T} C_D^{-1} \mathbf{d} \quad \text{and} \quad \|\mathbf{m}\|_M^2 = \mathbf{m}^T C_M^{-1} \mathbf{m} ,$$

where C_D is the data covariance matrix, C_M is the a priori model covariance matrix, the superscript T denotes the transpose of the matrix and * denotes the complex conjugate. The data and model covariance matrices used were $0.025 \mathbf{I}$ and \mathbf{I} , respectively, where \mathbf{I} is the identity matrix. The misfit function $S(\mathbf{m})$ between the real data \mathbf{d}_{obs} and the synthetic data \mathbf{d}_{cal} is computed and the model is optimised and updated starting from

an initial model \mathbf{m}_0 by varying Vp using the conjugate gradient technique as described by Kormendi and Dietrich (1991). Gradient inversion methods determine direction and step length for a model update based on the gradient of the misfit function. The convergence of the algorithm depends on the initial starting model \mathbf{m}_0 , so a good estimate of \mathbf{m}_0 is necessary for the inversion. These methods have been implemented in the FORTRAN program inv1d. Further details and examples concerning this code are given in Kormendi and Dietrich (1991) and Dietrich and Kormendi (1990).

Data pre-processing

Thorough preparation of the data set prior to $\tau - p$ transformation is essential to obtain adequate inversion results. Correction of spherical divergence has been applied using the estimate of a background velocity model. To avoid spatial aliasing in the data, it is necessary to have trace interval dx of $dx < v/(2f_{\text{max}})$. Hence the Nyquist ray parameter is $P_n = \frac{1}{2} (f_{\text{max}} * dx)$. To obtain the full frequency range, four CMP gathers were merged to form a Super CMP gather with an trace interval of 25 m. Missing traces were interpolated and minimum offset traces were extrapolated.

Source wavelet

An important factor in all waveform inversions is the estimation of the source wavelet. As seismograms are convolution of the source wavelet with the reflectivity series, errors in the source wavelet will directly account for errors in the final model. Ideally one would directly measure the far-field response of the airgun array. This could be achieved by an OBH tethered several hundred meters above the sea floor thus recording the airgun source signature including its full bubble train. As this was not done in this experiment, the source wavelet was extracted from the MCS data.

By deconvolving the seafloor multiple reflection with the seafloor primary the reflectivity response of the seafloor is obtained. Designing an inverse filter of the reflectivity and convolving it with the seafloor primary the source wavelet is obtained.

$$\text{Seabed} = S * R * F \quad ; \quad \text{Multiple} = - S * R * F * R$$

Where S is the source function, F is the instrument response, R is the seabed reflectivity and the star denotes the convolution operator.

Initial starting model

A good estimate of the large-scale P-wave velocity model describing the general background velocity trend is essential to ensure that the inversion for short-wavelength variations is started near the global minimum of the misfit function, or otherwise the inversion algorithm might get “trapped” in a local minimum. Various methods have been presented to determine an optimum long-wavelength background velocity model serving as the starting model in the inversion scheme. Singh and Minshull (1994) presented a two step method. First RMS velocities were estimated by maximizing the energy within a time window centered on individual reflectors along ellipses in the $\tau - p$ domain. In the second step, interval velocities for the observed reflections were searched simultaneously by maximizing the total energy of all trajectories. On the other hand Korenaga et al. (1997) used a traveltimes inversion to establish a long-wavelength background velocity model. However for this study the velocity information established

within the prestack depth migration by densely sampled focussing error analysis was used to construct the long-wavelength velocity model serving as initial model for the inversion. P-wave velocity values were taken from the prestack depth migration velocity model. The remaining parameters to establish the viscoelastic starting model of the subsurface are shear-wave velocity (V_s), the density (ρ) and the quality factors Q_p and Q_s characterizing the p-wave and s-wave attenuation respectively. These parameters are calculated from the p-wave velocity function using empirical relationships for V_s (Castagna et al. 1985) and density (Hamilton 1978). Effective quality factors of $Q_p=200$ and $Q_s=25$ are implemented for sediments (Hamilton 1972) and within the crust are set $Q_p=400$ and $Q_s=100$. During the inversion, V_s , density, Q_p and Q_s are kept constant, while only V_p is varied. However, by the velocity analysis performed within the prestack depth migration scheme, no conclusive velocities below the S-reflector could be obtained. This is mainly due to the lack of clear reflections recorded in the CMP gathers below the S-reflector. Thus there remains a lack of information about the sub-S velocities derived by the focussing error velocity analysis. However, Zelt et al. (2003) derived a velocity-depth model of the deep Galicia margin on the basis of a refraction and reflection tomography. In their velocity-depth model (Fig. 2.3.2) they show a sub-S velocity of 7.0 km/s. Thus for the starting model of the full waveform inversion a sub-S velocity of 7.0 was assumed.

Plane wave decomposition

The forward modeling algorithm and calculation of the misfit during the inversion is performed in the delay time – slowness domain. The plane – wave decomposition of a point – source seismogram obtained from horizontally stratified medium allows the separation of wave energy by angle of incidence. This enables a more rapid modeling, since it is faster to compute synthetic seismograms in the $\tau - p$ domain than in the $t - x$ domain (Singh et al. 1989). Transformation of the Super-CMP gather is performed utilizing the routine `segy_ftaup`. In the time domain, this program applies a slowness dependent aliasing removal proposed by Singh et al. (1989). A spatial damping filter is adopted to taper traces at large and small offsets to suppress artifacts. Next the data is transformed into the frequency domain, where a radon transformation of the data into

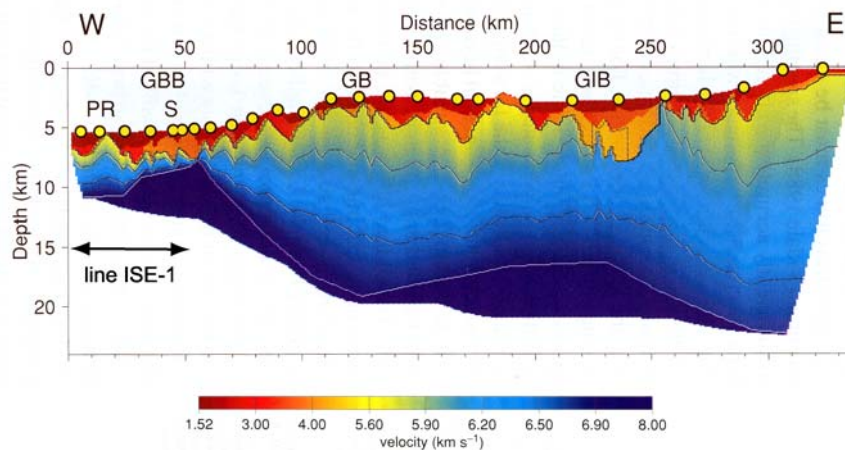


Fig. 2.3.2 : Velocity-depth model of the Galicia margin derived by Zelt et al. (2003) based on a refraction and reflection tomography. The most western part of this model is imaged by the multi-channel seismic line ISE-1 shown in Figs. 4.1.1 and 4.2.1. On the basis this model, a sub-S velocity of 7.0 km/s was assumed for the starting model of the full waveform inversion.

the frequency slowness domain is performed. Finally, the data is transformed back into delay time – slowness domain using the inverse Fourier transformation

Inversion

The starting model, the source wavelet and the Super-CMP gather are used as input for the full waveform inversion. All parameters except the p-wave velocity are kept constant in the inversion. The underlying assumption is that the observed S reflector can be related to significant changes in V_p , while ρ and V_s show little change. A strategy of progressive increase in bandwidth and slowness range during inversion as illustrated by Minshull et al. (1989) and Minshull and Singh (1993) is adopted for this data set. The inversion is performed in 5 runs of 15 iterations each progressively including higher frequencies. The final result from each run serves as the starting model of the next run. Finally, inversion is performed for the full slowness range and basic starting models to analyze uniqueness of determined results.

To analyse the nature of S and to test various geological models for S, the resulting final model is changed. At the depth of S a low velocity zone is inserted into the velocity model and then the inversion is rerun. The synthetic data resulting from this refined test model is then compared to the synthetic data of the original model and statistically checked to see if the fit in waveform is improved.

3.0 INTERPRETATION OF THE MCS DATA OF LINE ISE-2

The 80 km long seismic line ISE-2 is much longer and shows a greater variety of structural features as compared to the portion of line ISE-1 processed. Therefore, the results of processing of MCS-data of line ISE-2 are discussed here first. It represents the southernmost seismic section of that part of the Galicia margin which was studied geophysically in most detail (Fig. 1.2.2). It can extend our knowledge with respect to the effects of crustal stretching and especially with respect to an improved characterisation of the S-reflector and a better understanding of its origin and nature. As will be shown below several observations about hitherto little or not recognized structural features can be made from the depth migrated version of line ISE-2. In contrast to the portion of the GP seismic sections prestack migrated by Reston et al. (1996), line ISE-2 crosses the peridotite ridge.

3.1 POSTSTACK TIME MIGRATION

In the time migrated section of line ISE-2 several prominent structural features are clearly imaged. Four landward tilted crustal fault blocks labelled A to D in Fig. 3.1.1 are bounded westwards by normal faults F1 to F4. The peridotite ridge with clearly imaged slopes rises well above the sea floor. Underlying these rotated fault blocks S can be traced from about CMP 5000 to CMP 3000 as a bright reflector. The subseafloor consists of horizontally layered deep sea sediments, whereby the base of these undeformed postrift sediment sequence is well expressed seismically. However, the prerift and synrift sediments are in this time migrated section only poorly imaged with the exception of the distance between CMP 4000 and CMP 2900. Conformably overlying crustal fault block B a pile of prerift and synrift sediments is here observed, showing several internal reflections (Fig. 3.1.1). Near the center of the half graben between fault blocks B and C a wedge-shaped westward dipping body can be recognised. Its frontal portion directly overlies the S-reflector.

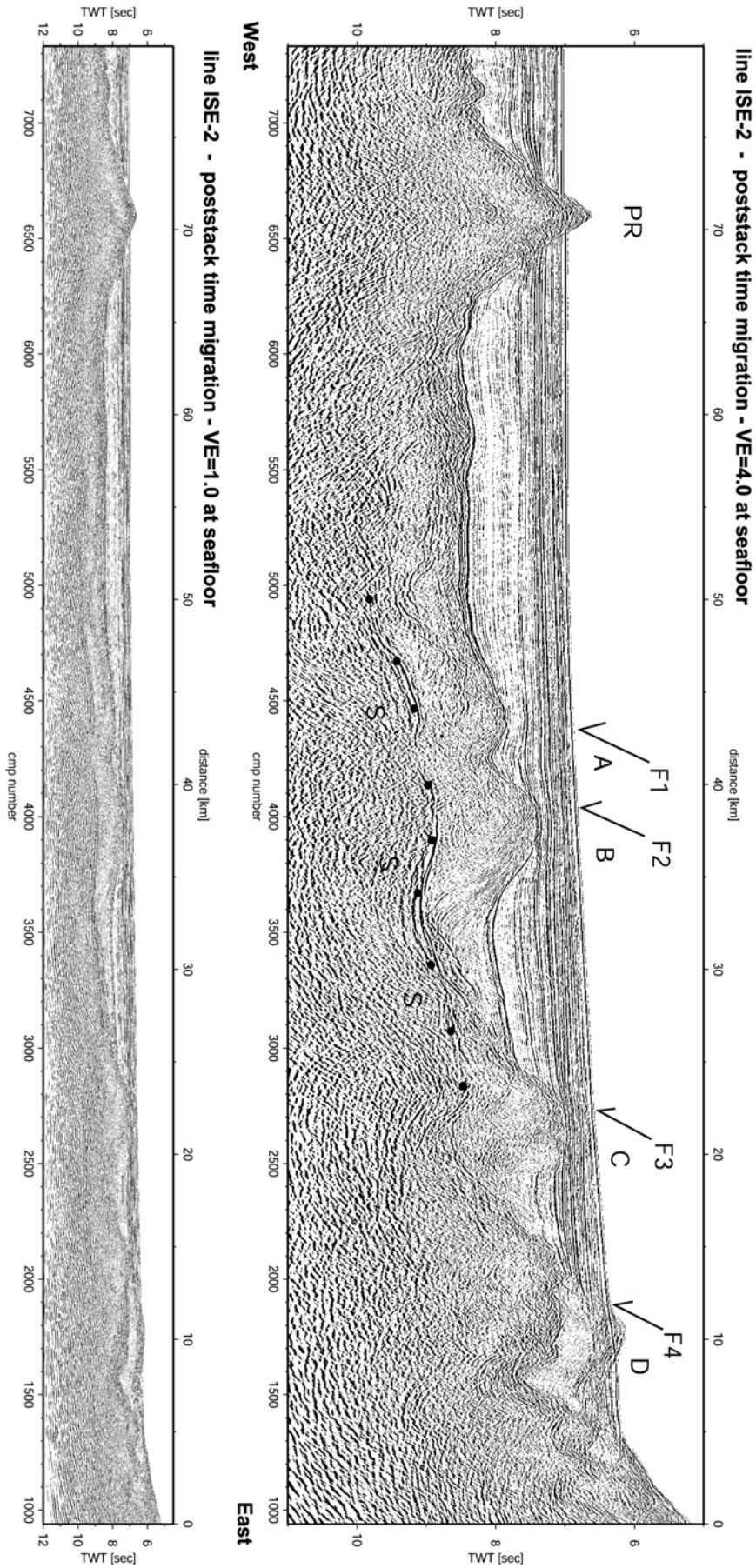


Fig. 3.1.1 : Poststack time migrated image of seismic line ISE-2. Vertical exaggeration at seafloor is 4.0 and 1.0 (above and below respectively). As subsurface velocities are increasing, vertical exaggeration is decreasing for later travel times.

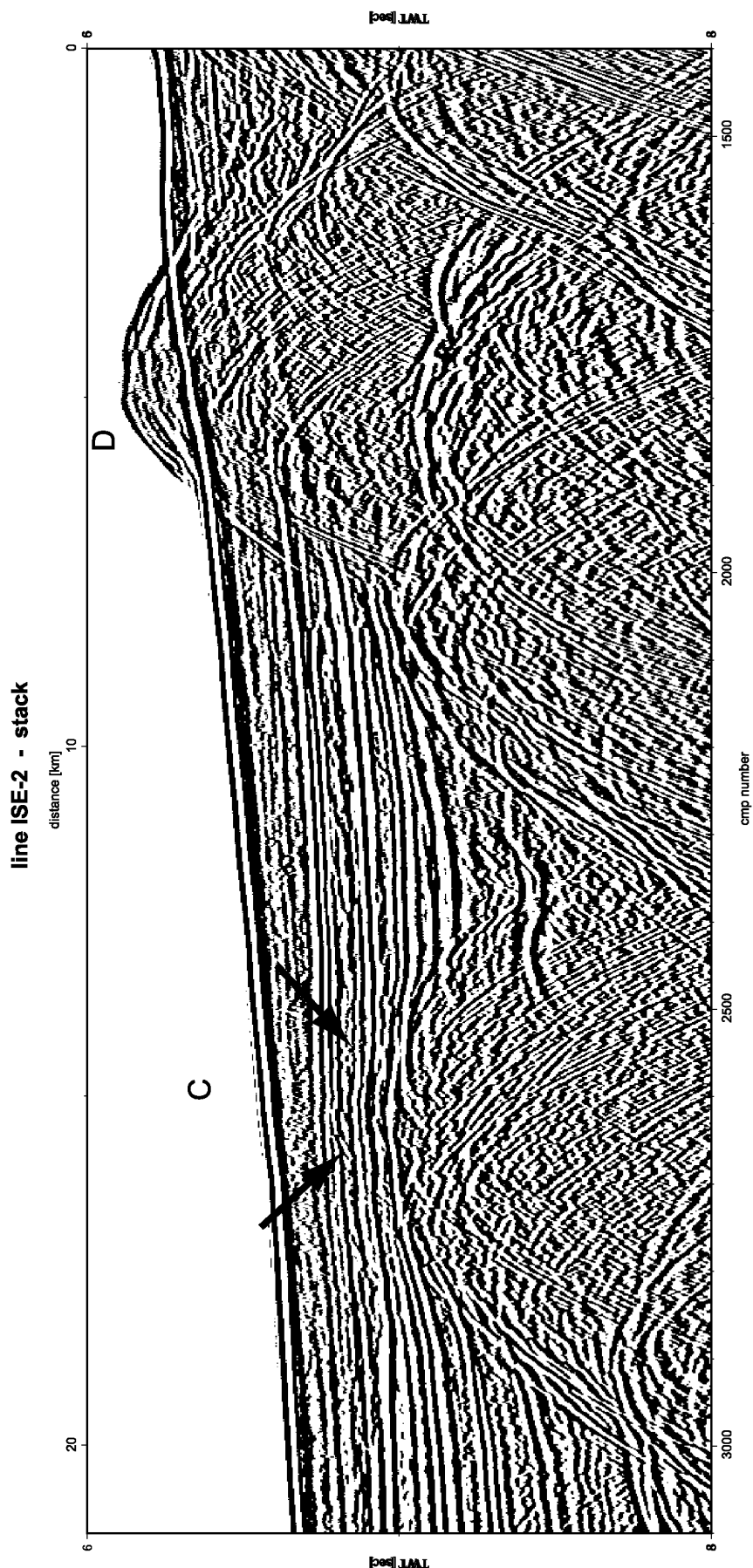


Fig. 3.1.2 : Detail of stack image of line ISE-2 showing the upper part of fault block C and D. Note that fault block D is located slightly offshore from this seismic line, i.e. seismic signals from the slope of fault block D are obliquely reflected into the position of this line, while the sea floor reflection is crosscutting the top of fault block D. The apparently flat top of fault block C can be attributed to a similar constellation. A weak diffraction hyperbola, originating from the offshore topmost part of fault block C, can be seen through the horizontally layered sediment strata (arrows).

These and additional structural features are imaged more clearly and in a geometrically more accurate relationship in the depth migrated section of this line. Therefore, a more detailed discussion of these observations is given in section 3.2. However, another striking observation should be mentioned here. Between about CMP 4200 and CMP 4300 the S-reflector appears to be discontinuous. Similar observations have been made before and convincingly interpreted as artefacts. Reston et al. (1996) pointed out that in such cases not the S-reflector itself is discontinuous rather than its reflection due to the focussing and defocussing effects of a structurally complex overburden and the resulting variable signal-to-noise levels.

Fig. 3.1.2 shows a portion of the time-migrated line ISE-2 in more detail. Between about CMP 1650 and CMP 1900 the strong sea floor reflection runs across the seismic image of the crustal fault block D. This observation indicates that fault block D is not directly traversed by line ISE-2. Instead this fault block is located slightly offline. Seismic signals from the slopes of fault block D are obliquely reflected into the position of line ISE-2.

3.2 PRESTACK DEPTH MIGRATION

Line ISE-2 shows a number of remarkable structural configurations which are clearly imaged in the prestack depth migration cross section (Fig. 3.2.1). The overall structural picture can be seen from the cross section showing the results of the velocity distribution model (Fig. 3.2.2). The continental crust appears to be thinned by stretching to an even higher degree as compared to the area crossed by line 1 and the GP-lines further north (Reston et al. 1996). Crustal thicknesses vary between about 3.2 and 1.5 km over most of the distance between CMP 5000 and the eastern edge of this line. The effect of an extreme degree of stretching is observed between CMP 3700 and CMP 3300 where the mantle is directly overlain by sediments indicating a complete basement separation between adjacent fault blocks. Fault blocks A and B have apparently moved westwards along the detachment as an isolated body of continental crust, whereas fault blocks C and D remained in contact with the continental crust to the east. Therefore, the S-reflector can indeed be classified here as a true detachment as

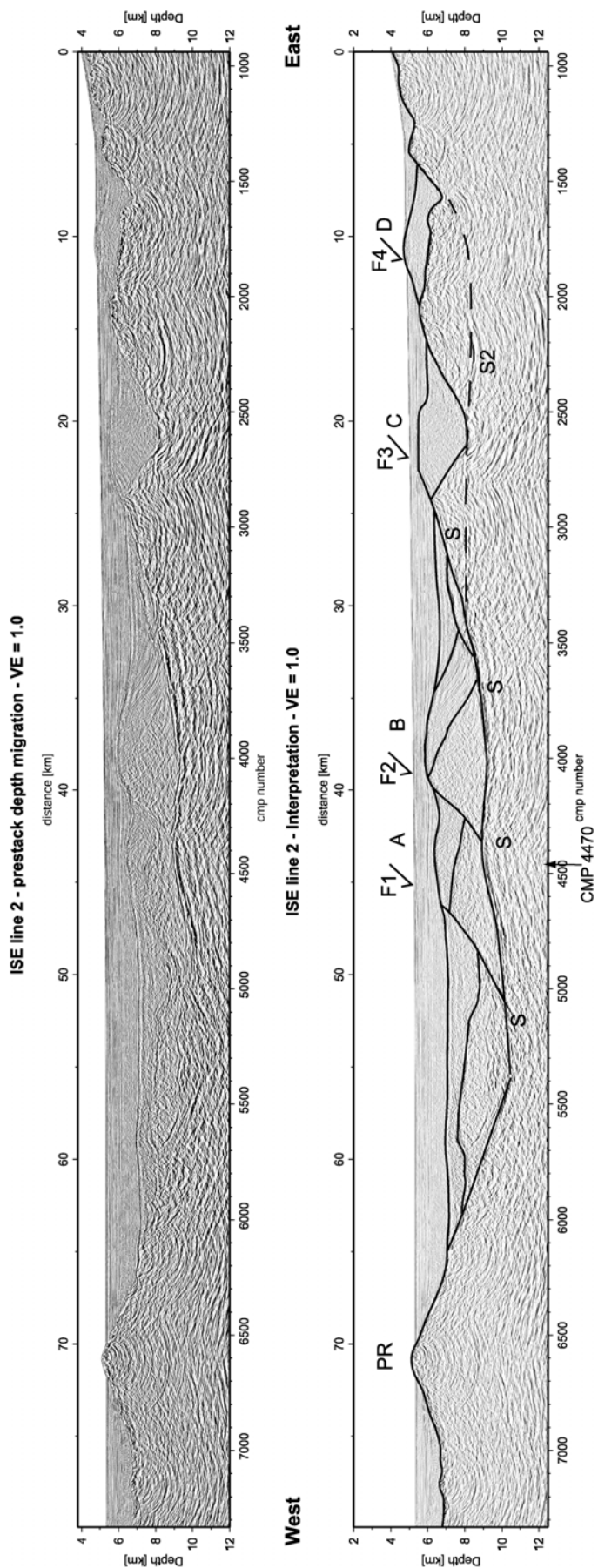


Fig. 3.2.1 : Prestack depth migrated image of line ISE-2, vertical exaggeration is 1.0. Note position of CMP 4470, which was used for full waveform inversion.

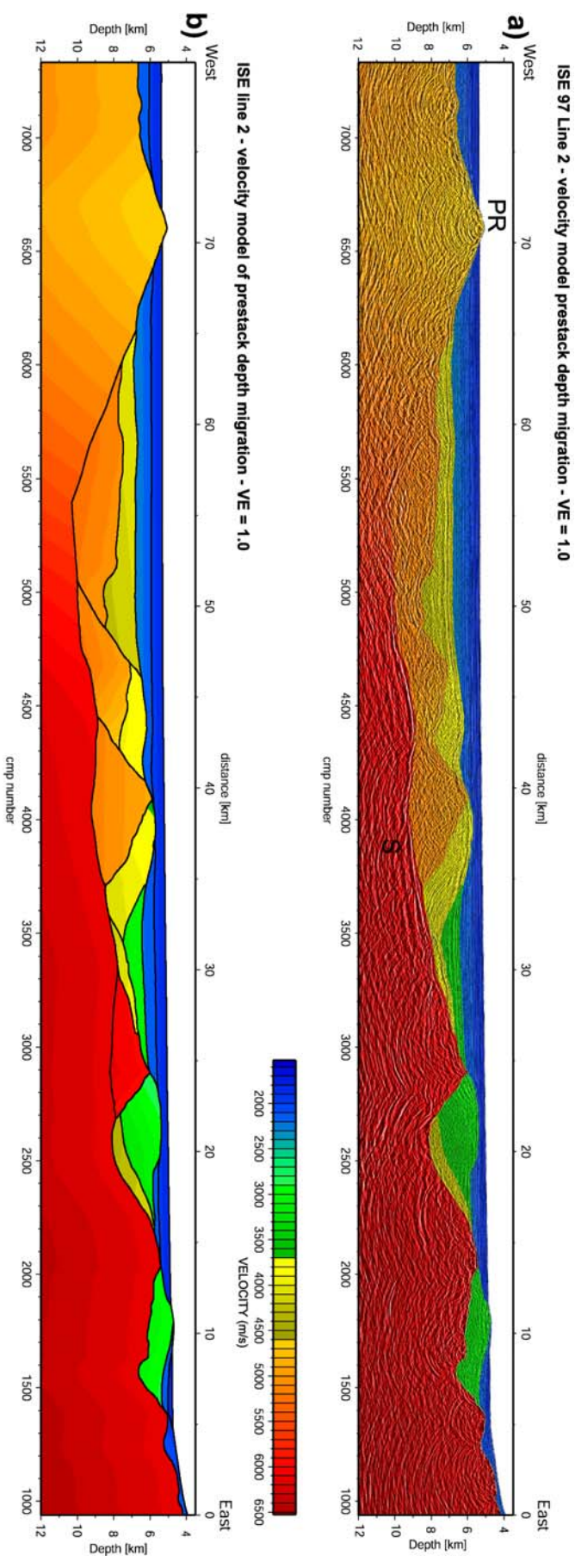


Fig. 3.2.2 : Velocity model of prestack depth migration of line ISE-2 in true scale. (a) Velocity model overlain on seismic image. (b) Velocity model including velocity domains derived in prestack depth migration. Velocities deep in section below S and peridotite ridge (PR) are poorly constrained.

defined by Pérez-Gussinyé et al. (2001), i.e. “a low-angle surface onto which other structures detach”. In accordance with these authors the area to the west of fault block A in line 2 is classified as the continent-ocean-transition zone (COT). An even more isolated and further transported block of continental crust has been observed further south where the continent-ocean transition zone is wider in a cross section connecting sites 1070, 1069 and 1065 of ODP leg 173 (Whitmarsh et al. 1998).

In this context it appears interesting to note that there is in line ISE-2 a significant but irregular variation of dips of the block bounding normal faults. The shallowest dip with an angle of 20° has the fault which is bounding block C (named F3 in Fig. 3.2.3). This fault appears to continue in a listric fashion directly into the S-reflector, i.e. the breakaway point appears to be located near CMP 2900. A similar, yet not that well developed structural configuration is observed between CMP 1850 and CMP 2050 in line GP-102 (Reston et al. 1996, Fig. 10) which is located about six km to the north. Whereas separation of the frontal fault blocks from the continental crust to the east has barely been initiated there, separation has significantly progressed in the area of line ISE-2. This observation is interpreted to reflect a somewhat higher degree of stretching here as compared to the areas further north along the Galicia margin. This regional difference in degree of stretching observed from comparison of seismic lines 2 and GP-102 may also be reflected by the offset of the peridotite ridge near 42°N (Beslier et al. 1993). The other block bounding faults imaged in line ISE-2 have dip angles varying between 28° and 40° (F4 and F2 respectively in cross section shown in Fig 3.2.3). Faults F1 and F2 terminate abruptly on contact with the S-reflector.

The S-reflector is in line ISE-2 clearly imaged between CMP 4900 and CMP 3400 as a west dipping reflection. Around CMP 3400 it is about 8 km deep, whereas 20 km to the west at CMP 4900 it has reached a depth of 10 km (Fig. 3.2.1). A remarkable feature concerns the observation that the S-reflector appears to be in direct contact with the eastern slope of the peridotite ridge near CMP 5400 (Fig. 3.2.4). This was not seen in the GP-lines to the north (Reston et al. 1996). However, the reflection from S between CMP 5400 and CMP 4900 is considerably weaker than east of CMP 4900. In the interpretation of line GP-12 the contact between the eastern flank of the peridotite ridge

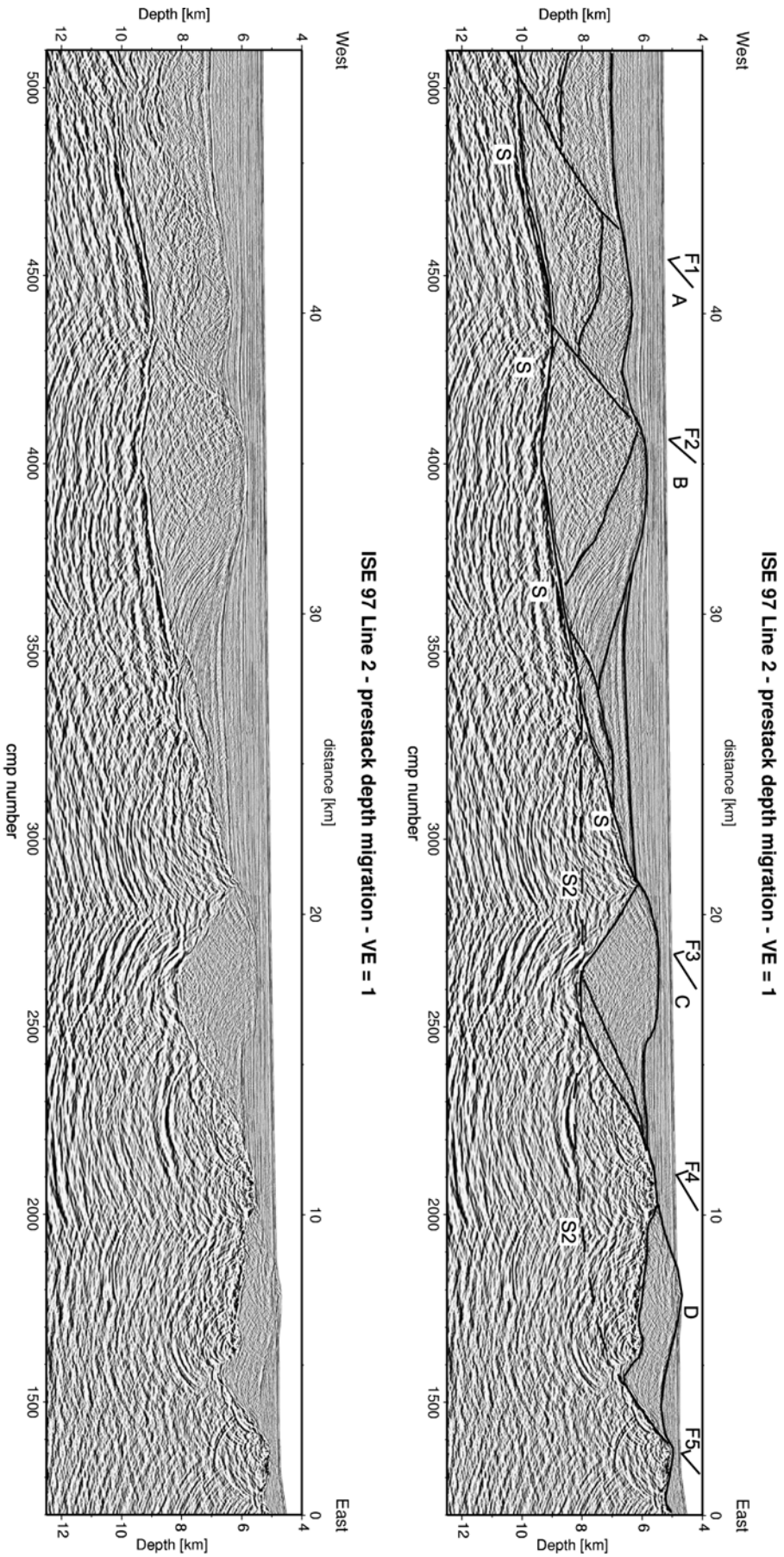


Fig. 3.2.3 : Detail of western part of prestack depth migrated image of line ISE-2. Vertical exaggeration is 1.0 .

and the S-reflector remained unclear (Pérez-Gussinyé et al. 2001, Fig. 3). The broad half graben in front of F1 is occupied to a large extent by a body which probably represents a crustal fault block. It was back tilted and highly tectonized due to the rise of the peridotite ridge. Although its general shape is reasonably well imaged, no clear internal structures can be interpreted. The peridotite ridge forms at the sea floor a 2 km wide elevation the summit of which rises about 250 m above the surrounding sea floor. No sediments can be seen on top of the summit of the peridotite ridge. A regional trend to much lower p-wave velocities towards the summit of the peridotite ridge (Fig. 3.2.2) is interpreted to result from increasing degrees of serpentinization as the mantle peridotite gets closer and closer to the sea floor. Between CMP 4800 and CMP 4000 the S-reflector shows a modest undulation. The eastward continuation of the S-reflector beyond CMP 3400 appears unclear. As discussed above the interpretation is favored here that S grades into the normal fault F3 (Fig. 3.2.3). Eastwards of CMP 3400 S is split into a second reflection labeled S2 in Fig. 3.2.1 and 3.2.3, which is, however, not as clearly imaged as the uprising branch. An alternative interpretation of the structural situation to the east of CMP 3400 would be that S does not, as discussed above, grade into F3. Instead the eastward continuation of S would be S2. This would imply that the breakaway point would be located further east around CMP 1400. Another observation concerning the shape of the S-reflector concerns a slight undulation between CMP 4000 and CMP 4900 (Fig. 3.2.1).

Another interesting structural configuration not seen in the GP-lines is imaged directly above S between CMP 3500 and CMP 3100 (Fig. 3.2.3). This lenticular shaped body is interpreted as a clastic wedge which may have been deposited on the western slope of the fault block C. This may have resulted from oversteepening of the slope at an earlier stage of stretching when the normal fault F3 was dipping at a much higher angle. Alternatively, this wedge may represent a fault sliver. There is a weak indication that prerift and synrift sedimentary strata on top of fault block B are onlapping onto the western contact of this presumed clastic wedge. Perhaps there is another clastic wedge in front of fault F4 as shown in Fig. 3.2.3. However, this observation is less clear. A similar wedge-shape body has been

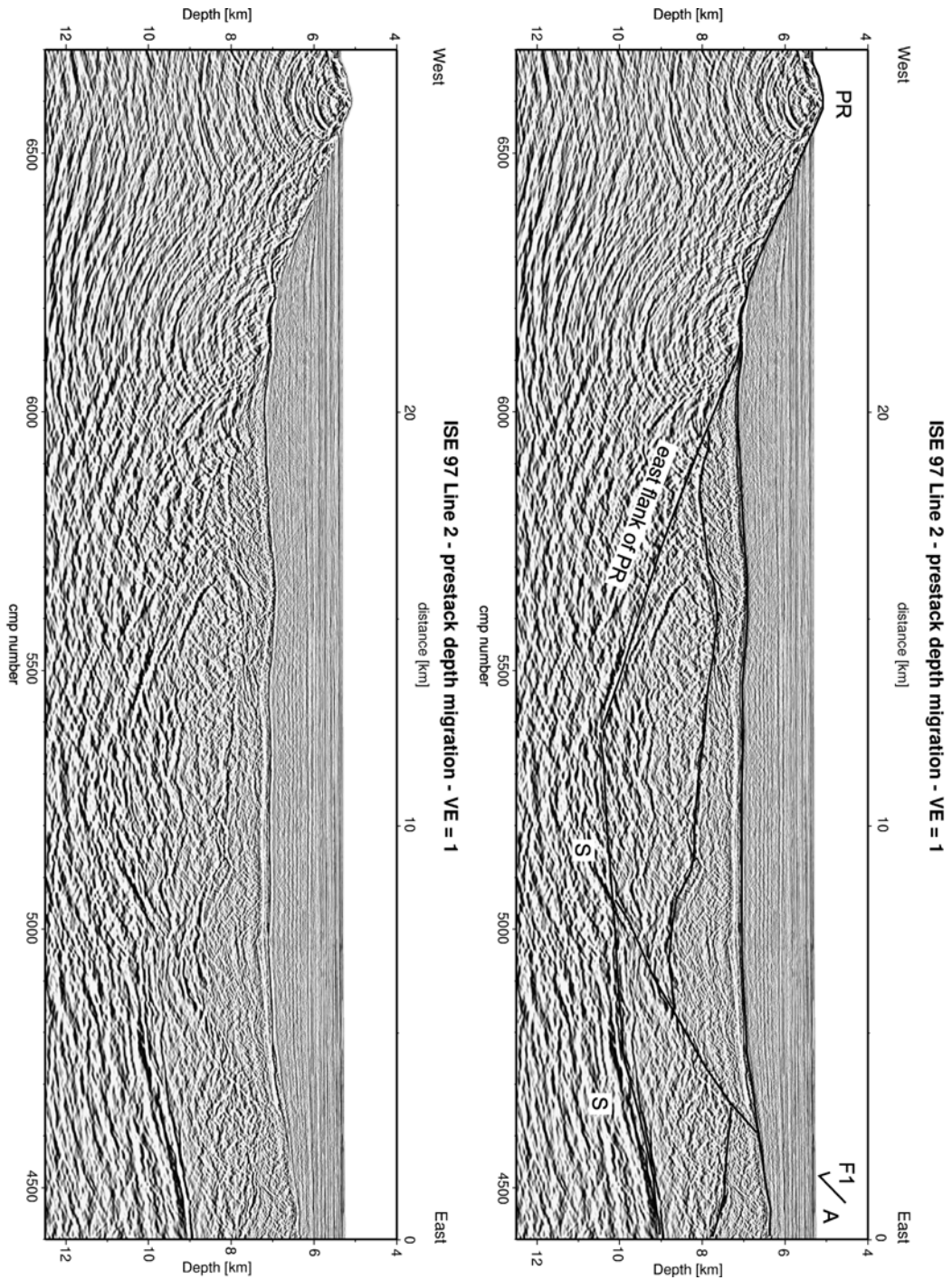


Fig. 3.2.4 : Detail of prestack depth migrated image of line ISE-2 shown in vertical exaggeration of 1.0 .

documented by Mauffret and Montardet (1987) in line GP-12 and interpreted similarly as a result of large scale erosion.

P-wave velocities of the continental crust fault blocks consisting of granodiorite basement (Boillot and Winterer 1988) appear to decrease from east to west (Fig. 3.2.2), i.e. from block C to block A (about 5.3 to 4.7 km/s respectively). This may perhaps be

caused by the fact that fault blocks A and B have, as discussed above, been dissected completely from the remaining continental crust and slid a certain distance along the detachment, whereas block C has just rotated. It is possible that the continental crust of fault blocks A and B have, therefore, experienced more dilatational stress resulting in a higher degree of fracturing. A similar observation applies to the back-tilted fault block in front of block A.

The conclusions by Reston et al. (1996) for the GP-lines with respect to the interpretation of the sedimentary sequence covering the tilted continental crustal fault blocks can be confirmed for line ISE-2. The prerift and synrift I - sequence has p-wave velocities ranging from 3.4 to 4.0 km/s (Fig. 3.2.2). It has been shown to consist of Tithonian-age shallow-water platform carbonates overlain by Early Cretaceous clastic sediments deposited during the early rifting phase (Boillot and Winterer 1988, Moullade et al. 1988, Mauffret and Montadert 1987). These synrift I strata are tilted in the same way as the underlying crustal fault blocks. During another phase of extension, the synrift II sequence sediments were deposited. They show a clear trend of increasing thickness towards the axial center of the half grabens between the rotated fault blocks, as imaged in line 2 e.g. between CMP 3700 and CMP 2900 (Fig 3.2.3). Like the underlying sediments the synrift II sequence has been sampled by ODP drill sites and documented to consist of Barremian to Aptian clastics (Mauffret and Montadert 1987, Boillot and Winterer 1988). The postrift sediments imaged in line 2 as a blanket of two layers with p-wave velocities varying between 1.8 and 2.3 km/s (Fig. 3.2.2) can in accordance with Mauffret and Montadert (1987) be interpreted to range in age from Santonian to Eocene and Miocene to recent respectively. The seismic stratigraphy and the implication with respect to the temporal evolution of stretching has been well documented for the GP-lines by Mauffret and Montadert (1987). One particular observation is of interest. Mauffret and Montadert (1987) have recognized a sedimentary unit which is seismically transparent, i.e. their Formation 3. They have interpreted this seismic transparent facies to consist of Albian black shales. A thin layer of similar seismic appearance is seen in line 2 just as the uppermost part of the synrift II sequence between about CMP 5700 and CMP 4700 (Fig. 3.2.4) and less clearly between CMP 3600 and CMP 3000 (Fig. 3.2.3). This layer could perhaps be interpreted as the Albian black shales.

3.3 FULL WAVEFORM INVERSION

To reveal the detailed internal structure of the S reflector a full waveform inversion study was conducted. For this purpose CMP gathers 4470-4473 were merged together to form a super-cmp gather (Fig. 3.3.1). By forming a super-cmp gather the trace-to-trace distance is decreased to 25 m, thus reducing aliasing effects during delay time slowness transformation (Fig 3.3.1). This super-cmp gather will be simply referred to as CMP 4470 from now on. At this location S shows the best signal-to-noise ratio within all CMP gathers. The inversion strategy consists of mainly two steps – a traveltime inversion and a waveform inversion. The full waveform inversion is an optimisation process, with the objective to minimize the misfit between synthetic and observed seismic data in a sample-by-sample comparison.

The source wavelet for the inversion was derived from the seabed reflection and its first multiple (Fig. 3.3.2), assuming that the seabed wavelet is the convolution of the source wavelet and the reflectivity series, and that the multiple results from a polarity reversal and from a second convolution with the seabed reflectivity series (Minshull et al, 1994). The source wavelet was scaled to a peak-to-peak amplitude of 1.0. The velocity and density of the sediments immediately beneath the sea floor are adjusted in the way to produce a reflection coefficient of 0.22.

The data and source wavelet were then Fourier transformed into the frequency-slowness domain. The waveform inversion consists of five runs with increasing ranges of frequency and slownesses. During each run, 15 iterations were performed. This approach contrasts with gradient-based inversions that converge to a local minimum of the misfit function in that it accounts for longer wavelength changes in the velocity/depth function before determining the finer details of the velocity structure. The final model of each run was used as the starting model of the next run. The last few iterations of the fifth run with slowness range up to 0.25 s/m and a broad frequency range of 5-55 Hz resulted in very little change of the misfit function (0,45%), indicating convergence to a minimum value. Only the p-wave velocity was inverted within each

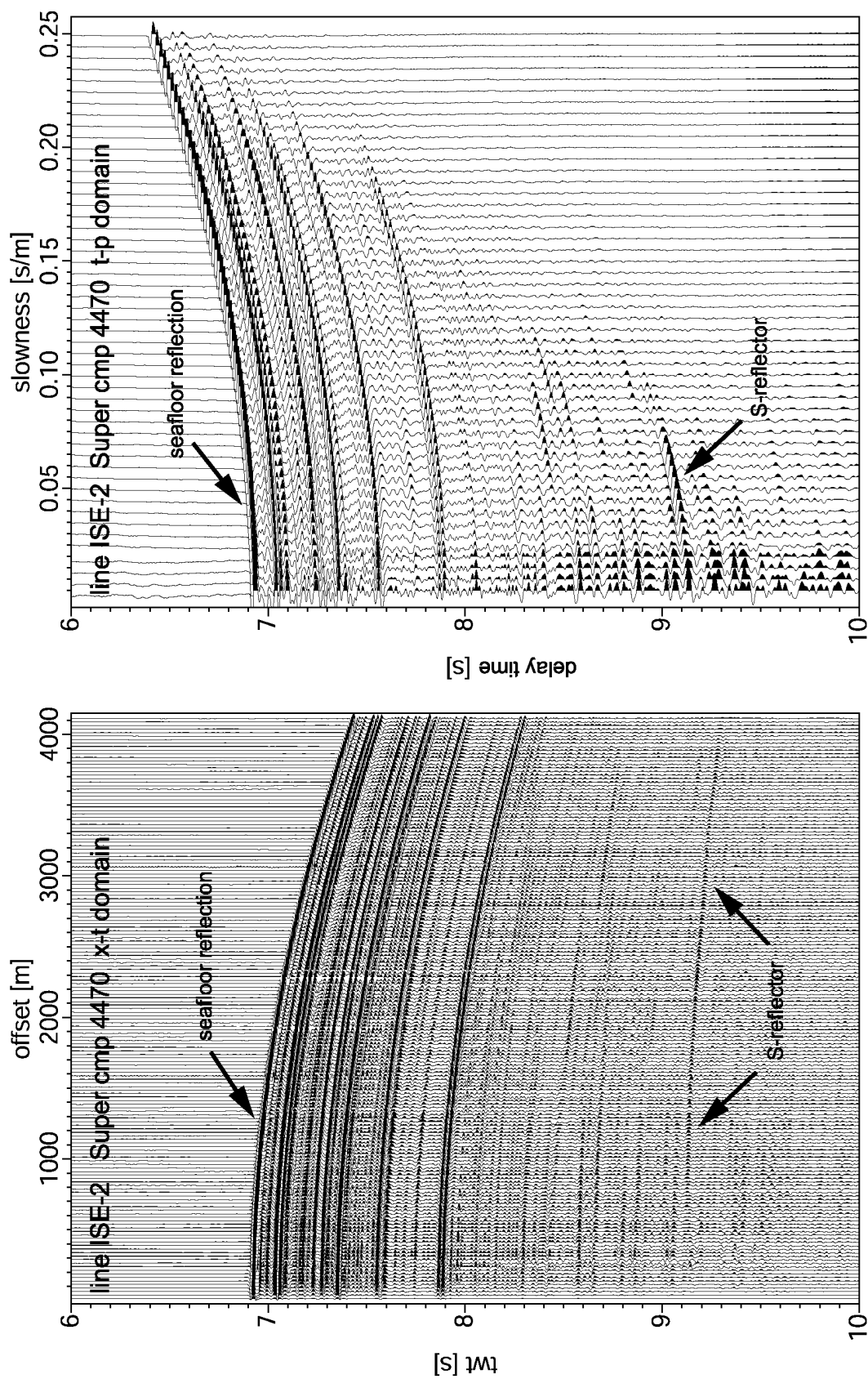


Fig. 3.3.1 : a) Super CMP gather 4470, merged together from 4 neighbouring CMP gathers. At a traveltime of 9,1 seconds the positive polarity, bright S-reflector can be seen. b) Super CMP gather 4470 transformed into the delay time - slowness domain.

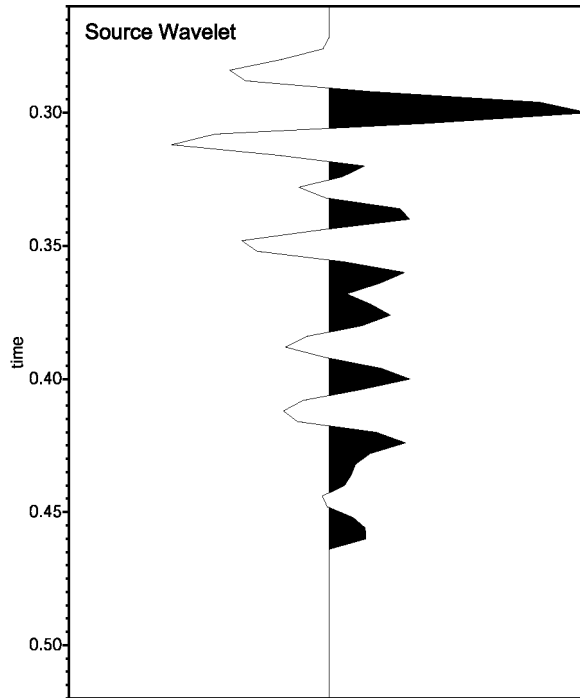


Fig. 3.3.2 : Source wavelet used in the inversion scheme, derived from the seabed reflection and its multiple.

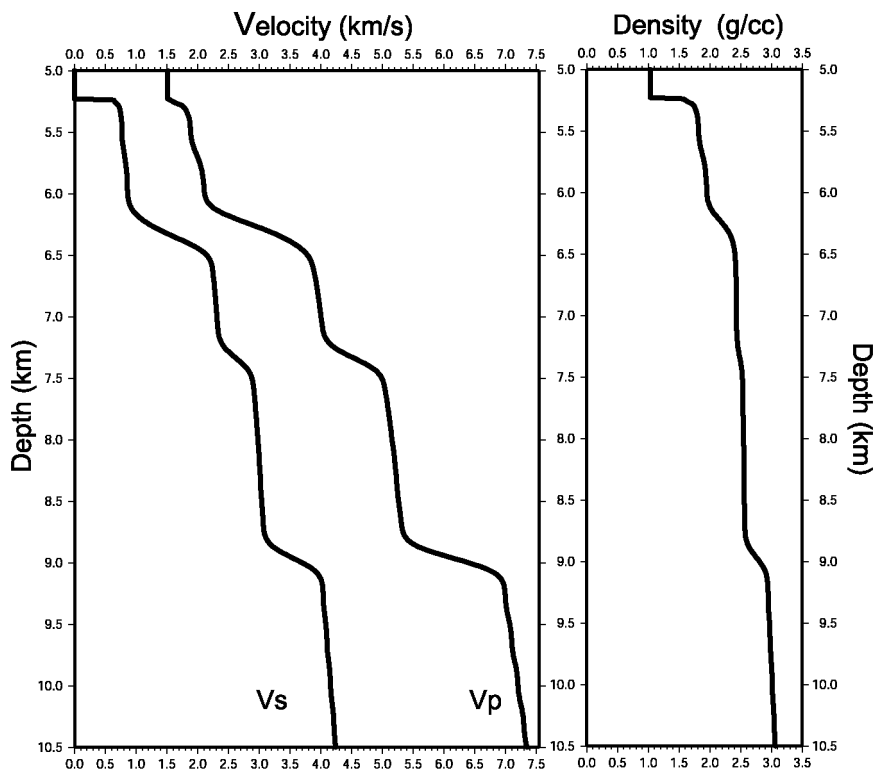


Fig. 3.3.3 : Smoothed starting model for the full waveform inversion. S-wave velocity and density are calculated from P-wave velocity. Attenuation values Q are constant with depth within sediments and crust.

iteration, whereas the remaining earth parameters ($V_{s,\rho,Qp,Qs}$) describing the subsurface were kept constant.

For the background velocity model serving as starting model for the waveform inversion the velocity model derived within the prestack depth migration algorithm was used (Fig 3.3.3). The prestack depth migration velocity model is obtained by densely sampled common-reflection-point velocity analysis. Based on the absence of any coherent reflections below the S-reflector, the downward continuation of velocities below S remains undefined. However, based on refraction and reflection tomography of OBS data, Zelt et al. (2003) derived a velocity-depth model of line ISE-1 (Fig. 2.3.2). In their model they achieve a velocity of 7.0-7.6 km/s for the mantle directly below the S-reflector. Based on these results a sub-S velocity of 7.0 km/s was assumed for the background velocity model serving as starting model for the waveform inversion. Finally, the model was discretized at 10 m intervals and smoothing was applied using a 26 m running average window to avoid large discontinuities at the reflectors.

The resulting best fit velocity model after five inversion runs is shown in Figure 3.3.4 as a black line, overlying the background velocity distribution (grey line). At the depth of S at approx. 9 km a distinct velocity structure is resolved. We resolve at a depth of 8.86 km a locally sharp decrease in V_p from 5.45 km/s to 5.2 km/s. Only another tens of meters deeper V_p is oscillating around its background velocity trend again. This local minimum in the fine scale velocity-depth model is a distinct feature. This means that by sending the source wavelet through the earth model, we obtain synthetic data which match the observed reflection from S with respect to its amplitude, phase and traveltime. The synthetic data based on the obtained fine-scale velocity model is shown in Figure 3.3.5 in grey, overlying the observed data plotted in black. Between 0.9-2.0 seconds the seabed reflection and the subseabed reflections within the sediments show a very good match in amplitude, phase and traveltime. This is an essential precondition to achieve a good match in the deeper levels (at the depth of S) as well. The synthetic S reflection does indeed show a good match to the observed reflection. To quantify the fit between synthetic and observed data a correlation coefficient R is calculated. A value of $R=1.0$ denotes a perfect fit whereas a value of $R=0.0$ equals to no fit between the compared data. The overall correlation coefficient of the complete synthetic CMP-

gather is $R=0.91$. It indicates that there is a 91% fit between the observed data and the synthetic data with respect to amplitude, phase and velocity.

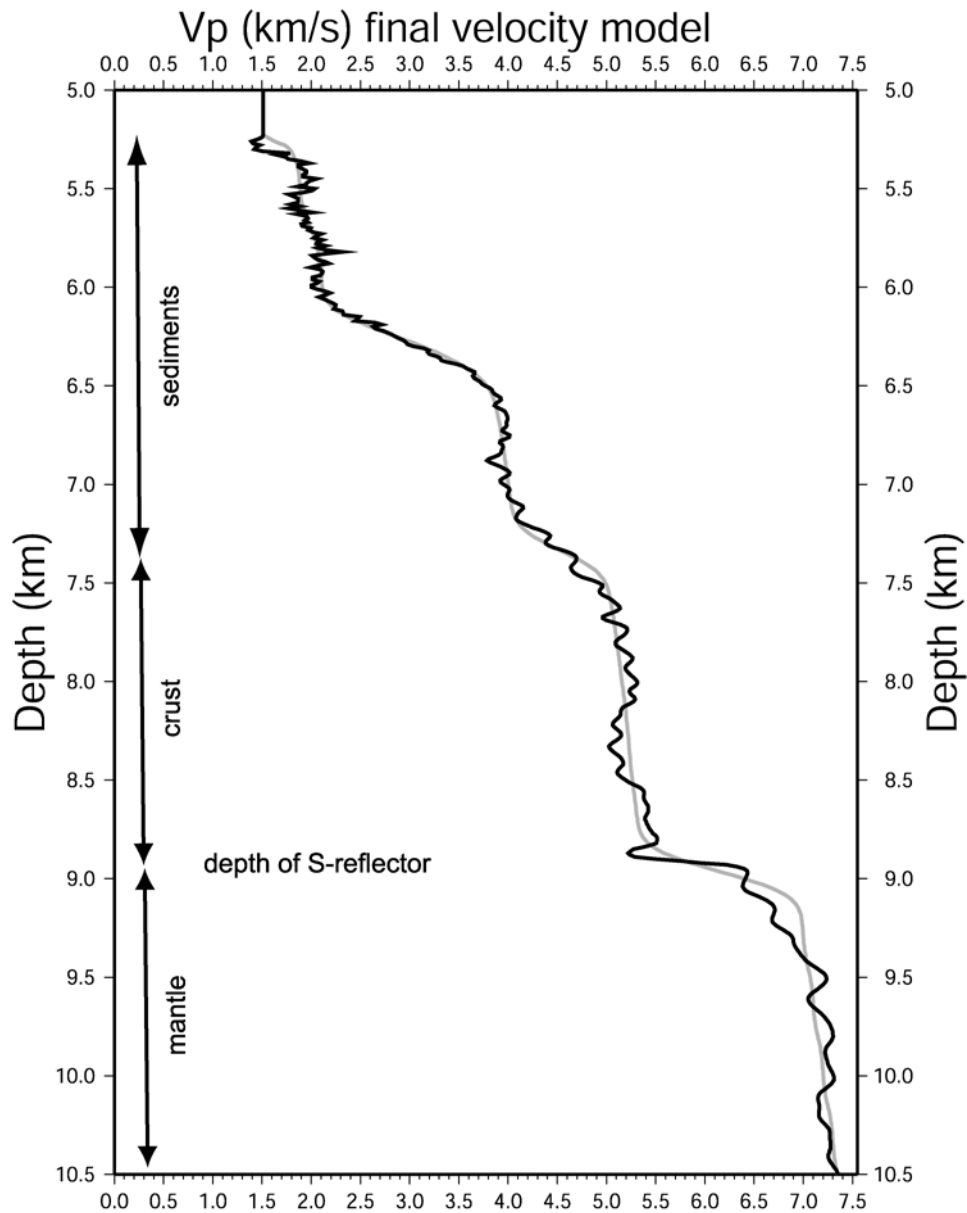


Fig. 3.3.4 : P-wave final velocity model (black line) after 5 inversion runs for the full slowness range with 15 iterations within each run. The p-wave starting model is plotted as grey line. At the depth of the S-reflector a zone of reduced velocity overlying a stepwise velocity increase is resolved.

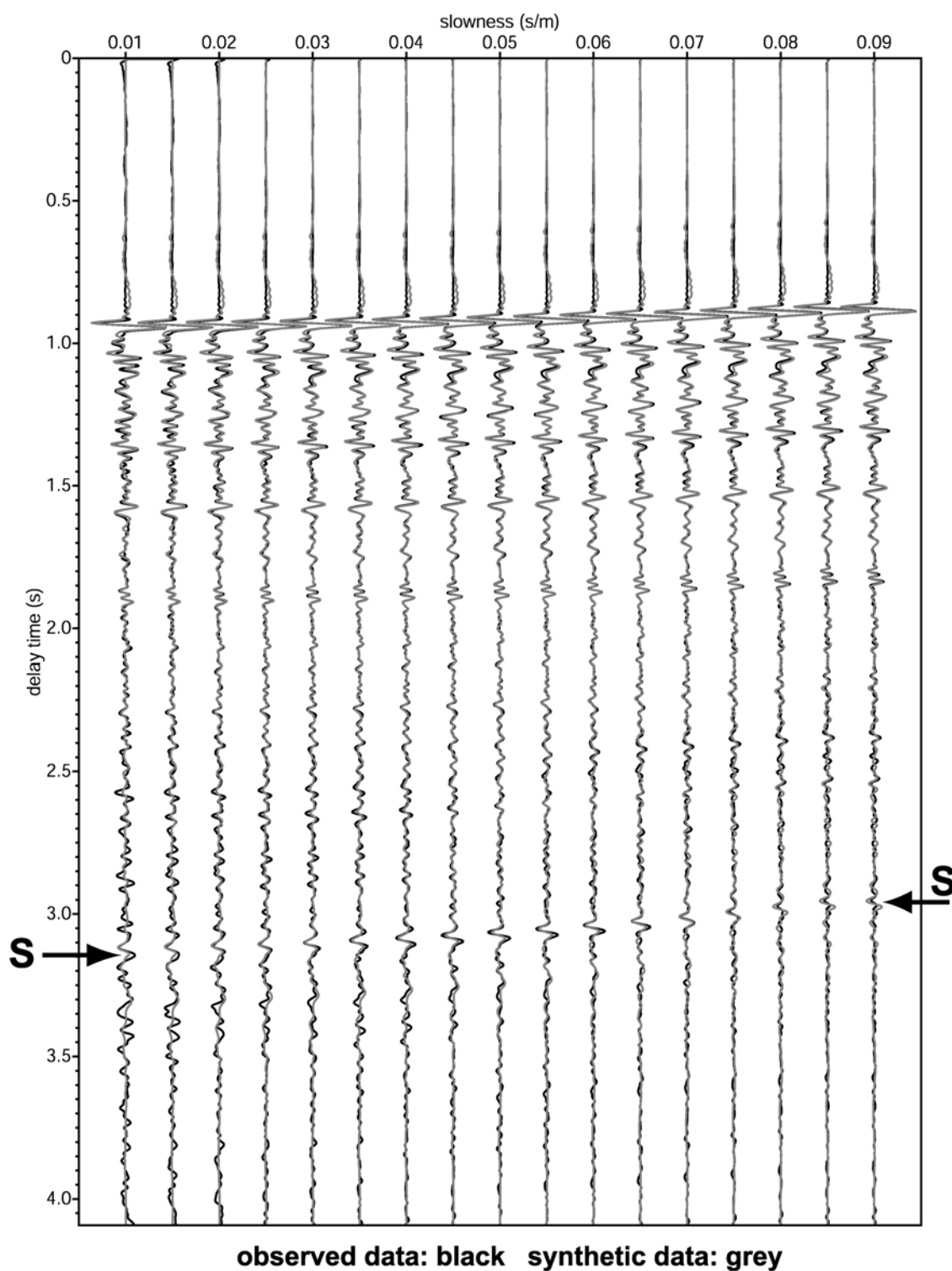


Fig. 3.3.5: Observed data (black) from CDP4470, line ISE-2, in the delay time – slowness domain plotted with the best fit synthetic data (grey) calculated from fine scale P-wave velocity model (Fig. 3.3.4).

To further investigate the nature of the velocity distribution around S and to evaluate its significance, a number of perturbed starting models were inverted. As shown in Fig. 3.3.6 the best fit velocity model was modified in the vicinity of S and zones of reduced velocity were incorporated in new starting models. Rerunning the full waveform inversion scheme, this time using the refined velocity model with the incorporated 50m and 100m low velocity zones as the starting models, yields new synthetic data. The misfit in waveform at the S-reflector is calculated in a 350 ms window around the S-reflector in terms of total residual energy divided by total energy of the observed data.

The results shown in Fig. 3.3.6 indicate that starting model (b) achieves the best waveform fit for S. Thus we conclude that the S reflection in the vicinity of CMP 4470 represents a 50 m zone of reduced velocity above a stepwise increase in velocity. As shown in Fig. 3.3.4 p-wave velocities of the lowermost crust is about 5.45 km/s decreasing to 5.2 km/s and increasing significantly towards 7.0 km/s. We believe that this zone of reduced velocity is the thickness of the fractured zone associated with the detachment fault. This 50 m thick, highly fractured zone would form the primary pathway for seawater to travel through the crust, finally into the mantle, where it would start serpentinisation of the mantle peridotite. Serpentinisation of mantle peridotite is known to dramatically decrease the friction coefficient thus acting as a lubricant for the detachment process and allowing the fault to stay active to almost horizontal dip.

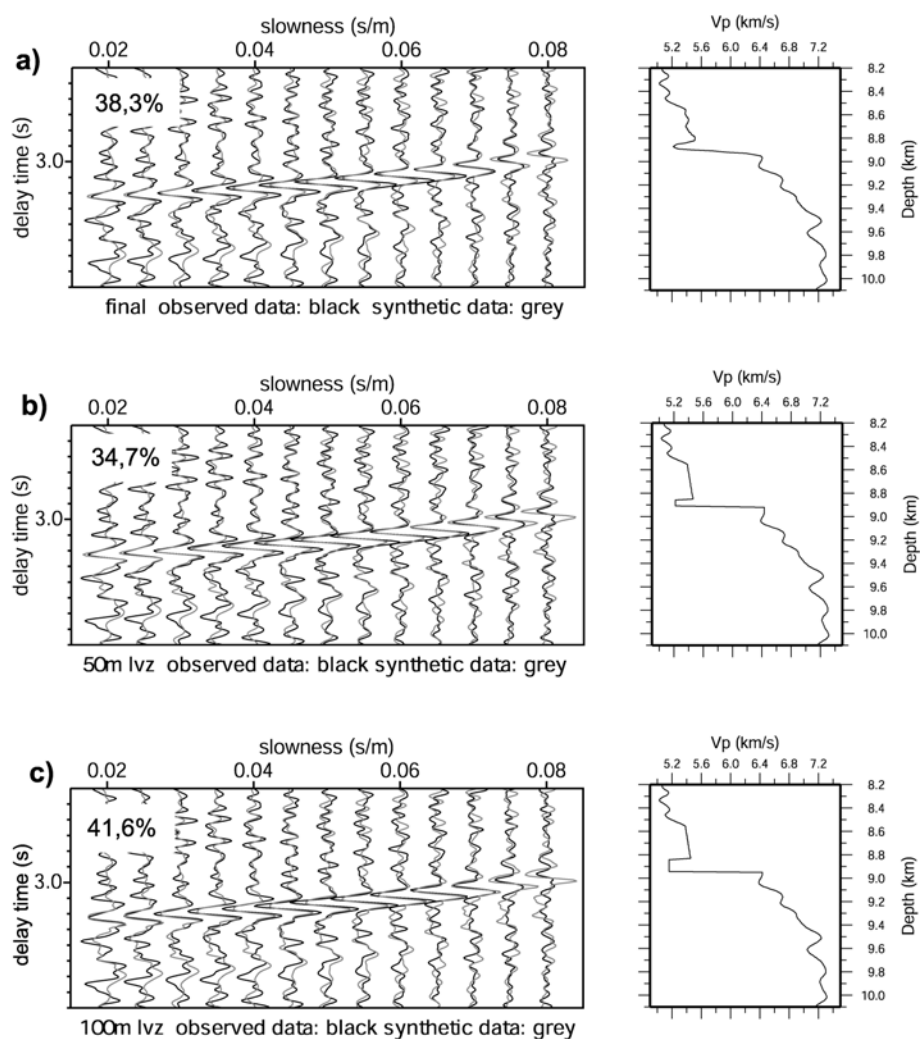


Fig. 3.3.6: Final velocity model (a) and starting models modified from (a) by incorporating (b) a 50m thick zone of reduced velocity above a stepwise velocity increase and (c) a 100m thick zone of reduced velocity above a stepwise velocity increase. Misfit values calculated in a 350 ms window around S are indicated. Starting model (b) shows best waveform fit form the S-reflector.

4.0 INTERPRETATION OF THE MCS-DATA OF LINE ISE-1

The 55 km long line ISE-1 runs parallel to, and is nearly identical with line GP-12 (Fig. 1.2.2), which was interpreted by Reston et al. (1996). However, the lateral extension of both seismic lines is not identical. Line ISE-1 is extended further westward for a distance of about 20 km traversing the peridotite ridge, while the processed part of line GP-12 shown in Reston et al. (1996) does not reach up to this ridge. On the other hand the processed part of line GP-12 shown by these authors extends about 15 km further in eastern direction.

4.1 POSTSTACK TIME MIGRATION

In the time-migrated section of line ISE-1 S is clearly shown as a continuous weakly undulating and westward dipping reflector between the eastern end of this line and about CMP 2650. As on line ISE-2 four tilted crustal blocks labelled A to D in Fig. 4.1.1 can be recognised. Also, the peridotite ridge, which is here not elevated as much above the seafloor is clearly imaged. The geometries of the sedimentary sequences covering this crustal topography can in the time migrated section not be properly defined. However, the horizontal stratification of the thick pile of the postrift sediments is clearly imaged.

4.2 PRESTACK DEPTH MIGRATION

The depth migrated version of line ISE-1 shows in general a similar structural situation as discussed above for line ISE-2. Four landward rotated fault blocks consisting of

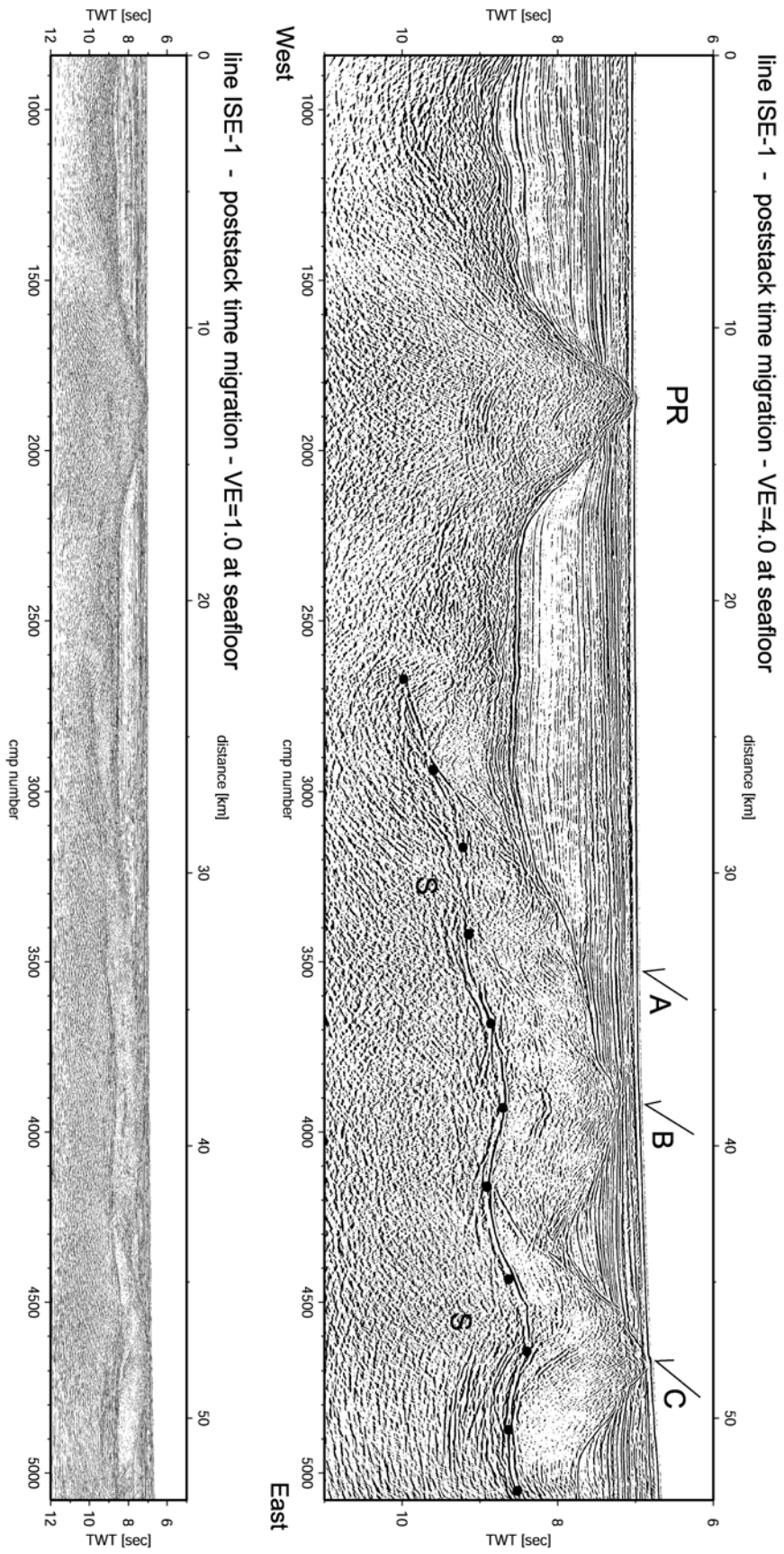


Fig. 4.1.1 : Poststack time migrated image of line ISE-1. Vertical exaggeration at seafloor is 4.0 and 1.0 (above and below respectively). As subsurface velocities are increasing, vertical exaggeration is decreasing at later travel times.

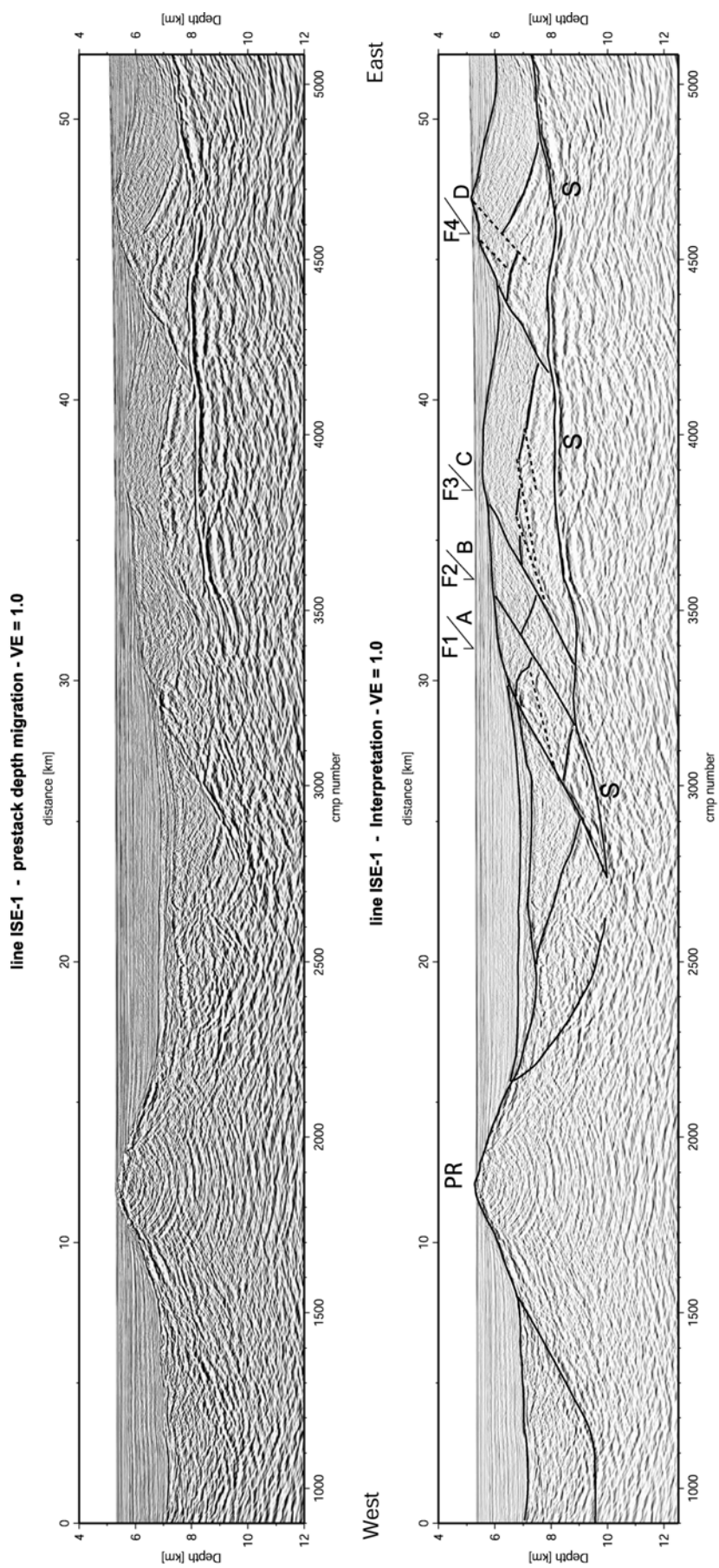
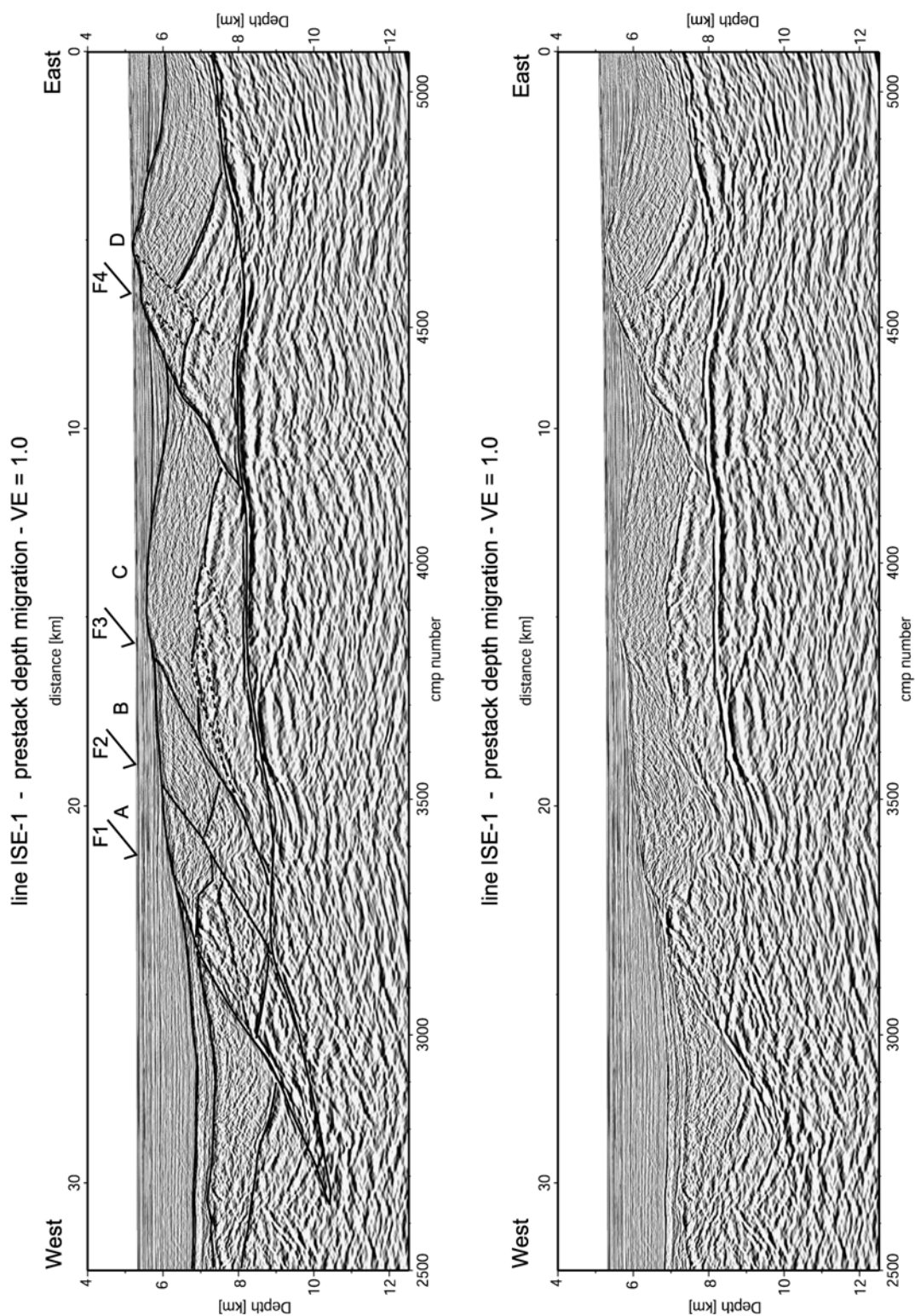


Fig 4.2.1 : Prestack depth migrated image of line ISE-1.

continental crust and overlying prerift and synrift I age sediments are clearly imaged (Fig. 4.2.1). However, in this cross section the block bounding normal faults F1 to F4 have more uniform dips in this cross section varying between about 30° and 35°. Like in Line ISE-2 all four block-bounding faults terminate abruptly on the S-reflector. The thickness of the stretched continental crust varies along a major part of this cross section between about 0.8 and 2.0 km. To the east of CMP 4800 sediments directly overlie the S-reflector, i.e. crustal fault blocks A to D have completely broken away from the continental crust to the east and have moved for a certain distance along the detachment. As discussed above in chapter 3.2 this observation confirms again the classification of S as a genuine detachment fault, which was first documented by Reston et al. (1996). The break-away point must be located beyond the eastern end of line ISE-1. It can, however, not clearly be recognised either in that part of line GP-12 (Reston et al. 1996) which represents more or less the eastern extension of line ISE-1. Therefore, the entire distance crossed by line ISE-1 can be classified as belonging to the continent-ocean transition (COT) zone.

S is a very strong reflection with a shallow dip westward over most of the distance between CMP 3500 and the eastern end of line ISE-1. The depth of S increases from about 7.3 km to about 8.5 km (Fig. 4.2.1). Towards the west beyond CMP 3500 the S-reflector is less clearly imaged (Fig. 4.2.2) and shows a significantly steeper dip westward of CMP 3200 (Fig. 4.2.1). For a short distance westward of about CMP 2750 where it has reached a depth of about 10 km, the S-reflector cannot be imaged. However, it may again be interpreted defining the eastern flank of the peridotite ridge (Fig 4.2.1). Most of this slope is covered by a body which as on line ISE-2 is interpreted as a back-tilted and highly tectonised crustal fault block. Back-tilting may have been caused by the rise of the peridotite ridge. In contrast to the line ISE-2 the peridotite ridge is here barely exposed at the sea floor. Finally, a weak undulation of the S-reflector is observed between CMP 2800 and CMP 3400 (Fig. 4.2.1).

The interpretation of the sedimentary sequences which cover in line ISE-1 this topography of rotated crustal fault blocks is similar to the one discussed above for line ISE-2. Fault blocks A to D are conformably overlain by thick piles of sediments interpreted as the prerift and synrift I sequence. Within these piles no clear internal structures are imaged except above fault block D and between about CMP 4600 and



CMP 4800 where reflections from sedimentary stratification run parallel to that of the top of the continental crust (Fig. 4.2.2). The prerift and synrift I sediments are exposed on the sea floor as the top of fault block D. A thin wedge of sediments interpreted as the

synrift II sequence in accordance with Reston et al. (1996, GP-12) are imaged between CMP 2200 and CMP 3200 overlying the back-tilted crustal fault block and a thick wedge-shaped body consisting of sediments of uncertain age. Slumped and tectonically disturbed sediments of the prerift and synrift I sequence may make up a major part of this volume. As the topmost part of this synrift II sequence a thin interval is imaged (Fig. 4.2.2) which may in terms of seismic expression represent the seismically transparent facies described by Mauffret and Montadert (1987) and interpreted as Albian-age black shales. Thin wedges of sediments classified as the synrift II sequence are observed like in line ISE-2 again filling the narrow half graben structures between fault blocks C and D as well the one to the east of block D. It is interesting to note that there appears to be little or no half graben structure developed between fault blocks A and B as well as between blocks B and C. The well stratified postrift sediments imaged in line ISE-1 can on the basis of results from the velocity model of the prestack depth migration perhaps be subdivided into three intervals (Fig 4.2.2). Stratigraphic ages and lithologies of all sedimentary sequences discussed here for line ISE-1 are the same as discussed in chapter 3.2 .

The top of the basement of fault block C, consisting of continental crust, is not a smooth surface. Instead it can be seen in the prestack depth migrated image to be dissected by small stepwise offsets (Figs. 4.2.1 and 4.2.2). These offsets in the topography of the basement of fault block C are interpreted to be caused by low-angle normal faults (shown as dashed lines in Fig. 4.2.2). These low-angle normal faults are thought to indicate an earlier phase of faulting preceding the faulting phase leading to the development of faults F1 – F4. However, it can not be inferred from the seismic image if and how far the low-angle faults transect the pre- and synrift sediment sequence overlying fault block C. Similar stepwise offsets dissecting the top of the pre- and synrift sediments, which would indicate a continuation of these low-angle faults through this pile of sediments, cannot be imaged. However, this might simply be beyond the seismic resolution of this experiment. A similar and even larger offset is imaged in the basement topography of fault block D. In this block the normal fault seems to be considerably steeper as compared to the faults in the basement of fault block C. However, in block D these normal fault seems to transect the overlying pre- and synrift

sediment sequence as can be inferred by the irregular surface of the pre- and synrift sediments in the frontal part of fault block D.

The early-generation faults shown in Fig. 4.2.2 as dashed lines are considerably less clearly imaged as the faults F1-F4. However, it is inferred that these structures indicate an early faulting phase that was overprinted in a later faulting phase leading to the formation of faults F1-F4. Thus their seismic expression is weaker than that of faults F1-F4. Nevertheless, it is a seismically inferred hint towards multiple phases of faulting in the rifting history of this margin. Multiple phases of faulting in the development of this margin have been documented before on the basis of another independent observation made in ODP Site 1065 in the Iberia Abyssal Plain. Site 1065 drilled the top of a continental tilted block, penetrating pre-rift sedimentary units. On the basis of data from the Formation MicroScanner (FMS) logging tool, a borehole imaging tool, Basile (2000) documented two distinct block tilting phases. The first tilt phase was previously unknown and had not been identified on the time-migrated seismic line CAM 144 imaging the tilted fault block of ODP site 1065. The author proposes two important changes in the rifting history of this margin "... first the change in extension orientation; and second the change from narrow, shallow and probably numerous tilted blocks to few large and deep blocks ...".

The distribution of p-wave velocities modeled from the prestack depth migration clearly reflects the overall structural configuration discussed above (Fig 4.2.3) As compared to line ISE-2 p-wave velocities of the crustal fault blocks A to D appear more uniform. Slightly lower p-wave velocities near the lower end of the back-tilted fault block may reflect the highly tectonised nature of this rock mass. P-wave velocities of the prerift and synrift I sequence sediments above fault blocks A to D are slightly higher as compared to those for the synrift II sequence sediments. Like observed in line ISE-2 a trend of decreasing p-wave velocities towards the top of the peridotite ridge probably reflects increasing degrees of serpentinization due to more intensive exposure of mantle peridotite to sea water (Fig. 4.2.3).

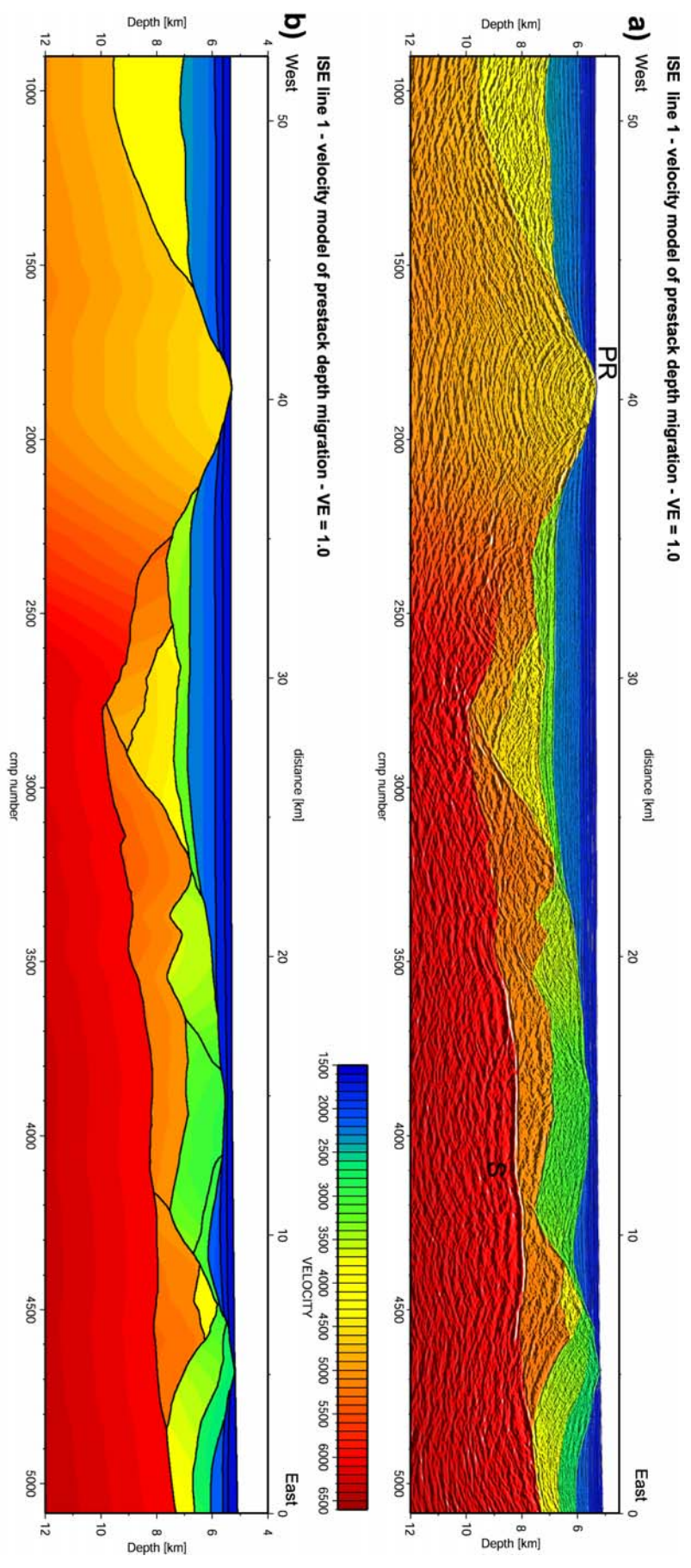


Fig. 4.2.3 : Velocity model of prestack depth migration of line ISE-1 in true scale. (a) Velocity model overlain on seismic image (b) Velocity model including the velocity domains. Velocities deep in section below S and peridotite ridge (PR) are poorly constrained.

5.0 DISCUSSION

As discussed in chapter 1.0 the precise role of the S-reflector in lithospheric extension and formation of the Iberia Margin has for a long time been hotly debated in the literature. The observations from poststack and prestack migration of lines ISE-1 and ISE-2, and especially the evidence obtained from full waveform inversion of a selected CMP-location discussed in the previous chapters have stimulated a new look at an old problem. A key for a better understanding of the origin and nature of the S-reflector was obtained by a review of the literature about the petrographic and petrophysical effects resulting from serpentinization of mantle peridotite. This process has been studied in detail by several authors on the basis of cores from ODP drilling. In this context it appears noteworthy that O'Hanley (1996) has characterized serpentinites as "records of tectonic and petrological history".

5.1 ORIGIN OF THE S-REFLECTOR

The various conceptual models which have been proposed in the literature to explain the nature of the S-reflector and its role with respect to continental extension along the Iberia margin have been summarized by Reston et al. (1996, Fig. 3) and Reston (1996, Fig. 3). In the latter paper he provided a detailed analysis of the seismic signature of the S-reflector, whereby S can be characterized seismically as a single interface representing a sharp boundary between very different rock types. In Reston et al. (1996) the authors concluded on the basis of structural analysis, that S is a top-to-the-west detachment fault.

Any interpretation of the nature of S must primarily be based on geophysical and geological evidence which can be summarized for the study area as follows:

a) Observations from deep sea drilling and submersible diving have shown that the S-reflector is overlain by crystalline basement, i.e. it is intrabasement and does not represent an intrasedimentary reflector (Boillot et al. 1988b).

b) In most seismic sections S is a continuous gently seaward dipping reflection. A clear example of this kind is seen in line GP-102 (Fig. 1.2.3 reproduced from Reston et al. 1996). Likewise, in the cross sections of lines ISE-1 and ISE-2 the S-reflector is imaged in a similar way.

c) In some seismic sections S is an undulating or domal-shaped reflection. A domal expression of S is seen e.g. in line GP-11 (Reston et al. 1996, Fig. 7). Undulations of S are observed in line ISE-1 between CMP 2800 and CMP 3400 (Fig. 4.2.1) as well as in line ISE-2 between CMP 4000 and CMP 5000 (Fig. 3.2.3).

d) The S-reflector passes without offset beneath the rotated fault blocks of thinned continental crust. The block-bounding faults stop abruptly at S. This was first noticed by Hoffmann and Reston (1992) and is seen clearly for the block-bounding faults F1 to F4 in line ISE-1 as well as for their equivalents F1 and F2 in line ISE-2 (Fig. 4.2.2 and Fig. 3.2.3 respectively).

e) In several seismic sections the S-reflector can be traced up to the basement/postrift sediment interface, e.g. towards the east of line GP-12 (Reston et al. 1996). This is even more clearly observed in line ISE-2 between crustal fault blocks B and C (Fig. 3.2.1 and 3.2.3).

f) In several seismic sections the S-reflector is towards the east split into two or more equally bright reflections as documented e.g. for line GP-11 (Reston et al. 1996, Fig. 7). Perhaps a similar, yet less clearly imaged, observation can be made in line ISE-2 eastward of CMP 3400 (Fig. 3.2.3). Reston et al. (1996) interpreted this split of S as branches of the same detachment system and hypothesized that the deepest of these branches might represent the crust mantle boundary (Reston et al. 1996, Fig. 16). If so, the S-reflector changes its geological significance across the margin. Over most of the

western part of these seismic cross sections and up to this branching point S represents the contact between lower continental crust and mantle peridotite, which is here the crust-mantle-boundary. To the east of this branching point S cuts into the continental crust, i.e. separating upper crustal from lower crustal rocks as proposed by Reston (1996, Fig. 16) as a possible explanation for line GP-12 and reproduced here as Fig. 5.1.1.

g) The structural relationship between the S-reflector and the peridotite ridge to the west is in all previously published seismic sections due to very complex structural situation of the overburden unclear. However, a situation where the S-reflector can be traced directly up to the peridotite ridge with some confidence is seen in line ISE-2 (Fig. 3.2.4). A possible interpretation is that the east flank of the peridotite ridge represents here just the continuation of S which was warped upward with the rise of the peridotite ridge. Concomitantly the frontal fault block was back-tilted and its rocks highly tectonized as discussed in chapter 3.2. In the GP-lines Reston et al. (1996) have interpreted the east flank of the peridotite ridge as a separate structure dipping to the east as also shown in Fig. 5.1.1. Based on new evidence from the depth migrated section of line ISE-2 this previous interpretation of the east flank of the peridotite ridge cannot be confirmed, i.e. it appears to be the true continuation of the S-reflector.

The observations discussed in chapter 3.0 and 4.0 fully support the interpretation of S as a low-angle, intrabasement detachment fault which has played a crucial role in continental breakup and rifting (Sibuet 1992; Reston et al. 1996, Reston 1996). They also confirm the conclusion by Reston (1996) that S is a top-to-the west detachment fault. The main unresolved problems concern the precise nature and the origin of the S-reflector. In order to solve these problems a new look at the seismic characteristics of the S-reflector is discussed below. However, first the previously proposed explanation of the nature and origin of S is briefly reviewed. Reston (1996) compared the waveform of the sea floor and that of the S-reflector. Based on the apparent similarity between both the author concluded that the S-reflector is a reflection from a single interface, i.e. from a sharp tectonic contact between different lithologies above and below. In addition, based on complex trace analysis the author showed that the instantaneous fre-

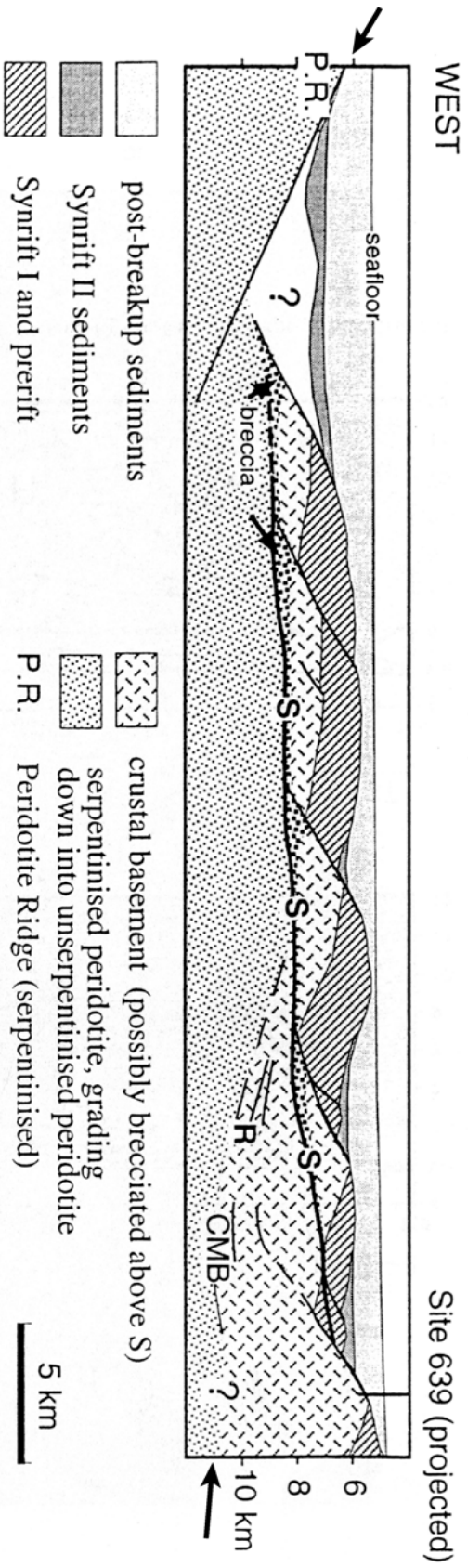


Fig. 5.1.1 : Interpretation of seismic line GP-12 by Reston et al. (1996, Fig. 16). Note that the east flank of the peridotite ridge was here interpreted as an eastward dipping structure (arrow) but its relationship to the S-reflector and the rotated fault blocks remained unclear. Note also that S is cutting into the continental crust over the eastern part of this cross section, i.e. the crust-mantle-boundary (CMB) is here deeper than S (arrow).

quency of S is that expected for a single interface, but indicated that “..., if S were a thin layer, it would have to be consistently of this thickness range (ca. 35-60 m thick).” However, Reston (1996) pointed out that his approach could not resolve a possible velocity decrease immediately above S, perhaps corresponding to a region of brecciation. Therefore, the application of a new and more sophisticated seismic analysis technique in the present study, i.e. the full waveform inversion, allows now to resolve further subtle features of this interface. As explained in detail in chapter 3.3, the S-reflector at CMP 4470 in line ISE-2 is not only a sharp stepwise interface between two lithologies of contrasting seismic characteristics. In addition S is best explained here as an approx. 50 m thick low-velocity interval (P-wave velocity 5.2 km/s) between a stepwise P-wave velocity increase from 5.45 to 7.0 km. The hypothesis favored here is based on the assumption that the S-reflector represents, at least over most of the area, a tectonic crust-mantle boundary separating serpentinitized peridotite below from a granodioritic continental crust above as previously argued by Boillot et al. (1989). If so, a clue to unravel the origin and nature of the S-reflector is concerned with an understanding of the process of serpentinitization and its effects on changing the density and the physical properties of the original peridotite.

Serpentinites are hydrated peridotites containing significant quantities of the serpentine minerals lizardite, chrysotile or antigorite with accessory magnetite, brucite and Mg- and Ca-Al silicates (O’Hanley 1996). It is well known that serpentinitization reactions require water to get in contact with mantle peridotite. Infiltration of water across the crust and down to mantle peridotite in the Iberia margin area could have occurred over an extended period of time. Deep dilatational faults and associated fracture systems as fluid conduits developed between about 140 to 135 Ma. Due to crustal stretching and resulting unroofing mantle unroofing and emplacement of serpentinitized peridotite at the seafloor occurred at about 125 Ma ago (Whitmarsh and Sawyer 1996). Skelton and Valley (2000) have, based on studies of cores from ODP leg 173, shown the exhumed peridotite is 95-100% serpentinitized. A reconstruction of the hypothetical temporal evolution of crustal extension for a margin of the “West Iberia type” was made by Pérez-Gussinyé et al. (2001). As shown in Fig. 5.1.2 reproduced from this work from 11.5 m.y. on after onset of extension stretching factors of about 4-5 have been reached so that the entire crust had become brittle. Under those conditions deep extensional

faults have cut into the mantle allowing infiltration of sea water causing serpentinization of peridotite. According to these authors the formation of mantle serpentinites resulted in the development of S as a detachment fault which appears to have been active at angles as low as 20° . Moreover, Pérez-Gussinyé et al. (2001) have suggested that extension proceeded in a more heterogeneous way after the onset of serpentinization resulting in “isolated blocks of crust floating in a sea of serpentinites”. This characterisation applies indeed to the structural situation of fault blocks A and B in line ISE-2 (Fig. 3.2.3) as well as of fault blocks A to D in line ISE-1 (Fig. 4.2.1). In this context they have coined the term “serpentinite margin” for the West Iberia margin.

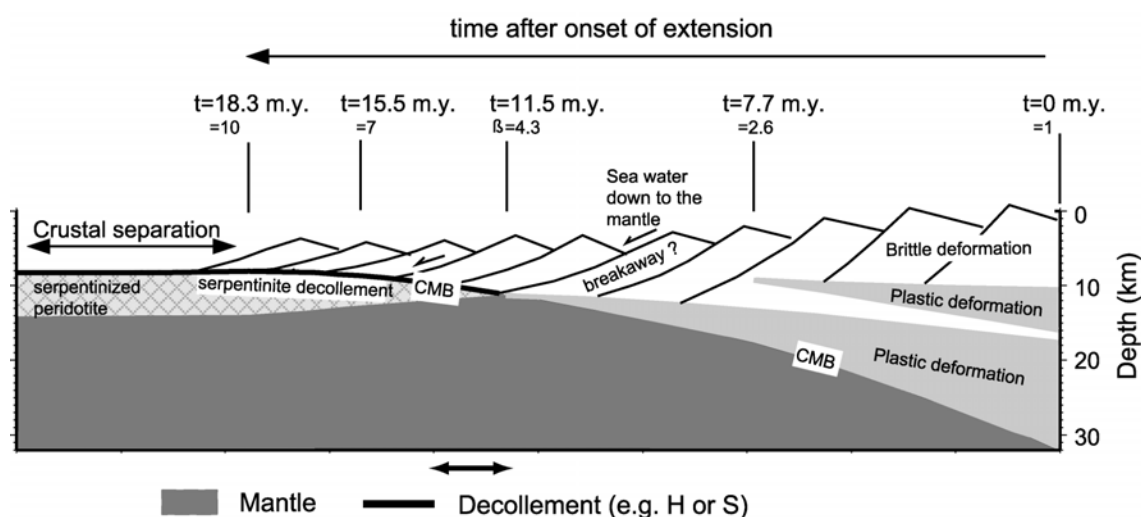
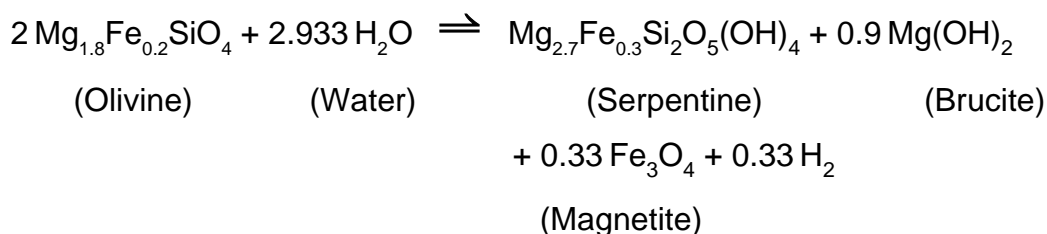


Fig 5.1.2 : Cartoon explaining the hypothetical temporal evolution of crustal extension for a margin of the "West Iberia"-type based on modeling of the thermal and rheological history depending on the initial lithospheric structure, rift duration and stretching factors (reproduced from Pérez-Gussinyé 2000). Note structural configuration and stretching stage (arrow) which represent the boundary conditions of the conceptual model proposed here to explain the origin of the S-reflector (Fig. 5.1.3)

Serpentinization of mantle peridotite is believed to have played a key role in the tectonic evolution and style of slow spreading ridges (Francis, 1981). Exhumed peridotite is 95 to 100% serpentinised and the serpentinization front is believed to extend to about 2 to 3 km depth. Generally speaking the process of serpentinization represents the formation of serpentine minerals from pre-existing anhydrous minerals

like olivine and pyroxen. Alt and Shanks (1998) have listed an example of serpentinization reaction :



These mineral alteration reactions can proceed in two different temperature regimes. High-temperature serpentinization (200°-400°C) occurs at transform faults near slow spreading ridges (Francis, 1981). Here fractured crust allows sea water to penetrate to great depth leading to serpentinization of unexposed mantle peridotite (Bougault et al. 1993; Coulton et al. 1995). In contrast low-temperature serpentinization of mantle peridotites has been documented in the Galicia margin area in a regime characterized by temperature of about 20° to 200°C and high water/rock ratios (Alt and Shanks 1998). O'Hanley (1996) quotes temperatures between 80°C and 170°C for this type of serpentinization reactions and states that they occur at relatively shallow depths under the ocean floor. For the Galicia margin area he implies a genetic relationship between serpentinization and the origin of detachment faults. Skelton and Valley (2000) have for the ocean-continent transition (OCT) beneath the Iberia Abyssal Plain concluded that serpentinization has occurred indeed in two stages. For ODP-Sites 1068 and 1070 they have documented two separate sea water infiltration events. During the ealier event pervasive infiltration of relatively warm sea water (>175°C) resulted in serpentinization of the uppermost mantle before it was exhumed. In the later event comparatively cool seawater (50°-150°C) was infiltrated in a structurally focussed way into the exhumed mantle, i.e. along deep normal faults.

From a geophysical point of view the most relevant effects of serpentinization concern the change in physical properties with the conversion of mantle peridotite to partially or completely serpentinized mantle rocks. According to Francis (1981) a completely

serpentinized mantle rock has a density of 2.55 g/cm^3 while a 50% serpentinization has resulted in a density of 2.90 g/cm^3 and a P-wave velocity of about 6.7 km/s . Skelton and Valley (2000) have for serpentinized peridotites of ODP sites 1068 and 1070 determined densities of $2.55\text{-}2.60 \text{ g/cm}^3$ as compared to 3.3 g/cm^3 for unaltered peridotite. Also, they have emphasized the low frictional strength of serpentinite. The topmost portion of the serpentinised mantle thus represents a low shear strength zone which is favorable for the development of detachment faults. Serpentine masses are also well known for their ability to flow plastically at low stresses. Therefore, serpentine can act as a lubricant facilitating the rotation of fault blocks.

Another important process probably associated with serpentinization is volume expansion. If a given volume of peridotite has experienced complete serpentinization its density has decreased from 3.3 to 2.55 g/cm^3 . Unless this process occurred in an open system, whereby reaction products can be transported away (which appears very unlikely for the upper mantle at great depth), this density decrease can only be accomplished by volume expansion. Volume expansion in terms results in generation of very high pore fluid pressures. Each deep normal fault cutting into the mantle is likely to be accompanied by zones of intense fracturing. Sea water effectively penetrates these fracture zones. The walls of these fractures are the sites where serpentinization reactions proceed. As these reactions progress volume expansion occurs leading to a reduction of the original fracture porosity. This in terms results in generation of extremely high pore fluid pressures. Generation of high pore pressures due to serpentinisation has been discussed previously by Escartín et al. (1997). Any such pressures which are exceeding hydrostatic pressure are termed overpressures. Sibson (2000) pointed out that “fluid overpressuring does also occur in crystalline rocks, but is localised within the normal fault zones which function as fluid conduits”. At pore fluid overpressures 0.8 times lithostatic pressure rocks are hydrofractured. MacDonald and Fyfe (1985) concluded that serpentinization “is geologically rapid controlled by the rate at which water is supplied to the reaction surfaces”. Also, they have calculated that a 1 km thick interval of peridotite at 300°C is serpentinised in about one million years. Hostetler et al. (1966) calculated the percent increase in volume due to serpentinization based on measured modes of both unaltered and serpentinized peridotite. They determined a range of 26 to

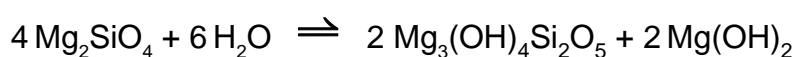
50% volume increase depending on the degree of serpentinization. Large volumes of mantle rock which have been fully serpentinised by high-temperature serpentinization at great depth represent, therefore, low-density bodies which will rise reaching the seafloor under certain circumstances. In this way the peridotite ridge along the ocean/continent transition zone of the Galicia margin could have been formed by isostatic uprise.

The question whether or not high pore fluid pressures localised around active normal faults can in the tectonic regime discussed here have been generated at all has been disputed on the basis of two arguments. One concerns the problem whether the sea water penetrated into a fault and fracture zone in the mantle is not completely consumed by serpentinization reactions. There may be no pore fluids left over or pore pressures may even drop. The following simple mass balance-type calculation allows to estimate the volume of water consumed for the hydration reactions of serpentinization:

Boundary conditions

- Serpentinization at constant mass but associated with volume expansion.
- Composition of peridotite consisting entirely of forsterite (Mg-olivine). This simplification appears in this context justified since peridotite consists to about 75% of olivine while the remaining 25% are pyroxenes, which are also hydrated in the serpentinization reactions.

Reaction equation



forsterite + water \Rightarrow chrysotile + brucite

converted into mass units utilising molar weights :

MgO = 40 , H₂O = 18 , SiO₂ = 60

forsterite (2 MgO + SiO₂) = 140

chrysotile (3 MgO + 2 SiO₂ + 2 H₂O) = 276

brucite (1 MgO + 1 H₂O) = 58

yields :

560 g/mol forsterite + 108 g/mol water (infiltrated) \Rightarrow

552 g/mol chrysotile + 116 g/mol brucite

mass units converted into volume units utilising density values :

forsterite = 3,2 g/cm³ ; chrysotile = 2,5 g/cm³ ; brucite = 2,4 g/cm³ ; water = 1.0 g/cm³

gives :

175 cm³ forsterite + 108 cm³ water = 221 cm³ chrysotile + 48 cm³ brucite

volume ratio of water : forsterite = 108 : 175 = 0.62

Result :

For serpentinization of a volume of 1m³ forsterite about 620 l of sea water are consumed in the hydration reactions.

In this simlified example 175 cm³ of forsterite are by hydration reactions converted into 269 cm³ of serpentine minerals. This corresponds to a volume expansion of the solid phase by 54 %. The volume of the aqueous phase, which is dynamically introduced via the fracture porosity while the serpentinization reactions proceed, is largely compensated by closure of the fracture system due to swelling of the solid phase. The reaction scheme considered here represents certainly a maximum case scenario. In reality both the volume of water consumed as well as the volume expansion due to serpentinization of peridotite will be somewhat lower because this calculation was made for a volume of pure forsterite. The purpose of this excercise was only to get order-of-magnitude estimates.

The large volume of water consumed by serpentinization can only be explained if the volume relationships between water intake, water consumption and replenishment as well as expansion of the solid phase are considered in a dynamic sense while hydration reactions proceed. Let us assume that this standard volume of 1 m³ forsterite is due to its close proximity to a normal fault criss-crossed by fractures. If six fractures each with a width of 1,03 cm are assumed this total fracture volume has to be replenished 10 times with sea water in oder to achieve a complete serpentinization. In summary, based on

this calculation there appears to be a discrepancy between the large volume of water required for serpentinization, which implies an open fracture system and the volume expansion of the solid phase which would lead to its rapid closure. MacDonald and Fyfe (1985) have pointed out this problem : Serpentinization "... will rapidly reduce the initial rock porosity to near zero. Thus, if there is any further reaction, the process must generate large volumetric strains and high stresses. If the stresses are sufficient, olivine and pyroxene will deform by cataclastic flow ... and new fractures will form in the rock ... ". According to MacDonald and Fyfe (1985) serpentinites and partially serpentinized peridotites get in this way intensively microfractured. They conclude that this microfracture system "... is in accord with rather rapid water flow rates." Also, they have measured the volume porosity of serpentinized peridotites in the order of 2-3%.

Rise of pore fluid pressures can only be initiated if the pore system becomes closed, i.e. fractures get sealed by expansion of the solid phase. Microfractures are very heterogeneously distributed throughout the rock matrix. Therefore, it can be expected that sealing of these microfractures occurs in a randomly oriented fashion. In this way it is likely that at some stage of the reaction residual stringers of water get trapped within sealed microfracture porosity or intergranular pore spaces. With further progress of the serpentinization reaction and additional swelling of the solid phase these pore fluids will get overpressured.

In the course of the serpentinization reaction there are two additional processes which can be expected to contribute significantly towards generation of overpressures: i) generation of methane, and ii) volume expansion of the aqueous phase due to heating. Generation of methane under the strongly reducing conditions of serpentinization is well known, e.g. Whitmarsh et al. (1998) have documented high methane concentrations in samples of serpentinized peridotites from ODP-cores from the Iberia margin area. Therefore, as soon as the permeability of the system, i.e. microfractures and matrix, becomes extremely low this gas cannot escape and gets trapped. Methane will be dissolved in the pore water leading to increased fluid pressures. If saturation levels are exceeded methane will be present as a gas phase. All of these conditions will result in generation of pore pressure. An additional argument in favour of the development of pore fluid overpressures during the latest stages of the serpentinization process is based on the fact that it is an exothermic reaction. Schroeder et al. (2002)

have noted that 67 Joule of heat are produced per cubic centimeter of peridotite serpentinized. For a hydrothermal vent field driven by exothermic serpentinization reactions they have estimated a rise of the water temperature from ambient sea floor conditions to about 100 °C . It is clear that the heat produced by the serpentinization reactions results in a volume expansion of the fluid phase. This will translate into a significant pressure component if the fluid phase is trapped in a closed system.

An argument in favour of generation of pore fluid overpressures due to serpentinisation – despite water consumption by hydration reactions – was recently made in a study by Hopkinson et al. (2004). They concluded “... that heating of solutions ... at the serpentinization front, combined with swelling pressures exerted by peridotite hydration and changes to the chemistry of aqueous solutions within the highly reducing environment at the serpentinization front, served to promote high pore fluid pressures ... “.

The other argument against the development of overpressures in this tectonic regime concerns a theoretical consideration : In order to build up fluid overpressures a closed system is required. However, it is suggested that in an extensional regime no closed system could exist (Wills and Buck, 1997). Although this may be true in an overall sense, it will be argued below that localised cells of overpressured rocks sealed-in as a consequence of serpentinization reactions around fault and fracture zones can indeed develop as transient phenomena.

The above outlined drastic changes of physical properties of mantle rocks associated with serpentinization must have played an important role with respect to the origin and nature of the detachment fault imaged as the S-reflector. In Fig. 5.1.3 a new hypothesis is illustrated schematically how serpentinization due to infiltration of seawater into the upper mantle could have affected the tectonic evolution and style of the COT zone of the Galicia margin. The qualitative two-dimensional tectonic model shown in cartoon fashion in Fig. 5.1.3 is proposed here to explain the origin of the S-reflector. This conceptual model is proposed for the following situation of continental extension and is based on the assumptions specified below :

- a) An advanced stage of crustal extension, i.e. stage 1 of Fig. 5.1.3 depicts a structural situation around stretching factors of $\beta=4.3$ as modeled by Pérez-Gussinyé et al. (2001) and reproduced in Fig. 5.1.2. At this stage the thickness of the continental crust is reduced to about 6-8 km. The frontal and oceanward portion of the stretched continental crust shown in stage 1 has moved into the brittle regime so that deep normal faults can cut across the entire crust and sea water can infiltrate the mantle. However, the lowermost portion of the landward extension of the crust depicted in stage 1 remains still in the ductile regime so that normal fault F5 does not reach into the mantle.
- b) This model to explain the origin of the S-reflector applies only to that part of the Iberia margin where S separates continental crust above from mantle peridotite below.
- c) Crustal stretching is not a continuous process but proceeds in many small intermittent steps. During each step landward rotation of the frontal blocks increases.
- d) Where the crust is in the brittle regime normal faults cut sequentially to deeper structural levels as thinning of crust increases, thus reaching deeper into the upper mantle step by step.
- e) Infiltration of seawater into the mantle through those deep normal faults as long as they are active.

This conceptual model was in parts adopted and modified from a model by Francis (1981) for the effects of faulting and sea water infiltration into the upper mantle near slow spreading ridges. Stage 1 of Fig. 5.1.3 shows schematically the frontal portion of the stretched continental crust with several fault blocks rotated to different degrees separated by normal faults and overlain by prerift sediments. Mantle peridotite is moderately altered to a certain depth by high-temperature serpentinization through pervasive infiltration of sea water (legend b in Fig. 5.1.3). This process will be discussed in more detail in chapter 5.2. The deep normal faults F2 to F4 have cut into the upper mantle juxtaposing granodioritic continental crust against mantle peridotite and permitting infiltration of sea water to great depth. Sea water influx along the

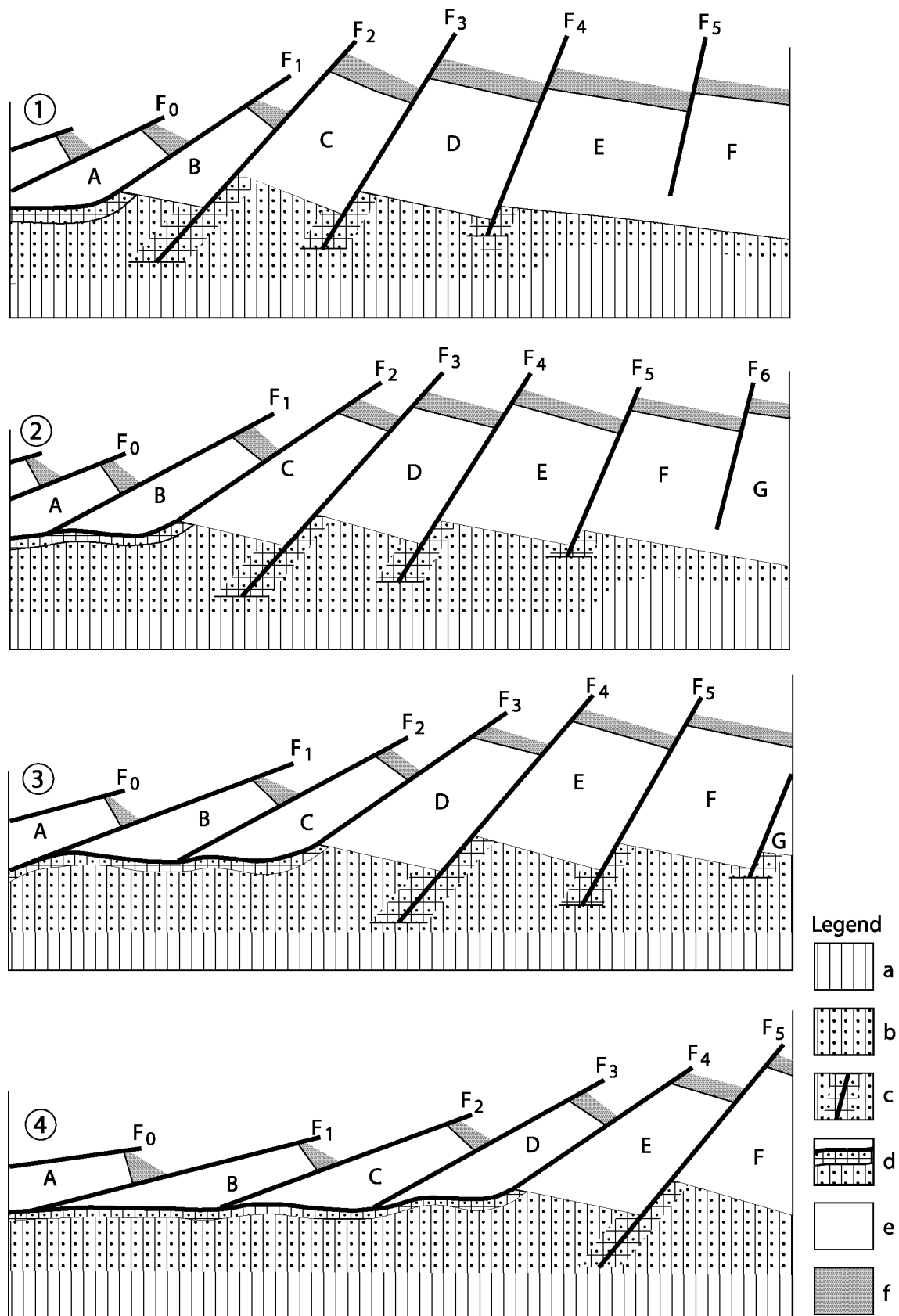


Fig. 5.1.3 : see next page for figure caption.

Fig. 5.1.3 : Schematic representation of the proposed hypothesis to explain the origin of the S-reflector as a detachment fault in the Galicia Margin area in the course of continental extension.

Stage 1 : Uppermost interval of mantle peridotite has prior to this situation been serpentinised to a moderate extent by pervasive infiltration of sea water through lower crust (legend b - for explanation see Fig. 5.2.1). Normal faults F2 to F4 are deepened into the mantle to increasing depth in a seaward direction. Influx of sea water at high rates leads to complete serpentinization of mantle volumes around each fault (legend c). In the course of serpentinization hydrothermal convection in the fracture system around fault F2 results in the formation of a seal by mineral precipitations near the crust/mantle boundary. Residual pore fluids trapped below get overpressured due to volume expansion. Note greater volumes of overpressured serpentine masses on upthrown blocks. Cross-hatched volume of completely serpentinized mantle around fault F2 represents a localised ductile regime.

Stage 2 : Lower branch of fault F2 and associated fracture zone is obliterated in this ductile volume. Therefore, fault F2 stops abruptly near crust/mantle boundary. Overpressured serpentine masses get squeezed laterally into and along crust/mantle boundary forming there a thin interval with chaotic internal structure which becomes part of the detachment. Due to new phase of stretching fault seal around F2 is re-opened leading to release of overpressures.

Stage 3 : With further stretching step same series of processes is repeated for fault F3. Thin interval of serpentine masses, which was overpressured while it became squeezed along crust/mantle boundary, is connected with equivalent interval originating from activity of fault F2. Note that rotation of fault blocks A to C is facilitated due to underlying zone of serpentine lubricant.

Stage 4 : With continued stretching these processes are repeated several times so that the low-angle detachment fault is growing in landward direction (legend d). Note also that the detachment can have a domal shape due to local plastic flow of serpentine masses filling void spaces below rotated fault blocks.

The seaward dip of the detachment (not shown in this figure) may allow dissection of several frontal fault blocks from the continental crust like observed in ISE-1 and ISE-2 seismic cross sections. For more details of this proposed hypothesis to explain the origin of the S-reflector see text.

Legend :

- (a) = unaltered mantle peridotite
- (b) = mantle peridotite serpentinised to a moderate extent by pervasive infiltration of sea water through lower continental crust.
- (c) = complete serpentinisation of peridotite around deep normal fault.
- (d) = detachment fault imaged as the S-reflector
- (e) = continental crust
- (f) = sediments of prerift and synrift I sequence

fault zones comes in contact with mantle peridotite first and over a larger area on the upthrown blocks. Let us consider this process around fault F2 offsetting blocks B and C where it is most advanced. Due to a larger contact area with the sea water impregnated fault plane on the upthrown block a significantly greater volume of mantle peridotite is

subjected to renewed serpentinization on the upthrown block as compared to the situation on the downthrown block. Serpentinization is an exothermic reaction (O'Hanley 1996). At an advanced degree of this reaction water near the bottom of fault and fracture zone F2 will be heated and loaded with solutes. It will rise upwards and eventually a localised convection cell will develop over the total length of this fault and fracture zone within the mantle. According to Hopkinson et al. (2004) this will ultimately lead to formation of a seal of the fault zone near the crust/mantle boundary by hydrothermal mineral precipitation. Influx of seawater will cease and with continuation of the serpentinization of the fractured mantle below this seal overpressures will build up. The overpressured serpentine masses in the cross-hatched volume around fault F2 represents a localised ductile regime. Consequently, that branch of the fault penetrating the mantle and its associated fracture zone will ultimately be obliterated. Fault F2 stops then abruptly at the crust mantle boundary. Overpressures may be that high that serpentine masses will be squeezed laterally into and along the crust/mantle boundary which may, due to prior stretching events, represent a zone of structural weakness (stage 2 in Fig. 5.1.3). In this way the formation of a narrow interval of serpentine masses with chaotic and brecciated internal structure is initiated, which will ultimately become part of the detachment. Also, during the transition from stage 1 to stage 2 in Fig. 5.1.3 thinning of the crust and mantle exhumation has progressed to a stage that normal fault F5 is now located within the brittle regime. More details of these processes will be discussed below on the basis of another schematic illustration (Fig. 5.1.4).

Between stage 1 and stage 2 of Fig. 5.1.3 a renewed phase of stretching is assumed leading to further rotation of fault F2 and block C. This extensional event has also opened the fault seal allowing pore fluid overpressures of the serpentine masses to be gradually released. In summary, fault F2 has acted as a valve which was closed near the crust/mantle boundary during times of tectonic quiescence due to hydrothermal cementation of the fault gouges. This allowed pore fluid overpressures to build up around the serpentinization front below. With renewed stretching the valve of fault F2 was re-opened resulting in gradual release of overpressures. At the same time fault F3 is deepened into the mantle and the same processes are repeated here as in case of fault F2 (stage 3 of Fig. 5.1.3). Another stretching step initiates the same cycle of events with

respect to fault F4. This has resulted in the formation of a low-angle, seaward dipping detachment fault (stage 4 of Fig. 5.1.3). This landward growth of the detachment fault continues as long as stretching prevails and high-angle normal faults are deepened into the mantle.

The hypothesis proposed here to explain the origin of the low-angle detachment imaged as the S-reflector appears to be supported by results of a study recently published by Hopkinson et al. (2004). Based on detailed mineralogical, textural and geochemical analyses of cores from sites 1068 of ODP-leg 173 located to the south of the study area they have emphasized the role of pore fluid overpressures with respect to the evolution of a major low-angle detachment fault in the area of the Hobby High. They propose the model of a fault-valve hydrothermal system whereby "... the detachment sustained cycles of fault seal rupture, hydrothermal discharge with regeneration of fault seals and high pore fluid pressures occurring due to post-slip hydrothermal cementation and ongoing serpentinization."

An attempt to explain in more detail the evolution of fault F2 in Fig. 5.1.3 and its contribution towards formation of the detachment with progress of serpentinisation reactions is illustrated schematically in Fig. 5.1.4. Stage 1 shows this steep normal fault and associated fracture zone shortly after deep penetration into the mantle. Mantle peridotite has been moderately serpentinized due to prior infiltration of sea water in a pervasive fashion as discussed in chapter 5.2. Due to massive influx of sea water complete serpentinization will now be achieved for the entire fractured mantle volume around this fault. The serpentinization front is progressing in accordance with sea water influx facilitated by further stretching (stage 2). At some point between stage 2 and stage 3 this fault and fracture zone has experienced sealing by hydrothermal mineral precipitation near the crust/mantle interface of the upthrown block. Therefore, pore fluids trapped in this closed system will get overpressured as discussed above. Since the volume of completely serpentinised peridotite around the lower branch of fault represents a local cell of ductile regime, this fault and fracture zone becomes obliterated. Due to significant reduction of shear strength of the material of this cell with overpressuring, serpentine masses are squeezed laterally into the crust/mantle zone (stage 3). Repetition of this series of processes at neighbouring faults will ultimately

form a thin interval of plastically displaced serpentine masses with chaotic and brecciated internal structure (stage 4), which is part of the detachment allowing tectonic

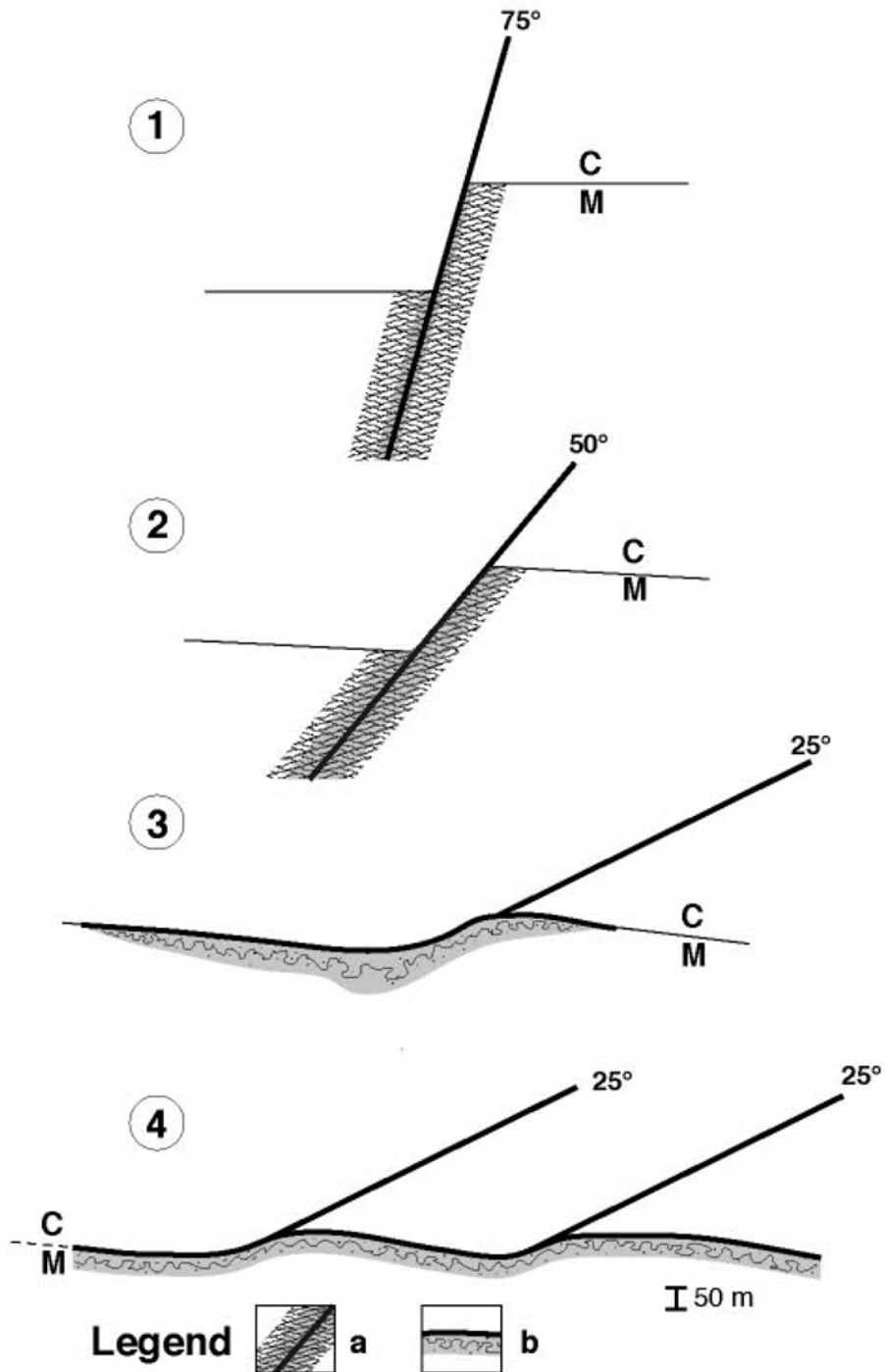


Fig. 5.1.4 : Schematic representation of the proposed hypothesis to explain the evolution of a steep normal fault, which has penetrated deeply into the mantle, with serpentinisation due to sea water influx. (figure caption continuous next page)

Stage 1 : Fault and associated fracture zone. Serpentinization front is progressing away from the fault.

Stage 2 : After another stretching step and rotation of the fault nearly entire volume of fractured mantle peridotite is completely serpentinised. The fault zone becomes gradually sealed near the crust/mantle boundary due to cementation by hydrothermal mineral precipitations. Residual pore fluids trapped below this fault seal become overpressured. Note larger volume of serpentinised peridotite on upthrown block.

Stage 3 : With further stretching and complete serpentinization of the entire fractured volume lower branch of this fault and its fracture zone is in this local cell of a ductile regime obliterated. Resulting reduction of shear strength leads to plastic squeezing of serpentine masses into the crust/mantle contact zone.

Stage 4 : Repeat of this series of processes at neighbouring faults leads to formation of a thin continuous interval of displaced serpentine masses along the crust/mantle interface, which is part of the detachment seismically imaged as the S-reflector. For a more detailed explanation of the processes discussed here see text.

Legend :

- (a) fault and associated fracture zone with advancing serpentinization front (gray)
- (b) thin interval of serpentine masses with chaotic and brecciated internal structure.

movements even at very low angles. This thin interval is seismically imaged as the S-reflector.

In the hypothesis presented here to explain the origin of S as a regional low-angle detachment fault, generation of pore fluid overpressures due to serpentinization represents an important process. However, it is emphasised that overpressures are considered here as a transient phenomenon. As long as sea water influx into the mantle through deep normal faults continues hydrostatic pore fluid pressures prevail. As soon as serpentinization reactions have progressed to a stage that hydrothermal sealing of the deep normal faults occurs a closed system is established. Below the fault seals pore fluid overpressures will build up in the above discussed manner. A similar effect was discussed by Axen (1992) who argued that low-permeability material near the surface of a preexisting fault could locally contain elevated pore pressures. The argument made here that high pore fluid pressures play an important role is also supported by the work of Floyd et al. (2001). For a low-angle normal fault in the Woodlark basin they calculated high porosity values which they concluded "... is best explained by the

presence of high pore fluid pressures in the fault zone. Fluid pressures must be near-lithostatic, otherwise the pore spaces would close under the weight of the overburden.”

Like any conceptual model, the one proposed here in Fig. 5.1.3 and Fig. 5.1.4 is qualitative and represents a simplification of the natural situation. However, the proposed model can explain in a qualitative way the formation of an extended low-angle detachment fault starting with a sequence of high-angle normal faults which cut due to individual stretching events stepwise deeper into the mantle. Since stretching steps are interrupted by periods of tectonic quiescence these deep normal faults are repeatedly opened and closed. With respect to the transmissibility of fluids they function in a valve-like fashion: i) initially open allowing massive influx of sea water leading to serpentinization of mantle peridotite, ii) then gradually closed due to sealing by hydrothermal precipitation of mineral cements, which results in build-up of pore fluid overpressures near the serpentinization front, and iii) re-opened again with another stretching step allowing release of pore fluid overpressures. Serpentine acting as a lubricant allows not only rotation of fault blocks but also their lateral transport by sliding action along the detachment. In support of the conceptual model presented here Whitmarsh et al. (2000) suggested that the detachment beneath the Iberia abyssal plain may have originated from extinct low-angle normal faults.

In this way the detachment imaged as the S-reflector could have gradually developed across the COT-zone of the Galicia margin. Furthermore, this proposed model can explain several observations from seismic lines ISE-1 and ISE-2 as well as from previous lines (Reston et al., 1996). This concerns especially the geometric relationships between the S-reflector and the block bounding faults, which stop abruptly at the detachment, as explained above. Good examples of this kind are faults F1 to F4 and F1 to F2 in line ISE-1 and ISE-2 respectively (Fig. 4.2.2 and 3.2.3). Undulating portions of the S-reflector may result from slightly different angles of rotation between adjacent fault blocks and hence irregular lower contacts of the rotated crustal fault blocks which have triggered mobilisation of serpentine masses in a lateral direction. As mentioned previously such undulations are seen in both ISE lines (Fig. 4.2.2 and 3.2.3). The

smooth domal feature of the S-reflector observed by Reston et al. (1996) in line GP-11 may have resulted from isostatic rise of a larger volume of serpentinised mantle in the center below this domal structure in combination with unloading effects due to thinning of the overlying continental crust. Structural configurations where the S-reflector is cutting up towards the base of the prerift and synrift sediment sequence like observed in line ISE-2 (Fig. 3.2.3), where S gradually merges into fault F3, corresponds to a stage in the evolution of the detachment which is equivalent to the situation of fault F4 in stage 4 of Fig. 5.1.3.

The role of serpentinization with respect to the geometry of deep normal faults and their conversion into a large-scale detachment as outlined here in the discussion of Fig. 5.1.3 appears to be analogous to observations documented by Escartín et al. (1997) for the oceanic crust at slow spreading ridges. They showed that “the presence of serpentinite can reduce the integrated strength of the oceanic lithosphere by up to 30%”. Especially, they argued that “... the mechanical properties of serpentinites favor strain localisation and may provide a mechanism for the development of long-lived, low-angle faults”. They point out that serpentinization which is localized to fault planes can also result in variations of fault geometry and fault spacing. The important role of volume expansion due to complete serpentinization of mantle peridotite underlying young oceanic crust was documented by Francis (1981). He concluded that local serpentinization along fault planes where mantle peridotite is juxtaposed against crust can result in volume expansion by 45% and uplift of the footwall block by several hundred meters. In terms of the depth level and structural situation – steep normal faults extending into the mantle – the process which Francis (1981) has documented for the oceanic crust near slow spreading ridges are believed to have occurred in a similar way in the COT zone part of the present study area. Volume expansion due to serpentinization at depth – the scenario which Francis (1981) has discussed is at 8 to 9 km depth – implies generation of pore fluid overpressures. The importance of local serpentinization restricted to fault zones, as argued above in the context of Fig. 5.1.3, has been emphasized also by Bogolepov (1970). He pointed out that local serpentinization restricted to fractures and shear zones results in complete serpentinization of peridotite adjacent to the fracture

zone, whereas regional serpentinization occurring in a pervasive fashion leads only to partial serpentinization.

5.2 NATURE OF THE S-REFLECTOR

The S-reflector at CMP 4470 in line ISE-2 is interpreted as a thin zone of reduced velocity between a stepwise increase of compressional wave velocities as discussed in chapter 3.3. Insofar this interpretation represents a refinement of the model which Reston (1996) have proposed to explain the nature of S. In order to explain the nature of this thin low-velocity zone it is proposed that serpentinization of the uppermost mantle peridotite has at this location occurred in two stages as illustrated schematically in Fig. 5.2.1. The boundary conditions and assumptions for this qualitative two-dimensional model are the same as outlined for Fig. 5.1.3. Stage 1 of Fig 5.2.1 depicts a less advanced stretching situation as compared to stage 2 which is identical to stage 1 of Fig. 5.1.3. In stage 1 of Fig. 5.2.1 the steep normal faults have not yet cut through the entire continental crust, but have approached the boundary with the mantle to increasing degrees in a seaward direction. Sea water is percolating through these normal faults and associated fracture zones reaching the lower crust. There it continues to move towards and into the mantle in a pervasive fashion probably by diffusion. An initial stage of serpentinization of mantle peridotite, which occurred in a high-temperature regime due to pervasive infiltration of sea water through the crust, was documented by Skelton and Valley (200) for cores from ODP Leg 173. They concluded that the uppermost mantle was serpentinised at great depth prior to its exhumation. However, they did not comment about the transport mechanism of this pervasive fluid flow. In the vicinity of faults F0 to F2 sea water has slowly penetrated the mantle and has resulted in a moderate degree of serpentinization. The serpentinization front is gradually advancing towards fault block D. This first phase of serpentinization is probably achieved by relatively hot sea water since it could, due to the slow infiltration process in the lower crust, have thermally equilibrated. Later and at a more advanced stage of continental extension several normal faults are deepened into the mantle (stage 2, Fig. 5.2.1) allowing massive influxes of sea water. Since rate of penetration of sea water into the mantle is now higher sea water is cooler (50°-150°C). In the vicinity of each of these

deep normal faults the fracture system is filled with sea water leading to the above discussed series of processes, i.e. continuation of the serpentinization reactions ultimately to completion, initiation of hydrothermal convection and sealing by

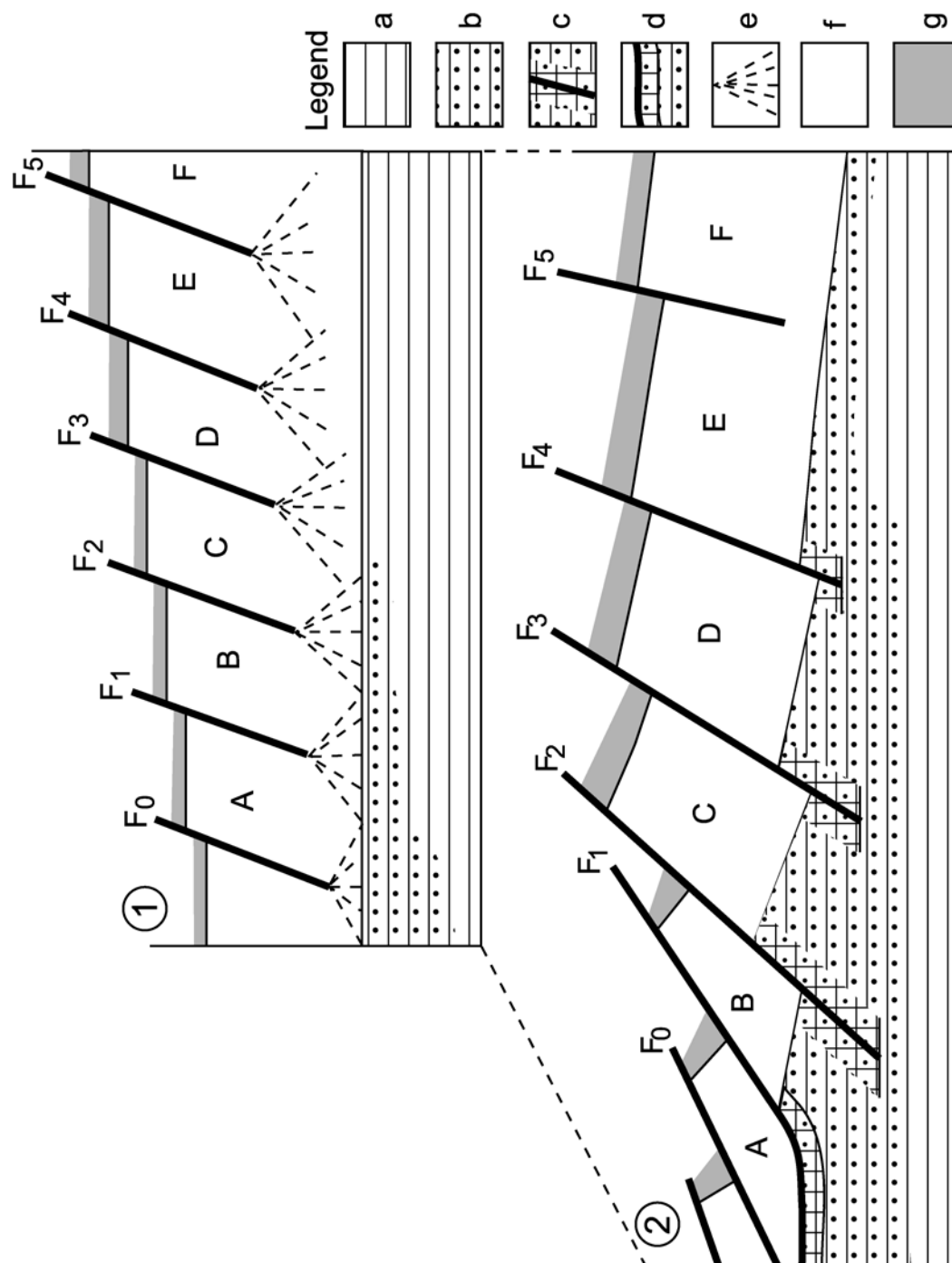


Fig. 5.2.1 : Schematic representation of the proposed hypothesis to explain how the nature of the S-reflector evolved as a result of serpentinisation which occurred in two separate phases during continental extension in the Iberia Margin area.

Phase 1 : During an early stage of stretching serpentinisation of mantle peridotite to a moderate extent is occurring by interaction with hot sea water. Elevated temperatures of sea water result from slow rates of penetration through the lowermost portion of the continental crust.

Phase 2 : During an advanced stage of stretching cool sea water rapidly influxing through normal faults F2 to F4 result in complete serpentinization by low temperature reactions in mantle volumes adjacent to each fault. Details of the effects of the associated mineral alterations and changes of petrophysical properties are explained in the text. Further explanation of processes occurring during this structural configuration – see Fig. 5.1.3 .

Legend :

(a) to (d) = see legend of Fig. 5.1.3

(e) = pervasive transport of sea water through lowermost continental crust

(f) = continental crust

(g) = sediments of prerift and synrift I sequence

cementation, generation of pore fluid overpressures and mobilisation of serpentine masses along the crust/mantle boundary initiating the formation of a low-angle detachment.

The model illustrated schematically in Fig. 5.2.1 is simplified and does not show all intended structural features. In stage 1 the boundary between lower continental crust and the mantle is considerably deeper and in a higher temperature regimes as compared to stage 2. By then the much advanced stretching has resulted in a thinning of the extended continental crust and some uplift of the mantle. Therefore, a somewhat lower temperature regime prevails at this stage in the upper mantle. According to the model proposed by Pérez-Gussinyé et al. (2001, Fig. 5.1.2) crustal separation and mantle exhumation has occurred in this area at a stretching factor greater than $\beta=10$ and more than 18.3 m.y. after onset of stretching. A possible explanation why at the location of CMP 4470 two separate phases of serpentinization could have occurred is based on the assumption that the processes of stretching and related fault block movement were similar here as in ODP site locations further south. Basile (2000) documented for ODP site 1065 which was drilled on the top of a tilted continental block (about 30 km to the East of the Peridotite Ridge) two distinct block tilting phases. The first one occurred during late Jurassic, while the second one was related to the main Cretaceous rifting

phase. Both tilting events resulted in sedimentary instabilities and formation of listric faults and slumps (Basile 2000). The assumption is made then, that these separate tilting episodes and their structural effects on the crustal block could have resulted in two distinct sea water infiltration events. Faults and fracture systems created during the first tilting episode may not have penetrated the entire crust. Sea water which has entered this shallow fault and fracture system may have filtered through the bottom part of the crust in a pervasive fashion. Due to low permeabilities of crustal rocks this was a slow process allowing thermal equilibration of the infiltrated sea water. A limited supply of hot sea water due to the slow infiltration process resulted only in a partial serpentinization of the mantle peridotite. Only during the main rifting phase when an advanced stage of stretching was reached did these re-activated faults cut through the entire crust extending into the mantle allowing now infiltration of sea water through interconnected fracture permeabilities. Due to the resulting higher rate of influx the sea water was not completely equilibrated thermally, i.e. it was cooler than during the initial infiltration event. The higher supply of infiltrated sea water lead to a continuation of the serpentinization process and ultimately to complete serpentinization which triggered the initiation of the detachment in the above discussed manner. The reason for the advancement of the serpentinization front in a landward direction as schematically shown in Fig. 5.2.1 appears to be a consequence of differences in the ease of sea water infiltration into the mantle. With the thinning of the crust by extension in an oceanward direction, the abundance of fractures is likely to increase. Hence, sea water could have penetrated there at higher rates into the mantle resulting in a thicker interval of serpentinised peridotite.

In summary, it is proposed that the nature of the S-reflector at CMP 4470 in line ISE-2 which is interpreted as a low-velocity zone between a stepwise increase of p-wave velocities can be explained by the assumption of two discrete phases of serpentinization as outlined schematically in Fig. 5.2.1. The effects which the second stage serpentinization has had with respect to a change of the physical properties of this low-velocity zone can be quantified based on literature data. Christensen (1972) has experimentally measured seismic velocities of a series of peridotite samples which were serpentinised to different degrees. As shown in Fig. 5.2.2 his results can be used to convert the p-wave velocities of the 50 m thick zone of reduced velocity at CMP 4470

and the underlying interval into values for rock densities and volume percentages of serpentine. The p-wave velocities obtained by full waveform inversion discussed in chapter 3.3 are converted into the density values and the percentages of alteration of mantle peridotite into serpentine listed in Tab. 1 .

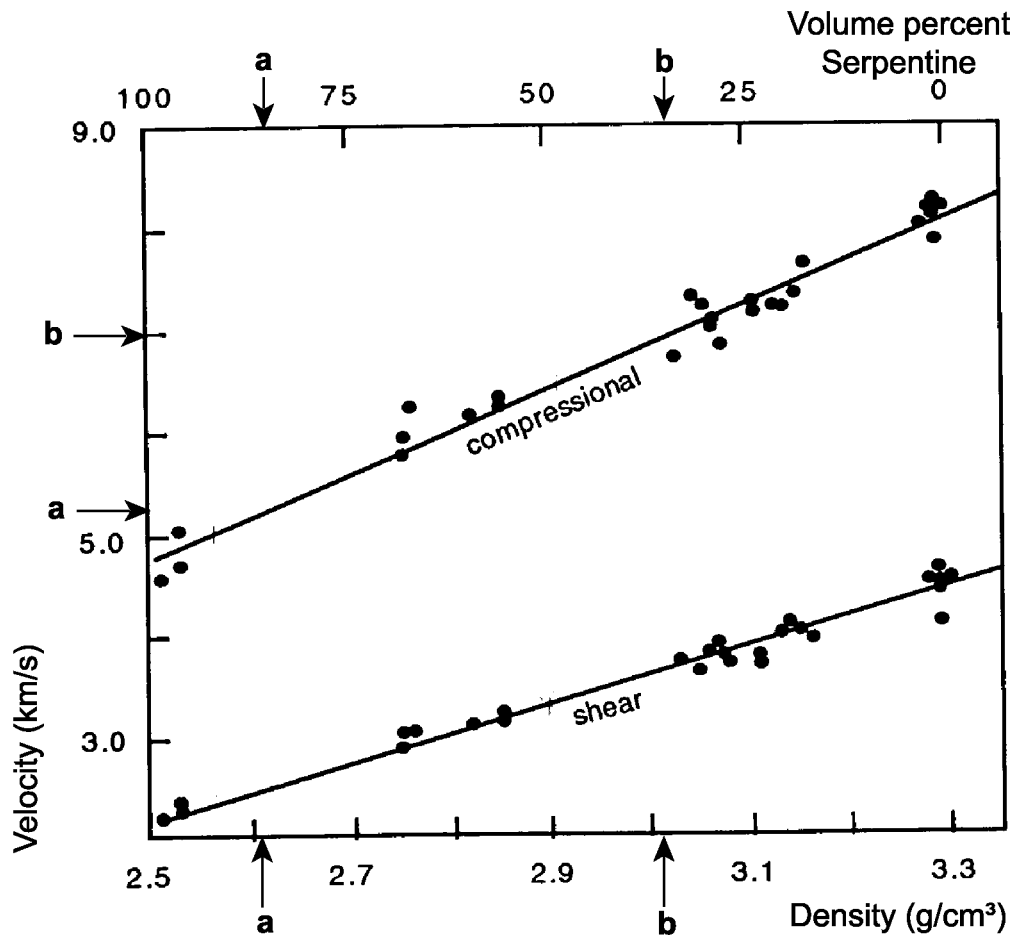


Fig. 5.2.2 : Seismic wave velocities of peridotites as a function of density and extent of serpentinization measured by Christensen (1972) at pressures of 10 kbar reproduced from O'Hanley (1996). P-wave velocities determined in the present study by full waveform inversion of S at CDP 4470 of line ISE-2 are converted into density and volume percent values of serpentine for the following intervals :

a = values for 50 m thick low velocity zone

b = values for serpentinised mantle peridotite below.

All values obtained in this way are listed in Tab. 1 .

Based on this conversion mantle peridotite has around the location of CMP 4470 been altered by an initial stage of serpentinization so that 33% of the rock volume is comprised of serpentine. This situation probably extends to several kilometers depth

and is believed to result from pervasive infiltration of hot sea water at great depth during a structural situation equivalent to stage 1 of Fig. 5.2.1 . The 50 m thick zone of reduced velocity imaged as the S-reflector resulted from additional progression of serpentinization reactions achieved by high influx of cooler sea water along the deep

	Vp (km/s) ^{a)}	Density (g/cm ³) ^{b)}	Volume % Serpentine ^{b)}
Lower continental crust	5.45	-	-
S = low velocity zone (strongly serpentinised mantle)	5.2	2.61	82%
Mantle peridotite (moderately serpentinised)	7.0	3.02	33%

Tab. 1 : Petrophysical properties, mineralogical composition and p-wave velocities of the S-reflector at CMP 4470 of line ISE-2 in comparison with corresponding properties of the intervals immediately above and below.

a) derived from full waveform inversion (this study)

b) P-wave velocities converted into these properties according to Fig. 5.2.3 (Christensen 1972).

normal fault F2 (Fig. 5.2.3) during a later extensional phase. The degree of serpentinization can be estimated as 82 volume percent serpentine. The density decrease from the moderately serpentinised mantle to the topmost 50 m mantle interval is the effect of an increasing degree of serpentinization. As also shown in Tab. 1 the second stage of serpentinization has resulted in a conversion of the original mantle peridotite into serpentine to 82% by volume.

A summary of the conclusions reached in the above discussion concerning the nature of the S-reflector in the study area is given in Fig. 5.2.3. The model of S as a first-order p-wave velocity discontinuity, which was previously proposed by Reston (1996) was refined in the present study on the basis of the results of the full waveform inversion of a selected CMP gather from line ISE-2. The stepwise variation of p-wave velocities were explained to reflect the changes in densities listed in Fig. 5.2.3. The reduced density of the thin low-velocity zone is interpreted to result from a higher degree of

serpentinization and associated changes of petrophysical properties. However, the conclusions summarised in Fig. 5.2.3 are based on full waveform inversion of only a single CMP gather. More control points of this kind would strengthen the validity of these conclusions. Also, the qualitative model proposed in the present study to explain

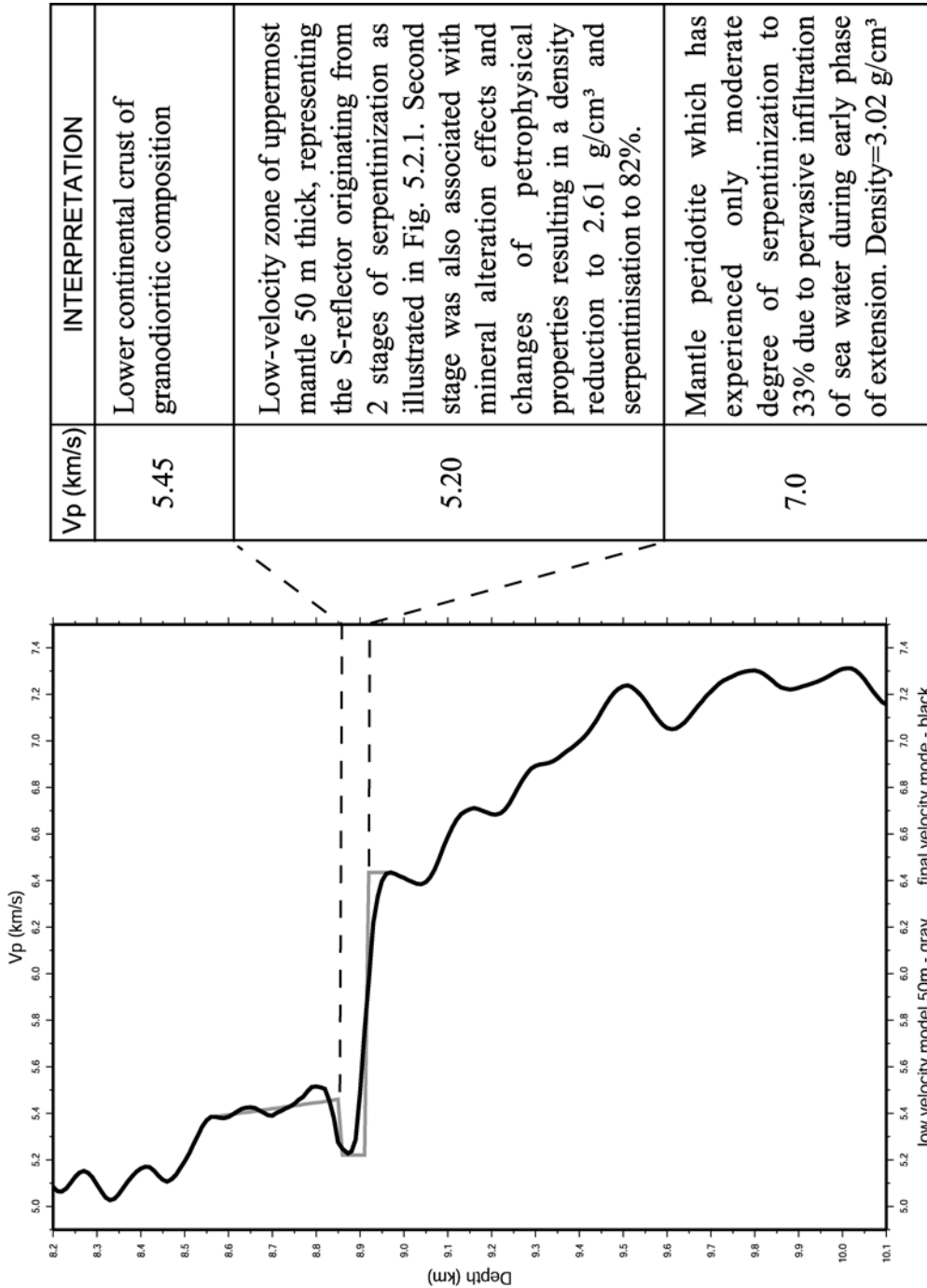


Fig. 5.2.3 : Summary of conclusions reached in the present study concerning the nature of the S-reflector in the Galicia margin area.

the nature and origin of the S-reflector in the Galicia margin area has to remain a hypothesis until the effects of the mineralogical, petrophysical and tectonic processes discussed in this context have been quantified by modeling. The ultimate test of the validity of the proposed model has to wait until the S-reflector will be penetrated by a future IODP drill hole.

6. DANKSAGUNG

Diese Arbeit wäre nicht zustande gekommen ohne die stetige und tatkräftige Unterstützung vieler Mitarbeiter der Abteilung Marine Geodynamik des GEOMAR. An erster Stelle möchte ich mich herzlich bedanken bei Herrn Prof. Dr. Tim Reston für die Beantragung des DFG-Projektes und die intensive Betreuung meiner Arbeit. Herrn Prof. Dr. Ernst Flüh danke ich herzlich für die Betreuung in der Anfangsphase meiner Arbeit.

Bedanken möchte ich mich natürlich auch bei meinen „Mitstreitern“ Cord Papenberg, Jörg Petersen, Anne Krabbenhöft, Lars Planert, Arnim Berhorst und Heidrun Kopp.

Bei Dr. Dirk Klaeschen bedanke ich mich für Einführung in die Geheimnisse der seismischen Datenbearbeitung.

Mein besonderer Dank gilt Herrn Dr. Tim Minshull für die freundliche Aufnahme in der Arbeitsgruppe „Subseafloor Processes“ am Southampton Oceanography Centre. Er hat mich in die Methodik der „full waveform inversion“ eingewiesen und aus seinem reichen Erfahrungsschatz viele nützliche Hinweise gegeben. Nur durch diese Unterstützung sind die neuen Erkenntnisse über die Natur des S-Reflektors im Untersuchungsgebiet ermöglicht worden.

Für die finanzielle Unterstützung des Projekts bedanke ich mich bei der Deutschen Forschungsgemeinschaft. Ein Marie-Curie-Stipendium ermöglichte mir einen achtmonatigen Aufenthalt am Southampton Oceanography Centre. Dafür danke ich der E.U., Brüssel.

7.0 LITERATURE

- Agrinier, P., G. Cornen and M.-O. Beslier, Mineralogical and oxygen isotopic features of serpentinites recovered from the ocean/continent transition in the Iberia Abyssal Plain, in *Proc. Ocean Drill. Program, Sci. Results*, 149, 541-552, 1996
- Alt, J.C. and W.C. Shanks, Sulfur in serpentinitized oceanic peridotites: Serpentinization processes and microbial sulfate reduction, *J. Geophys. Res.*, 103, 9917-9929, 1998
- Audebert, F. and J.-P. Diet, A Focus on focusing, 52nd EAEG meeting in Copenhagen, Denmark, expanded abstracts, European Association of Exploration Geophysicists, 107-108, 1990
- Axen, G.J., Pore pressure, stress increase and fault weakening in low-angle normal faulting, *J. Geophys. Res.*, 97, 8979-8991, 1992
- Barnes, A. and T.J. Reston, A study of two mid-crustal bright spots from southeast Georgia (USA), *Geophys. J. Int.*, 108, 683-691, 1992
- Basile, C., Late Jurassic sedimentation and deformation in the west Iberia continental margin: insights from FMS data, ODP Leg 173, *Mar. Petr. Geology*, 17, 709-721, 2000
- Beslier, M.-O., M. Ask and G. Boillot, Ocean-continent boundary in the Iberia Abyssal Plain from multichannel seismic data, *Tectonophys.*, 218, 383-393, 1993
- Bogolepov, V.G., Problems of serpentinisation of ultrabasic rocks, *Inter. Geol. Rev.*, 12, 421-432, 1970
- Boillot, G. and E. Winterer, Drilling on the Galicia margin: Retrospect and prospect, *Proc. Ocean Drill. Program Sci. Results*, 103, 809-828, 1988
- Boillot, G., J. Girardeau, and J. Kornprobst, The rifting of the Galicia margin: crustal thinning and emplacement of mantle rocks on the seafloor, in *Proc. ODP, Sci. Results*, 103, eds Boillot, G. Winterer, E.L., Collage Station, TX (Ocean Drilling Program), 741-756, 1988b
- Boillot, G., G. Féraudi, M. Recq, and J. Girardeau, Undercrusting by serpentinite beneath rifted margins: the example of the west Galicia margin (Spain), *Nature*, 341, 523-525, 1989
- Bougault, H., J.L. Charlou, Y. Fouquet, H.D. Needham, N. Vaslet, P. Appriou, P.J. Baptiste, P.A. Rona, L. Dimitriev and S. Silantiev, Fast and slow spreading ridges: Structure and hydrothermal activity, ultramafic topographic highs and CH₄ output, *J. Geophys. Res.*, 98, 9643-9651, 1993

- Chian, C., K.E. Loudon, T.A. Minshull and R.B. Whitmarsh, Deep structure of the ocean-continent transition in the southern Iberia Abyssal Plain from seismic refraction profiles: Ocean Drilling Program (Legs 149 and 173) transect, *J. Geophys. Res.*, *107*, 7443-7462, 1999
- Christensen, N.I., The abundance of serpentinites in the oceanic crust, *J. Geol.*, *80*, 709-719, 1972
- Coulton, A.J., G.D. Harper and D.S. O'Hanley, Oceanic versus emplacement age serpentinization in the Josephine ophiolite: Implications for the nature of the Moho at intermediate and slow spreading ridges, *J. Geophys. Res.*, *100*, 22245-22260, 1995
- Dean, S.M., T.A. Minshull, R.B. Whitmarsh, K.E. Loudon, Deep structure of the ocean-continent transition in the southern Iberia Abyssal Plain from seismic refraction profiles: II. The IAM-9 transect at 40°20'N, *J. Geophys. Res.*, *105*, 5859-5885, 2000
- de Charpal, O., P. Guennoc, L. Montadert and D. Roberts, Rifting, crustal attenuation and subsidence in the Bay of Biscay, *Nature*, *275*, 706-711, 1978
- Denelle, E., Y. Dezard and J. Raoult, 2-D prestack depth migration in the (S-G-W) domain, paper presented at 56th Meeting, Soc. of Explor. Geophys., Houston, Tex., 1986
- Dietrich, M. and F. Kormendi, Perturbation of the plane-wave reflectivity of a depth-dependent elastic medium by weak inhomogeneities, *Geophys. J. Int.*, *100*, 203-214, 1990
- Escartín, J., G. Hirth and B. Evans, Nondilatant brittle deformation of serpentinites: Implications for Mohr-Coulomb theory and strength of faults, *J. Geophys. Res.*, *102*, 2897-2913, 1997
- Floyd, J.S., J.C. Mutter, A.M. Goodliffe and B. Taylor, Evidence for fault weakness and fluid flow within an active low-angle normal fault, *Nature*, *411*, 779-783, 2001
- Francis, T.J.G., Serpentinisation faults and their role in tectonics of slow spreading ridges, *J. Geophys. Res.*, *86*, 11616-11622, 1981
- Froitzheim, N., and G. Manatschal, Kinematics of Jurassic rifting, mantle exhumation, and passive-margin formation in the Austroalpine and Penninic nappes (eastern Switzerland), *Geo. Soc. of American Bulletin*, *108*, 1120-1133, 1996
- Goodwin, E., G. Thompson and D. Okaya, Seismic identification of basement reflectors: the Bagdad reflection sequence in the Basin and Range Province – Colorado transition zone, Arizona, *Tectonics*, *8*, 821-831, 1989

-
- Hinz, K., A hypothesis on terrestrial catastrophes. Wedges of very thick oceanward dipping layers beneath passive continental margins – their origin and paleoenvironmental significance. *Geologisches Jahrbuch E22*, 3-28, 1981
- Hoffmann, H.J. and T.J. Reston, The nature of the S-reflector beneath the Galicia Bank rifted margin. Preliminary results from pre-stack depth migration, *Geology*, 20, 1091-1094, 1992
- Hopkinson, L., J.S. Beard and C.A. Boulter, The hydrothermal plumbing of a serpentinite-hosted detachment: evidence from the West Iberia non-volcanic rifted continental margin, *Marine Geology*, 204, 301-315, 2004
- Horsefield, S., Crustal structure across the continent-ocean boundary. PhD thesis, 215 pp., Cambridge Univ., Cambridge, United Kingdom, 1992
- Hostetler, P.B., R.G. Coleman, F.A. Mumpton, and B.W. Evans, Brucite in alpine serpentinites, *Am. Mineral*, 51, 75-98, 1966
- Juhlin, C., Interpretation of the reflections in the Siljan Ring area based on results from Gravberg-1 borehole, *Tectonophysics*, 173, 345-360, 1990
- Kennett, B.L.N. and N.J. Kerry, Seismic waves in a stratified half-space, *Geophys. J. Roy. Astr. Soc.*, 57, 557-583, 1979
- Korenaga, J., W.S. Holbrook, S.C. Singh and T.A. Minshull, Natural gas hydrates on the southeast U.S. margin: Constrains from full waveform and travelttime inversions of wide-angle seismic data, *J. Geophys. Res.*, 102, 15345-15365, 1997
- Kormendi, F. and M. Dietrich, Nonlinear waveform inversion of plane-wave seismograms in stratified elastic media, *Geophys.*, 56, 664-674, 1991
- Krawczyk, C.M., T.J. Reston, M.O. Beslier, and G. Boilot, Evidence for the detachment tectonics on the Iberia Abyssal Plain rifted margin, in *Proc. Ocean Drill. Program, Sci. Results*, 149, 603-615, 1996
- Larner, K., and C. Beasley, Cascaded migrations: improving the accuracy of finite-difference migration, *Geophys.*, 52, 618-643, 1987.
- Larsen, H.C. Investigations of rifted margins, *Joides Journal*, 28, No.1, 85-90, 2002
- Litak, R. and E. Hauser, 1992, The Bagdad Reflection Sequence as tabular mafic intrusions: evidence from seismic modelling of mapped exposures, *Geol. Soc. Am. Bull.*, 104, 1315-1325, 1992
- MacDonald, A.H. and W.S. Fyfe, Rate of serpentinitisation in seafloor environments, *Tectonophysics*, 116, 123-135, 1985

- Malod, J.A. and Mauffret, A., Iberian plate motions during the Mesozoic, *Tectonophys.*, 184, 261-278, 1990
- Mauffret, A. and L. Montadert, Rift tectonics on the passive continental margin off Galicia (Spain), *Mar. Pet. Geol.*, 40, 49-70, 1987
- Milikan, K.L., F.L. Lynch and K.E. Seifert, Marine weathering of serpentinites and serpentinite breccias, sites 897 and 899, Iberia Abyssal Plain, in *Proc. Ocean Drill. Program, Sci. Results*, 149, 529-558, 1996
- Minshull, T.A., S.C. Singh and G.K. Westbrook, Seismic velocity structure at a gas hydrate reflector, offshore western Colombia, from full waveform inversion, *J. Geophys. Res.*, 99, 4715-4734, 1994
- Minshull, T.A. and S.C. Singh, Shallow structure of oceanic crust in the western North Atlantic from seismic waveform inversion and modeling, *J. Geophys. Res.*, 98, 1777-1792, 1993
- Morgan, J.K. and K.L. Miliken, Petrography of calcite veins in serpentinitized peridotite basement rocks from the Iberia Abyssal Plain, sites 897 and 899: kinematic and environmental implications, in *Proc. Ocean Drill. Program, Sci. Results*, 149, 559-569, 1996
- Murillas, J., D. Mougénot, G. Boillot, M.C. Comas, E. Banda and A. Mauffret, Structure and Evolution of the Galicia Interior Basin (Atlantic western Iberian continental margin), *Tectonophys.*, 184, 297-319, 1990
- O'Hanley, D.S., *Serpentinites - records of tectonic and petrological history*, Oxford University Press, 1996
- Pérez-Gussinyé, M., T.J. Reston and J.P. Morgan, Serpentinisation and magmatism during extension at non-volcanic margins: the effect of initial lithospheric structure, *Geol. Soc. Lond. Spec. Publ.*, 187, 551-576, 2001
- Pickup, S.L.B., R.B. Whitmarsh, C.M.R. Fowler and T.J. Reston, Insight into the nature of the ocean-continent transition from deep multichannel seismic reflection profile, *Geology*, 24, 1079-1082, 1996
- Pinheiro, L.M., R.B. Whitmarsh, and P.R. Miles, The ocean-continent boundary off the western continental margin of Iberia, II. Crustal structure in the Tagus Abyssal Plain, *Geophys. J. Int.*, 109, 1106-124, 1992
- Pratt, T., E. Hauser, T. Hearn and T. Reston, Reflection polarity of the midcrustal surrency bright spot beneath southeastern Georgia: testing the fluid hypothesis, *J. Geophys. Res.*, 96, 10145-10158, 1991
- Rabinowitz, P.D., S.C. Cande and D.E. Hayes, Grand Banks and J-anomaly Ridge, *Science*, 202, 71-73, 1978

-
- Reid, I., Crustal structure of a nonvolcanic rifted margin east of Newfoundland, *J Geophys. Res.*, *99*, 15161-15180, 1994
- Reston, T.J., C.M. Krawczyk, and H.-J. Hoffmann, Detachment tectonics during Atlantic rifting: analysis and interpretation of the S reflection, the west Galicia margin, *Geol. Soc. Lond. Spec. Publ.*, *90*, 93-109, 1995
- Reston, T.J., C.M. Krawczyk, D. Klaeschen, The S-Reflector west of Galicia (Spain): Evidence from prestack depth migration for detachment faulting during continental breakup, *J. Geophys. Res.*, *101*, 8075-8091, 1996
- Reston, T.J., The S reflector west of Galicia: the seismic signature of a detachment fault, *Geophys. J. Int.*, *127*, 230-244, 1996
- Schroeder, T., B. John, and B.R. Forst, Geologic implications of seawater circulation through peridotite exposed at slow-spreading mid-ocean ridges, *Geology*, *30*, 367-370, 2002
- Sibson, R.H., Fluid involvement in normal faulting, *J. Geodyn.*, *29*, 469-499, 2000
- Sibuet, J.C., New constrains on the formation of the non-volcanic continental Galicia-Flemish Cap conjugate margins, *J. Geol. Soc. Lond.*, *149*, 829-840, 1992
- Singh, S.C. and T.A. Minshull, Velocity structure of a gas hydrate reflector at Ocean Drilling Program site 889 from global seismic waveform inversion, *J. Geophys. Res.*, *99*, 24221-24233, 1994
- Skelton, A.D.L. and J.W. Vally, The relative timing of serpentinisation and mantle exhumation at the ocean-continent transition, Iberia: constraints from oxygen isotopes, *Earth Planet. Sci. Let.*, *178*, 327-338, 2000
- Srivastava, S.P., Results from detailed aeromagnetic survey across the northeast Newfoundland margin, Part II, Early opening of the North Atlantic between the British Isles and Newfoundland, *Mar. Pet. Geol.*, *5*, 324-327, 1988
- Srivastava, S.P., and W.R. Roest, Nature of thin crust across the SW Greenland margin and its bearing on the location of the Continent-Ocean boundary. *Kluwer NATO ASI Series C*, *463*, 95-119, 1995
- Thompson, A.B., Metamorphism and fluids, p.223-248, in: Understanding the Earth, eds. Brown, G.C. et al. *Cambridge University Press*, 1992
- Tucholke, B.E. and W.J. Ludwig, Structure and origin of the J anomaly Ridge, western North Atlantic Ocean, *J. Geophys. Res.*, *87*, 9389-9407, 1982

- Whitmarsh, R.B. and P. Miles, Models of the development of the West Iberia rifted continental margin at 40°30' N deduced from surface and deep tow magnetic anomalies, *J. Geophys. Res.*, *100*, 3789-3806, 1995
- Whitmarsh, R.B., R.S. White, S.J. Horsefield, J. Sibuet, M. Recq and V. Louvel, The ocean-continent boundary off the western continental margin of Iberia: Crustal structure west of Galicia Bank, *J. Geophys. Res.*, *101*, 28291-28314, 1996
- Whitmarsh, R.B. and D.S. Sawyer, The ocean/continent transition beneath the Iberia Abyssal Plain and continental-rifting to seafloor-spreading processes, in *Proc. Ocean Drill. Program, Sci. Results*, *149*, 713-736, 1996
- Whitmarsh, R.B. and ODP Leg 173 Shipboard Scientific Party, Drilling reveals transition from continental breakup to early magmatic crust, *Eos, Transactions, American Geophysical Union*, *79*, 173, 180-181, 1998
- Whitmarsh R.B, S.M. Dean, T.A. Minshull and M. Tompkins, Tectonic implications of exposure of lower continental crust beneath the Iberia Abyssal Plain, Northeast Atlantic Ocean: Geophysical evidence, *Tectonics*, *19*, 919-942, 2000
- Wills, S. and W.R. Buck, Stress-field rotation and rooted detachment faults: A Coulomb failure analysis, *J. Geophys. Res.*, *102*, 20503-20514, 1997
- Wilson, R.C.L., R.N. Hiscott, M.G. Willis and F.M. Gradstein, The Lusitanian Basin of West-Central Portugal: Mesozoic and Tertiary Tectonic, Stratigraphic and Subsidence history, in *Extensional tectonics and stratigraphy of the North Atlantic*, *Am. Soc. Pet. Geol. Mem.*, *46*, 341-361, 1990
- Yilmaz, O, Seismic data processing, Investigations in geophysics, Vol. 2 – SEG, Tulsa (OK), 526 pp., 1987
- Zelt, C.A., K. Sain, J.V. Naumenko and D.S. Sawyer, Assessment of crustal velocity models using seismic refraction and reflection tomography, *Geophys. J. Int.*, *153*, 609-626, 2003

CURRICULUM VITAE

Name	Thomas Leythaeuser
Date & place of birth	10.03.69, London, U.K.
Citizenship	German
1975 – 1979	Gemeinschafts-Grundschule Laurensberg, Aachen
1979 – 1988	Anne-Frank-Gymnasium Aachen
1988 – 1989	Military service in the German Airforce (medical corps)
1989 – 1992	Study of physics at the Technical University Aachen (RWTH), Vordiplom degree in physics
1992 – 1993	Study of geophysics at University of Münster
1993 – 1997	Study of geophysics at University of Hamburg, Diplom degree in geophysics
06/2001 – 02/2002	EU Marie-Curie fellowship at Southampton Oceanography Center (SOC)
since 1998	Research Assistant at GEOMAR